

MAY 20
C/76302



FACILITY FORM 602	N70-15023	
	(ACCESSION NUMBER) 185	(THRU) 1
	(PAGES) NASA-CL# 86302	(CODE) 02
	(NACA CR OR TMX OR AD NUMBER)	(CATEGORY)



DYNAMICS RESEARCH CORPORATION

60 Concord Street
Wilmington, Massachusetts

Reproduced by
**NATIONAL TECHNICAL
 INFORMATION SERVICE**
 U.S. Department of Commerce
 Springfield, VA. 22151

195

001 2 - 710-00508

NAS 12-2150

R-106U

OPERATIONAL ALIGNMENT AND
CALIBRATION OF THE ISU FOR PHASE 2
OF THE V/STOL PROGRAM

Volume I Calibration

By William H. Fincke

December 1969

Prepared under Contract No. NAS12-2150 by
DYNAMICS RESEARCH CORPORATION
60 Concord Street
Wilmington, Massachusetts 01887

for Electronics Research Center

NATIONAL AERONAUTICS AND SPACE ADMINISTRATION

TABLE OF CONTENTS

	Page
1. SUMMARY	1-1
2. INTRODUCTION	2-1
2.1 General	2-1
2.2 Objectives and Scope of Calibration Study	2-2
2.3 Ground Rules of Calibration Study	2-4
3. SYMBOLS	3-1
4. ISU and INERTIAL SENSORS MATH MODELS	4-1
4.1 Accelerometer Math Model	4-2
4.2 Gyro Math Model	4-6
5. ISU and TEST EQUIPMENT CONFIGURATIONS	5-1
6. DESCRIPTION OF SYSTEM and TEST EQUIPMENT REQUIREMENTS	6-1
6.1 Description of System	6-2
6.2 Single-Axis Test Stand (SATS)	6-5
6.3 Two-Axis Fixture (TAF)	6-7
6.4 Optical Alignment Equipment	6-8
6.5 Data Collection System	6-9
7. DEVELOPMENT OF CALIBRATION EQUATIONS	7-1
7.1 Accelerometer Equations	7-3
7.2 Gyro Equations	7-7
7.3 Scale Factor Error Coefficient Equations	7-12
8. CALIBRATION TEST PROCEDURE	8-1
8.1 Development Considerations	8-5
8.2 Pre-Calibration Operational Procedure	8-9
8.3 Calibration Operational Procedure	8-13

TABLE OF CONTENTS (Cont'd)

		Page
9.	ESTIMATION OF CALIBRATION TERMS	9-1
9.1	Pre-calibration Calculations	9-5
9.2	Accelerometer Calibration Estimation Equations	9-8
9.3	Gyro Calibration Estimation Equations	9-11
10.	ERROR ANALYSIS	10-1
10.1	General Form of Error Equations	10-1
10.2	Pre-calibration Alignment Errors	10-3
10.3	Environmental Error Sources	10-4
10.4	Accelerometer Error Analysis	10-9
	10.4.1 Error Sensitivities	10-9
	10.4.2 Expected Accelerometer Calibration Precision	10-12
10.5	Gyro Error Analysis	10-15
	10.5.1 Error Sensitivities	10-15
	10.5.2 Expected Gyro Calibration Precision	10-19
11.	CONCLUSIONS	11-1
12.	RECOMMENDATIONS	12-1
13.	REFERENCES	13-1
APPENDICES:		
A.	DEVELOPMENT OF ACCELEROMETER MATH MODEL	A-1
B.	TABULATION OF CALIBRATION EQUATIONS	B-1
C.	CALIBRATION ESTIMATION EQUATIONS	C-1
	C.1 Equations for Estimating Calibration Terms Associated with the Accelerometers	C-1
	C.2 Equations for Estimating Calibration Terms Associated with the Gyros	C-2

TABLE OF CONTENTS (Cont'd)

	Page
APPENDICES (cont'd):	
D. EFFECT OF ENVIRONMENTAL ERROR SOURCES	D-1
D.1 Effect on Accelerometers	D-1
D.2 Effect on Gyros	D-4
E. ACCELEROMETER ERROR EQUATIONS	E-1
F. GYRO ERROR EQUATIONS	F-1
G. GLOSSARY	G-1

OPERATIONAL ALIGNMENT AND
CALIBRATION OF THE ISU FOR PHASE 2
OF THE V/STOL PROGRAM

Volume I Calibration

By William H. Fincke

DYNAMICS RESEARCH CORPORATION
60 Concord Street
Wilmington, Massachusetts 01887

1. SUMMARY

This volume of the final report presents a detailed design and analysis of a calibration scheme to be used for the strapdown inertial system for Phase 2 of the V/STOL Program. The calibration scheme is capable of being implemented under hanger conditions and runs can be completed within one 8-hour day. The precision of calibration is expected to be sufficient to support flight operations.

A total of 11 terms can be determined for each of the 3 gyros and 8 terms for each of the 3 accelerometers. These terms provide the matrix of misalignments between the ISU body axes and the input axes of each gyro and accelerometer. Second and third order scale factor error coefficients are also estimated as well as bias and gyro g sensitive coefficients. A second level of calibration can also provide estimates of cross compliance terms*. A detailed specification of the test procedure is

*If all terms are not to be calibrated, the process can be completed within 5 to 8 hours. Calibration of the gyro scale factor at a variety of rates will take longer.

provided, although details of the ISU alignment before each run have yet to be finalized.

The expected 1σ precision of calibration for the accelerometers is approximately $2 \widehat{\text{sec}}$ for misalignments, $4\mu\text{g}$ for bias, 3 to $13 \mu\text{g}$ for scale factor, and 6 to $12 \mu\text{g}/\text{g}^2$ for compliance terms. For the gyros, the expected 1σ precision is approximately $2 \widehat{\text{sec}}$ for misalignments, 8 mdh for bias, 20 mdh for scale factor at $2^\circ/\text{sec}$ (3 ppm), 6 to $10 \text{mdh}/\text{g}$ for mass unbalance terms, 11 to $14 \text{mdh}/\text{g}^2$ for major compliance terms and 15 to $20^* \text{mdh}/\text{g}^2$ for cross compliance terms.

The data reduction calculations have been made as simple as possible since estimation of the calibration terms may be done manually using only a desk calculator. Flexibility is provided in the least squares estimation of the scale factor error coefficients in that any number of input conditions can be accommodated. All calculations required to determine the calibration terms are provided.

A detailed error analysis of the calibration system was made that provided not only expected calibration estimation precision, but also formed the basis for specifying key performance requirements of the support equipment involved. Consideration was given to designing the system so as to minimize the complexity and number of test equipments required, thereby reducing the cost of implementing the system. Each major support equipment is described functionally.

* One of the terms for one of the accelerometers is expected to be $30 \text{mdh}/\text{g}^2$ (1σ).

2. INTRODUCTION

2.1 GENERAL

The purpose of these studies is to develop operational pre-flight alignment and calibration procedures for the strapdown inertial navigator to be used during Phase 2 of the V/STOL Program. The calibration procedure is designed to be one which can be implemented using the limited test equipment which will be available in the hangar. The alignment procedure is designed to be one which can be accomplished in the helicopter using the fixed point, on-board flight computer. Since the calibration and alignment procedure developments can be discussed separately and since many personnel at NASA-ERC are primarily interested in only one of these developments, the developments are discussed and documented in separate volumes: Volume 1 for the calibration procedure and Volume 2 for the alignment procedure.

Error analyses are presented which indicate the expected accuracies of the developed procedures. These error analyses, of course, are dependent on the assumed input error models. Developing models for the inertial sensors was one of the tasks performed as part of the overall study.

To the extent that they were known, input parameters for the study were supplied by NASA-ERC. These parameters describe the following types of inputs:

- specifications on the performance of the accelerometers and gyros,

- a description of the dynamic environment in which the alignment and calibration must be performed,
- a description of the test equipment that will be available for calibration in the hangar, and
- a description of the coordinate frames and the mounting of the inertial sensors in the strapdown system.

In those cases where the specifications and descriptions were incomplete, the associated error analyses must be considered preliminary in nature. In those cases where assumptions had to be made, the resultant error analysis provides information on how to set the performance specifications.

Throughout this report, references are made to a study made by UNIVAC [3, 4, 5]*. Whereas that study was concerned with calibration and alignment in the laboratory, this study is directed towards calibration in the field.

2.2 OBJECTIVES AND SCOPE OF CALIBRATION STUDY

The objectives of the ISU calibration procedure are as follows:

- estimate the inertial sensor calibration terms listed in Tables 4-3 and 4-5 of Section 4, with precision goals as indicated in the tables
- perform the calibration under field conditions (viz., in a hangar)

*References are indicated by numbers in brackets and listed in Section 13.

- perform the calibration in a minimum time period, with 8 hours as a goal. Equipment setup time and complexity is to be minimized, as well as pre-calibration activities and calculations
- data reduction is to be as simple as possible since it may be done manually

It is anticipated that the calibration procedure may be performed routinely once a week and more often if necessary, (e. g. , if an inertial sensor is changed or parameter changes are suspected).

The scope of the study is defined by the following tasks, as interpreted by certain ground rules discussed in the next section:

- develop inertial sensor models
- develop operational procedures to obtain the desired calibration terms, including an estimate of the time required to calibrate
- develop equations required to estimate the desired calibration terms
- specify critical functional and performance requirements of the associated test equipment
- identify the significant error sources and estimate the expected calibration precision

The study is considered to be a part of the total development effort required to implement the ISU calibration function, in that further trade-off studies are required, as well as detailed specification of the precalibration activities. The study should be considered as specifying

a base line system that can be developed and modified as necessary to arrive at a final design. In this sense many engineering judgements were exercised with the anticipation that design details may be changed, as required to provide a "balanced design".

2.3 GROUND RULES OF CALIBRATION STUDY

A set of ground rules were established at the beginning of the calibration study, to be used as a guide in developing the calibration system. These were discussed in Ref. 2 and further established as the study progressed. The ground rules of the study are as follows:

1. The ISU is to contain three Honeywell GG 334A gyros and three Kearfott 2401 pendulous accelerometers, using time-modulated pulsed torque-to-rebalance loops operating at 128 and 256 kHz respectively, and a maximum data sampling rate of 1 kHz.
2. Polarities of the calibration terms shall be as defined in Tables 4-2 and 4-4.
3. The ISU is to be mounted in a Two-Axis Fixture (TAF) as shown in Fig. 5-3 (this is a change from the convention used in the UNIVAC study (Refs. 3, 4 and 5)).
4. Accelerometer random noise is assumed to be negligible; gyro random noise is to be as specified in the UNIVAC study; torque-to-rebalance loop noise is no greater than the loop quantization, for both the accelerometers and the gyros.
5. The test stand base motion and effects on the gyro and accelerometer outputs are assumed to be the same as that presented in the UNIVAC study.
6. A Single-Axis Test Stand (SATS) with the rotary axis nominally vertical is to be used (in order to minimize costs). Data is to be taken only as a function of full table rotations.

7. A Two-Axis Fixture (TAF) is to be used to support the ISU. Accurate readouts of the TAF gimbals angles will be provided.
8. To reduce costs and since data recording is to be done manually, the data collection equipment is to be minimal. A minimum number of pulse counters should be used in trade-off with the objective to calibrate in one 8 hour day.
9. Since data reduction may be performed manually, the estimation equations should be as simple as possible (e. g., post run data filtering is to be avoided).
10. Least squares filtering of redundant data is to be minimized and used only when necessary to provide adequate sensitivity or flexibility to allow the inclusion of extra data when desired.
11. The calibration procedure is to be patterned after that used in the UNIVAC study, modified as necessary to reflect a single-axis test stand (rather than two axes) and pendulous accelerometers (rather than vibrating string accelerometers). It is desirable to use the same symbology, definitions, zero positions, etc.
12. The calibration procedure is to be based on using only test table rates and the gravity vector. Gyro scale factor error coefficients to be estimated using input rates between ± 1 and $\pm 60^\circ/\text{sec}$.
13. Error sensitivity equations are to be identified in support of possible tradeoffs that may be made as the design develops. The estimate of expected calibration precision is to be based on engineering judgements of acceptable error tolerances in the design in order to arrive at the base-line system.
14. Tradeoffs are to be minimized in this study in preference to the development of workable calibration procedures and specification of critical calibration system hardware requirements.
15. Details of the pre-calibration activities are to be developed separate from this study.

3. SYMBOLS

The symbols used in the ISU Calibration study are intended to be compatible to the maximum extent possible with those used in the UNIVAC Study [3, 4, 5] and in previous reports on this project [1, 2]. However, some deviations and redefinitions were necessary to avoid ambiguities, classify meanings, and provide consistency. Changes in these areas are noted specifically. The detailed lists of symbols are contained in the last Appendix, G, to facilitate rapid and convenient access whenever required.

The information contained in the Glossary, Appendix G, is intended to provide a central location for understanding all nomenclature used in the report. Four categories are defined, as follows:

- Formation of symbols
- List of prime symbols and abbreviations
- List of subscripts
- List of superscripts

Coordinate systems and related transformations are defined, where used, in Sections 5, 9 and Appendix B.

Positive quantities are defined in the direction of positive axes and positive angles are defined according to the right hand rule. Signs associated with nominally cardinal values of dot and cross products of vectors are defined as above and in terms of the coordinates in which the right hand term in the product is expressed. Positive values of the calibration terms are defined in Tables 4-2 and 4-4 in the Math Models Section (4).

4. ISU AND INERTIAL SENSORS MATH MODELS

The purpose of this section is to present the math models that will be used to characterize the ISU in general and the accelerometers and gyros in particular. The inertial sensors are discussed in Sections 4.1 and 4.2, whereas the ISU is considered below.

The structural alignment tolerances within the ISU are assumed to be as listed in Table 4-1. The ISU porro prism misalignment relative to the ISU optical cube is not considered in this study since the ISU cube is considered to be the prime reference during calibration.

<u>Definition of Misalignment</u>	<u>Value</u>
• Inertial sensor mounting error	6 $\widehat{\text{sec}}$ (max)
• Inertial sensor OA and SA (or PA) about IA	10 $\widehat{\text{min}}$ (max)
• ISU cube and inertial sensor mounting pads	6 $\widehat{\text{min}}$ (max)
• ISU cube and ISU mounting surface	6 $\widehat{\text{min}}$ (max)

Table 4-1 ISU Internal Alignment Errors

4.1 ACCELEROMETER MATH MODEL

The accelerometer math model is derived in Appendix A and repeated here, as follows:

$$\begin{aligned}
 \Delta V_C = \Delta \Phi^A \sum_1^N C_k = & \int_{t_0}^{t_N} (a_i)_j dt + \int_{t_0}^{t_N} [A_b + D_1 a_i + D_2 a_i^2 + D_3 a_i^3 \\
 & - C_P a_p + C_{IP} a_i a_p + C_{IO} a_i a_o - MOA a_p' \\
 & + MPA a_o' + Q_{IP} w_p w_i + J_A \dot{w}_o + D_b] dt \\
 & + e_q^A + e_n^A
 \end{aligned} \tag{4-1}$$

where

a_p' = acceleration in direction of ISU body axis to which accelerometer PA is nominally parallel

a_o' = acceleration in direction of ISU body axis to which accelerometer OA is nominally parallel

and in which e_n^A includes the effects of random accelerometer noise (e_{nr}^A) and dynamics of the accelerometer rebalance loop (e_{nreb}^A). The term D_b is the dynamic bias due to the nominal vibration environment. The torque-to-rebalance loop operates in the same fashion as the gyro, as explained in Refs. 1 and 9.

The C_P term in Eq. (4-1), which is proportional to mass unbalance along the accelerometer IA, is indistinguishable from MOA and so it will be dropped. In addition, the Q_{IP} and J_A terms may be deleted since accelerometer outputs are not recorded when the test table is rotating and the rates that do exist (earth rate components) are small. Other error effects considered negligible are:

- rotational cross coupling: $\delta a = \frac{m\ell^2}{K} a_i (w_p^2 - w_i^2 - w_o^2)$
- compliance: $\delta a = T_c(a_i, a_o, a_p)/m\ell$ (not including C_{IP} and C_{IO})
- cross-coupling of accelerations along OA

where $m\ell$ is the pendulosity of the accelerometer and K is the equivalent stiffness of the rebalance loop.

The effect of scale factor error is modeled as a third order polynomial in terms of acceleration along the IA, as shown in Eq. (4-1).

Sign conventions associated with the accelerometer calibration terms are contained in Table 4-2, and Table 4-3 lists numerical values of the calibration terms in Eq. (4-1). Table 4-3 also indicates the calibration terms to be estimated and the associated precision goals.

<u>Calibration Term</u>	<u>Symbol</u>	<u>Sign of Output Acceleration for Positive Value of Calibration Term</u>
Bias	A_b	positive
Compliance	C_{IP}, C_{IO}	same as sign of products of accelerations along (IA) (PA) and (IA) (OA), respectively.
Misalignments	MOA, MPA	opposite to acceleration along nominal PA and same as acceleration along nominal OA, respectively (corresponding to positive rotations of IA about OA and PA, respectively).
Accelerometer Scale Factor Error Coefficients	$\left\{ \begin{array}{l} D_1, D_3 \\ D_2 \end{array} \right.$	<p>same as acceleration along IA</p> <p>positive for either positive or negative acceleration along IA</p>

Table 4-2 Sign Conventions Associated with Accelerometer Calibration Terms

Symbol (1)	Name	Units	Nominal Value ⁽²⁾	Range (max) ⁽³⁾	Est. Prec. Goal (max) ⁽⁴⁾
$\Delta\Phi$	Scale factor (SF)	fps/pulse	.0025	$\pm 10\%$	-
A_b *	Bias	μg	50	± 175	< 25
D_1 *	SF error (SFE)	$\mu g/g$	50		< 25
D_2 *	2nd order SFE	$\mu g/g^2$			TBD
D_3 **	3rd order SFE	$\mu g/g^3$			TBD
C_{IP} **	Vibropendulous Coeff.	$\mu g/g^2$		~ 10	TBD
C_{IO} **	Compliance of pendulous axis	$\mu g/g^2$		~ 10	TBD
MOA*	Misalignment of IA about OA	$\widehat{\text{sec}}$	± 8	± 30	< 5
MPA*	Misalignment of IA about PA	$\widehat{\text{sec}}$	± 8	± 30	< 5

Notes: (1) A single asterisk refers to the basic calibration terms to be estimated. The double asterisk refers to additional terms to be estimated to provide a full calibration.

(2) Value at beginning of calibration run, for a normally operating ISU (average magnitude).

(3) Maximum value at beginning of calibration run, to be used for worst case design purposes.

(4) Maximum values are interpreted as being equivalent to a 3σ value. TBD indicates "to be determined".

Table 4-3 Numerical Tabulation of Accelerometer Calibration Parameters

4.2 GYRO MATH MODELS

The gyro math model was derived in Ref. 1 and is repeated here, as follows:

$$\begin{aligned}
 \Delta\psi_c = \Delta\Phi^G \sum_{k=1}^N C_k = & \int_{t_0}^{t_N} (w_i)_j dt + \int_{t_0}^{t_N} [R_b + B_1 a_i + B_S a_s + B_O a_o + C_{II} a_i^2 \\
 & + C_{SS} a_s^2 + C_{IS} a_i a_s + C_{IO} a_i a_o + C_{OS} a_o a_s \\
 & + Q_{IS} w_i w_s + Q_1 w_i + Q_2 w_i^2 - MOA w_s' \\
 & + MSA w_o' + J_G \dot{w}_o] dt + e_q^G + e_n^G
 \end{aligned}
 \tag{4-2}$$

where

w_s' = inertial rate about ISU body axis to which gyro SA is nominally parallel

w_o' = inertial rate about ISU body axis to which gyro OA is nominally parallel

and in which e_n^G includes the effects of random gyro noise (e_{nr}^G) and dynamics of the gyro gimbal/rebalance loop (e_{nreb}^G). The Q_{IS} and J_G terms may be deleted in the calibration process since they contribute a negligible effect to the gyro output.

The effect of scale factor error is modeled as a second order polynomial in terms of inertial rate about the IA, as shown in Eq. (4-2).

Sign conventions associated with the gyro calibration terms are contained in Table 4-4, and Table 4-5 lists numerical values of the calibration terms in Eq. (4-1). Table 4-5 also indicates the calibration terms to be estimated and the associated precision goals. The math model for internal random gyro drift rate (e_{nr}^G) is contained in Table 4-6 and is the one used in the UNIVAC study* as originally specified in Ref. 7.

* Appendix A (pp. A-8, 9) of Ref. 4

<u>Calibration Term</u>	<u>Symbol</u>	<u>Sign of Output Rate for Positive Value of Calibration Term</u>
Bias	R_b	positive (corresponding to a negative torque on float about OA)
Mass Unbalance	MULA	opposite to sign of acceleration along SA and IA, respectively (corresponding to mass unbalances along positive IA and SA)
	MUSA	
	B_I, B_S, B_O	same as sign of acceleration along IA, SA and OA, respectively
Major Compliance	C_{II}, C_{SS}	positive for positive or negative acceleration along IA and SA, respectively
Cross Compliance	C_{IS}, C_{IO}, C_{OS}	same as sign of products of accelerations along (IA)(SA), (IA)(OA) and (OA)(SA), respectively
Misalignments	MOA, MSA	opposite to rate about nominal SA and same as rate about nominal OA, respectively (corresponding to positive rotations of IA about OA and SA, respectively)
Scale Factor Error Coefficients	Q_1	same as rate about IA
	Q_2	positive for either positive or negative rate about IA

Table 4-4 Sign Conventions Associated with Gyro Calibration Terms

Symbol (1)	Name	Units	Nominal Value (2)	Range (max) (3)	Estimation Precision Goal (max) (4)
$\Delta\Phi$	Scale Factor (SF)	$\widehat{\text{sec}}/\text{pulse}$. 844 (0 to 30°/sec) 1. 688 (30 to 60°/sec)	$\pm 10\%$ $\pm 10\%$	-
R_b *	Bias	°/hr	± 0.100	0.200	< 0.020
Q_1 *	SF error (SFE)	ppm	± 200		< 50
Q_2 *	2nd order SFE	ppm/rad/sec	50		TBD
B_I *	Mass Unbalance along SA	°/hr/g	± 0.300	± 1.5	< 0.020
B_S *	Mass Unbalance along IA	°/hr/g	± 0.300	± 1.5	< 0.020
B_O **	Output axis acceleration sensitivity	°/hr/g	.040		< 0.020
C_{II} **	Compliance Coeff.	°/hr/g ²	.020		< 0.025
C_{SS} **	Compliance Coeff.	°/hr/g ²	.020		< 0.025
MOA *	Misalignment of IA about OA	$\widehat{\text{sec}}$	± 8	± 30	< 5
MSA *	Misalignment of IA about SA	$\widehat{\text{sec}}$	± 8	± 30	< 5
C_{IS} **	Compliance Coeff.	°/hr/g ²			< 0.025
C_{IO} **	Compliance Coeff.	°/hr/g ²			< 0.025
C_{OS} **	Compliance Coeff.	°/hr/g ²			< 0.025

Notes: (1) A single asterisk refers to the basic calibration terms to be estimated. The double asterisk refers to additional terms to be estimated to provide a full calibration.

(2) Value at beginning of calibration run, for a normally operating ISU (average magnitude).

(3) Maximum value at beginning of calibration run, to be used for worst case design purposes.

(4) Maximum values are interpreted as being equivalent to a 3 σ value. TBD indicates "to be determined".

Table 4-5 Numerical Tabulation of Gyro Calibration Parameters

The gyro random drift rate (\dot{e}_{nr}^G) is modeled in terms of power spectral density, as specified in Ref. 7 and Appendix A of Ref. 4.

$f(\text{Hz})$	PSD (\dot{e}_{nr}^G)*, $(\text{deg/hr})^2/\text{Hz}$
0 to $(100 \text{ hrs})^{-1}$	3.02×10^{-2}
$(100 \text{ hrs})^{-1}$ to 10^{-3}	$2.33 \times 10^{-13} f^{-2}$
10^{-3} to 8	2.33×10^{-7}
8 to 24	1×10^{-6}
above 24	$6 \times 10^{-4} f^{-2}$

The rms value of PSD (\dot{e}_{nr}^G) from $f = (14 \times 3600 \text{ sec/cycle})^{-1}$ to ∞ is 5 mdh.

Table 4-6 Gyro Internal Random Drift Rate Math Model

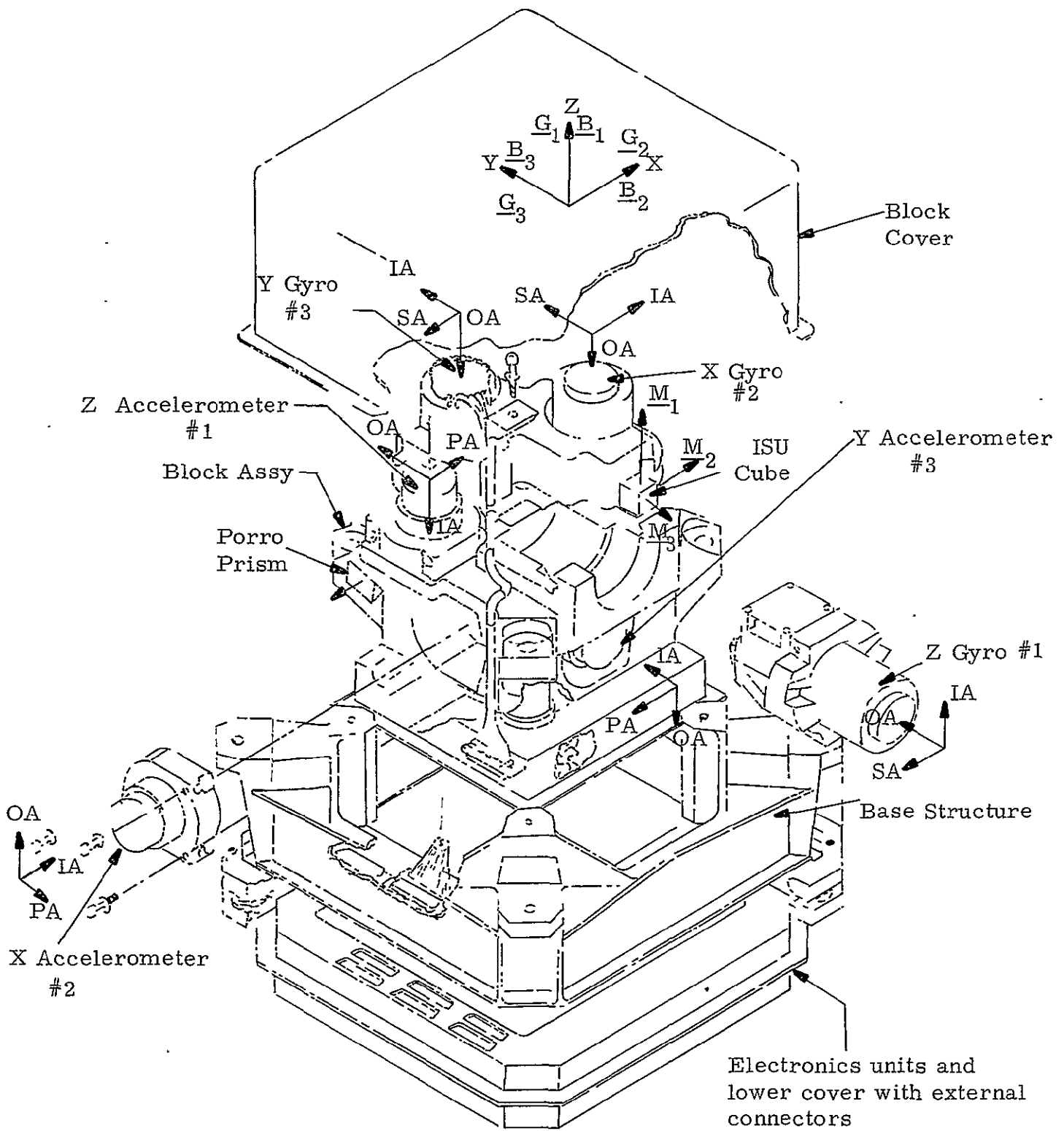
* A plot of the PSD has a large discontinuity at $f = (100 \times 3600 \text{ sec/cycle})^{-1}$; however, the effect of \dot{e}_{nr}^G in the calibration process is small.

5. ISU AND TEST EQUIPMENT CONFIGURATIONS

The configurations of the Inertial Sensing Unit (ISU) and required calibration test equipments are discussed in this section. In order to support subsequent analyses and understand the system operation, considerations are restricted here to geometrical relationships within the major equipments and definition of all necessary coordinate frames. Hardware considerations and functional descriptions are discussed in the next section (6).

The layout of the ISU is defined in [6] and repeated in Fig. 5-1. The change from the ARMA D4E vibrating string accelerometer to the Kearfott 2401 pendulum type of accelerometer is reflected in the figure, primarily as a reversal of the IAs and definition of OAs and PAs. The addition of a porro prism azimuth reference is also shown. In this study, the \underline{M}_2 or \underline{M}_3 faces of the ISU cube will be used as the azimuth reference and it is assumed that the alignment between the cube and the porro prism is determined separately. Note that the normal mounting position of the ISU in the aircraft is with the black cover down such that +z is down, x is forward and y is right.

The ISU cube and inertial sensor relative orientations indicated in Fig. 5-1 are repeated schematically in Fig. 5-2 for clarity, and the entire ISU has been rotated to show its orientation relative to earth coordinates for the zero positions of the Single-Axis Test Stand (SATS) and the Two-Axis Fixture (TAF). Detailed definitions of the coordinate frames



- Notes: (1) When installed in aircraft, Z is down, X is forward and Y is right.
- (2) The Body Axes (B_1, B_2, B_3) are defined by the ISU Cube faces, nominally in the directions of the gyro IAs.
- (3) The Mirror Axes (M_1, M_2, M_3) are defined by the visible surfaces of the ISU Cube.

Figure 5-1 Layout of Strapdown Inertial Sensing Unit (ISU)

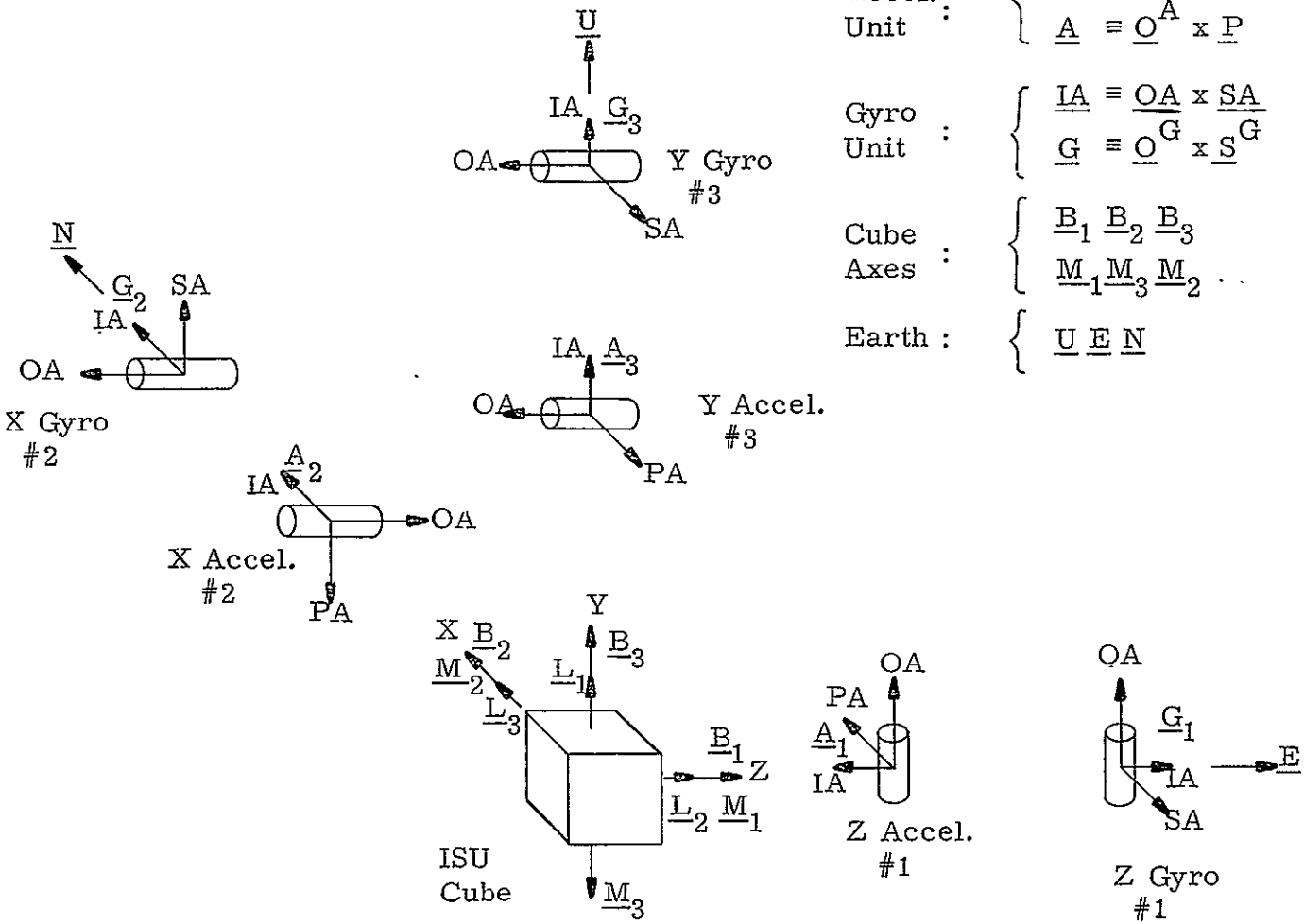
Right-handed Coordinate Frame

Accel. : $\left\{ \begin{array}{l} \underline{IA} \equiv \underline{OA} \times \underline{PA} \\ \underline{A} \equiv \underline{O}^A \times \underline{P} \end{array} \right.$

Gyro : $\left\{ \begin{array}{l} \underline{IA} \equiv \underline{OA} \times \underline{SA} \\ \underline{G} \equiv \underline{O}^G \times \underline{S}^G \end{array} \right.$

Cube Axes : $\left\{ \begin{array}{l} \underline{B}_1 \underline{B}_2 \underline{B}_3 \\ \underline{M}_1 \underline{M}_3 \underline{M}_2 \dots \end{array} \right.$

Earth : $\left\{ \begin{array}{l} \underline{U} \underline{E} \underline{N} \end{array} \right.$

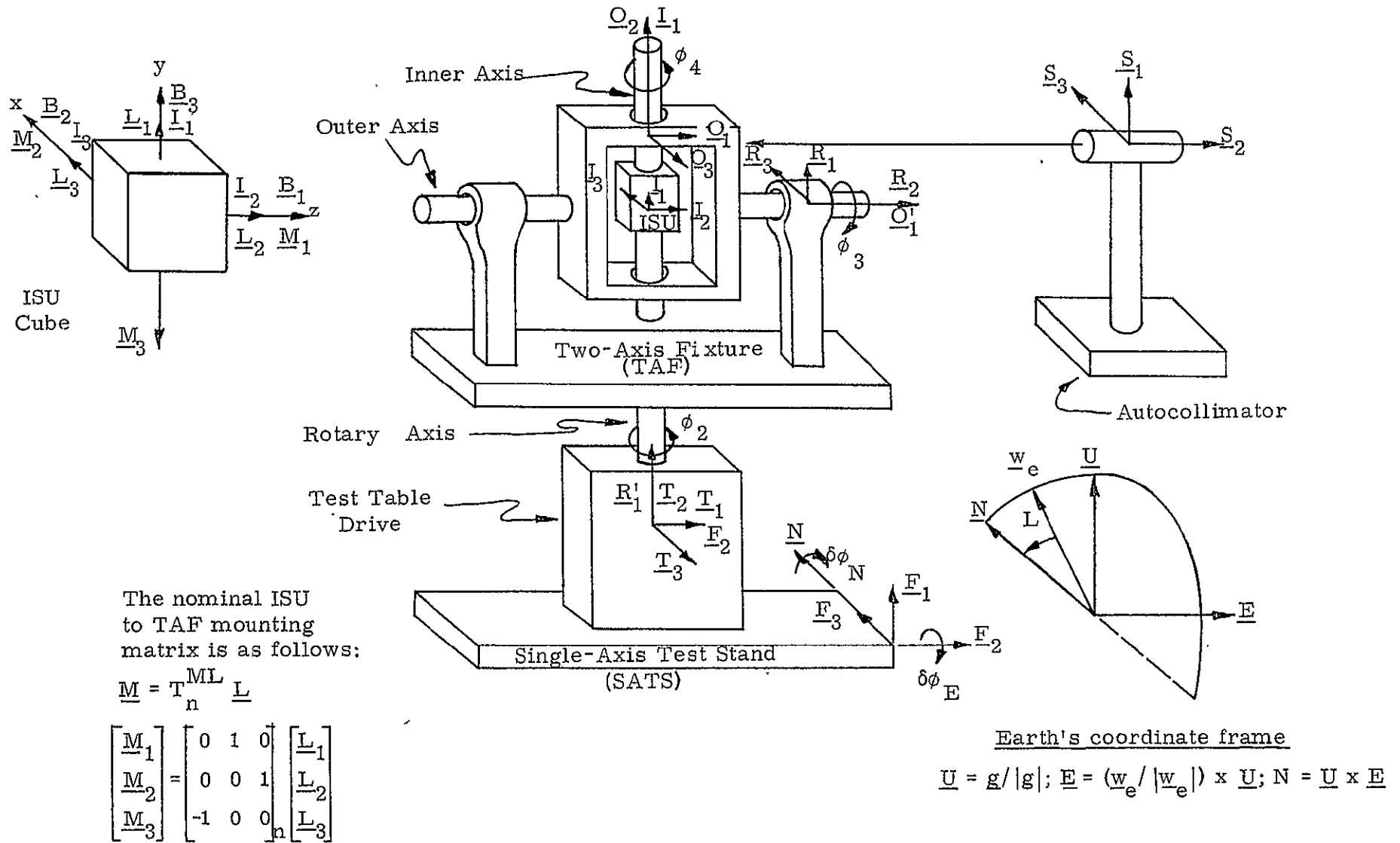


- Notes: (1) The ISU orientation relative to earth coordinates is shown for zero positions of SATS and TAF.
- (2) All coordinate sets are defined by unit vectors.
- (3) The Body Axes ($\underline{B}_1 \underline{B}_2 \underline{B}_3$) are defined by the orthogonal ISU cube faces, nominally in the directions of the gyro IAs (i. e. , $\underline{B}_1 \equiv \underline{M}_1$, $\underline{B}_2 \equiv \underline{M}_2$ and $\underline{B}_3 \equiv -\underline{M}_3$). All other coordinate sets are generally misaligned with respect to each other.
- (4) The nominal orientation of the Bubble Level coordinate frame ($\underline{L}_1 \underline{L}_2 \underline{L}_3$), which is fixed to the TAF inner gimbal, is shown for reference purposes.

Figure 5-2 ISU Cube and Inertial Sensor Orientations for ISU

shown in Fig. 5-2 are contained in Table 5-1. The positive ISU cube (mirror)axes were chosen to correspond to the visible faces of the cube. Except for \underline{M}_3 , the Mirror and Body axes coordinate frames are the same as in the Univac report [3], as are all of the gyro coordinates. The accelerometer system (IA) coordinates are also the same, except for \underline{A}_1 . Finally, the zero position of the ISU has been changed from that used in the Univac study. This was done primarily to facilitate mounting some electronics, along with the ISU, within the TAF.

The configuration of the major alignment equipments associated with the ISU is shown in Fig. 5-3, and Table 5-2 contains detailed definitions of the coordinate frames shown and how they are related. Unit vectors are used to define all coordinate axes. Unlike the Univac study, a test table trunnion axis is not provided, in order to reduce costs. The SATS and TAF are used to support the ISU in various orientations relative to the rotary axis and the Earth's coordinate frame. The autocollimator is used to measure the orientation of the ISU cube relative to vertical, about the \underline{S}_3 axis, and a set of at least three Bubble Levels (BL) are used to represent the inner gimbal axes of the TAF. The ways that these equipments are used is discussed in Sections 6 and 8. The ISU cube is shown in Fig. 5-3 for reference purposes to show the nominal relationships between the various cube and TAF coordinate frames.



- Notes:
- (1) The SATS and TAF are shown in their "zero" positions (i. e., $\phi_2 = \phi_3 = \phi_4 = 0$).
 - (2) The F and Earth's coordinate frames are assumed to be misaligned by $\delta\phi_N$, about \underline{N} .
 - (3) The Bubble Level coordinate frame is nominally defined by the inner gimbal coordinate frame.
 - (4) Nonorthogonalities of axes are indicated by defining the O and R coordinate frames as small rotations of the \underline{O}' and \underline{R}' frames about the \underline{O}'_3 and \underline{R}'_3 axes, respectively.

Inertial Sensing Unit (ISU)

- Mirror (M) $\underline{M}_1 \underline{M}_3 \underline{M}_2$ M is defined by the visible surfaces of the ISU cube and is assumed to be orthogonal and right-handed in the order listed.
- Body Axes (B) $\underline{B}_1 \underline{B}_2 \underline{B}_3$
 $\underline{B}_z \underline{B}_x \underline{B}_y$ B is defined by the ISU cube faces, nominally in the direction of the gyro IAs.
- Gyro System (G) $\underline{G}_1 \underline{G}_2 \underline{G}_3$ The elements of G correspond to the gyro IAs and are generally not orthogonal.
- Gyro Unit (GU) $\underline{G} = \underline{O} \underline{x} \underline{S} \underline{G}$ The gyro right-handed coordinate system is defined relative to the gyro case and is generally not orthogonal.
- Accelerometer System (A) $\underline{A}_1 \underline{A}_3 \underline{A}_2$ The elements of A correspond to the accelerometer IAs and are generally not orthogonal.
- Accelerometer Unit (AU) $\underline{A} = \underline{O} \underline{x} \underline{P}$ The accelerometer right-handed coordinate system is defined relative to the accelerometer case and is generally not orthogonal.

Earth Coordinate Frame

- Earth (E) $\left. \begin{array}{l} \text{(up)} \quad \underline{E}_1 \equiv \underline{U} \equiv (\underline{g} / |\underline{g}|) \\ \text{(East)} \quad \underline{E}_2 \equiv \underline{E} \equiv (\underline{w}_e / |\underline{w}_e|) \times \underline{U} \\ \text{(North)} \quad \underline{E}_3 \equiv \underline{N} \equiv \underline{U} \times \underline{E} \end{array} \right\} \text{E is defined by } \underline{g} \text{ and } \underline{w}_e \text{ as an orthogonal right-handed coordinate system.}$

Table 5-1 Definitions of ISU and Earth Coordinate Frames

All coordinate frames are defined by a triad of unit vectors, unless specified otherwise.

Optical Alignment Coordinate Frame

- Autocollimator (S) $\underline{S}_1 \equiv \underline{g} / |\underline{g}|$ $\underline{S}_2 \equiv$ line of sight $\underline{S}_3 \equiv \underline{S}_1 \times \underline{S}_2$ S is defined by \underline{g} and the optical line of sight.

Single-Axis Test Stand (SATS)

- SATS Frame (F) $\underline{F}_1 \underline{F}_2 \underline{F}_3$ F is fixed to the frame of the SATS
- Test Table (T) $\underline{T}_1 \underline{T}_2 \underline{T}_3$ T defines the rotary axis, but does not rotate.
- Rotary Frame' (R') $\underline{R}'_1 \underline{R}'_2 \underline{R}'_3$ R contains the rotary axis and rotates the test table

Two-Axis Fixture (TAF)

- Rotary frame (R) $\underline{R}_1 \underline{R}_2 \underline{R}_3$ R defines the outer gimbal axis and is misaligned with R' by MR_3' , about R_3' . $R = R'$ for $MR_3' = 0$ and does not rotate with the outer gimbal
- Outer Gimbal' (O') $\underline{O}'_1 \underline{O}'_2 \underline{O}'_3$ O' contains the outer gimbal axis and rotates with the outer gimbal
- Outer Gimbal (O) $\underline{O}_1 \underline{O}_2 \underline{O}_3$ O defines the inner gimbal axis and is misaligned with O' by MO_3' , about O_3' . $O = O'$ for $MO_3' = \text{zero}$ and does not rotate with the inner gimbal.
- Inner Gimbal (I) $\underline{I}_1 \underline{I}_2 \underline{I}_3$ I contains the inner gimbal axis and rotates with the inner gimbal
- Bubble Level (L) $\underline{L}_1 \underline{L}_2 \underline{L}_3$ A unit vector in the L frame is defined by the line through the ends of the level indication marks that points in the same nominal direction as the corresponding inner gimbal unit vector (see diagram). Elements of L are generally not orthogonal.

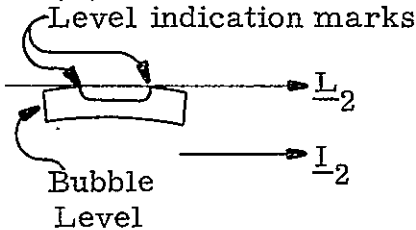


Table 5-2 Definitions of Test Equipment Coordinate Frames.

6. DESCRIPTION OF SYSTEM AND TEST EQUIPMENT REQUIREMENTS

The purpose of this section is to describe the total calibration system from the equipment viewpoint, considering both functional and performance requirements.

Not only will this help to understand the calibration process, but it is the means by which the key test equipment requirements will be established. After a brief description of the system, the following major test equipments are considered separately:

- Single-Axis Test Stand (SATS)
- Two-Axis Fixture (TAF)
- Optical Alignment Equipment
- Data Collection System
- Data Processing System

In conjunction with specifying the calibration procedure and the data processing equations, the error analysis of Section 10 and the test equipment requirements of this section were developed simultaneously in an attempt to achieve a balanced design. As mentioned earlier, however, the design described here is considered to be an initial or interim one, particularly in the area of the pre-calibration alignment equipments. In addition, the data collection system was not considered in detail in this study since no significant problems were anticipated. Instead, emphasis was placed upon determining procedures, estimation algorithms, expected accuracy,

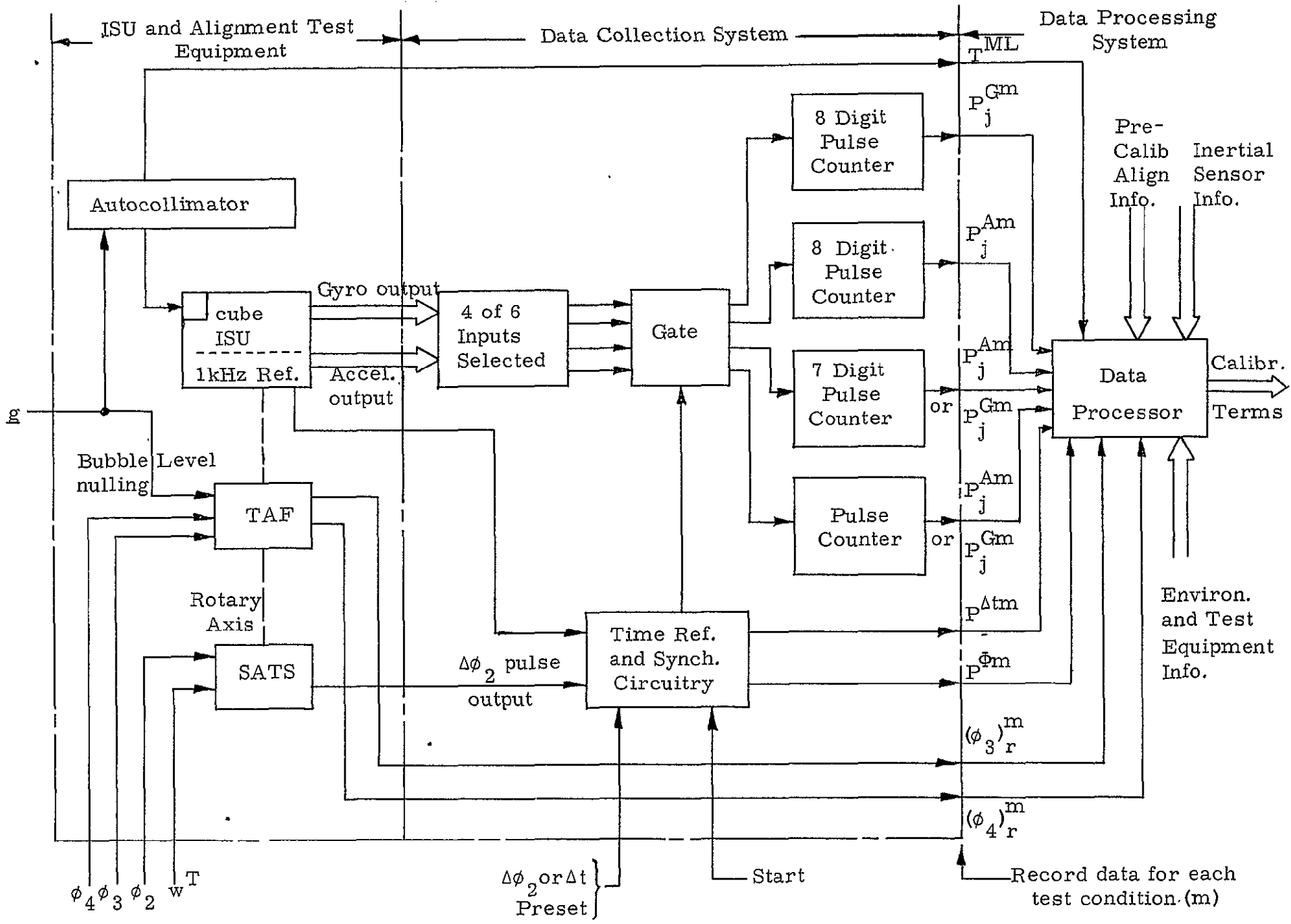
and requirements of the critical test equipments. The performance requirements specified herein therefore should be considered preliminary.

6.1 DESCRIPTION OF SYSTEM

A brief functional description of the major system equipments and their interrelationships is contained in this section. There are three primary functions performed by the equipments provided within the calibration system, as indicated in the functional schematic of Fig. 6-1. The first is the ISU support and alignment function. The second is the data collection (and recording) function, and the third is the function of processing the data obtained to determine the required calibration terms. Each of these functions is described next.

The ISU support and alignment function is provided by the Single-Axis Test Stand (SATS), Two-Axis Fixture (TAF) and an Autocollimator. The ISU to be calibrated is mounted within the TAF, which in turn is supported by the SATS. The geometry of the assembly is illustrated schematically in Fig. 5-3, and Fig. 5-1 is an illustration of the ISU. The autocollimator is referenced to the vertical (indicated by \underline{g} in Fig. 6-1) and with the bubble levels on the inner gimbal of the TAF nulled at three different orientations of the ISU, the transformation matrix between the ISU cube (mirror coordinates) and bubble levels (T^{ML}) is measured and recorded. The various orientations of the ISU are achieved by adjusting the TAF inner and outer gimbals about their respective axes and by rotating the entire TAF about the SATS rotary axis, which is nominally vertical.

Figure 6-1 Functional Schematic of Calibration System
6-3



Notes: (1) Not shown are power supplies, ISU electrical support equipment or all equipments required to install the Single-Axis Test Stand (SATS) and initially align and calibrate the Two-Axis Fixture (TAF).

Continuous precise readouts of the TAF inner and outer gimbal angles (ϕ_4 and ϕ_3) are provided. The test stand is also capable of driving the TAF and ISU at a rate (w^T) about the rotary axis and full revolutions of the test table are indicated by a pulse output. Before each run, the ISU is nominally oriented in the desired position and the Bubble Levels nulled by adjusting ϕ_3 and/or ϕ_4 . The gimbal angles obtained are labeled (ϕ_{3r}) and (ϕ_{4r}) and are recorded. Next, the gimbals are readjusted to indicate (ϕ_{3z}) and (ϕ_{4z}), which are equal to the nominal values desired plus the small corrections determined when the test equipment was originally zeroed.

The next major part of the calibration system is the Data Collection System. In order to minimize the cost of test equipment, only four pulse counters are provided to count the number of pulses generated within the ISU accelerometer and gyro rebalance loops. It is therefore necessary to select the inertial sensor outputs, as shown in Fig. 6-1. A timing reference is used to control the start and stop times over which pulses are counted, and it indicates the corresponding elapsed time. It is synchronized with the 1k Hz reference in the ISU such that counts are started and ended only for full cycles and when the 1kHz reference is zero. Initiation of the counts is controlled by one of two independent variables which must be pre-selected. When the table is non-rotating, time is selected as the independent variable and when the start command is given, pulse counting is initiated as soon as the next full 1k Hz cycle is started, as described above. Counting continues until the elapsed time is equal to a value preset into the time reference. The actual stop time is determined as explained above. When the table is rotating, test table angle (ϕ_2) is selected as the

independent variable. The SATS is designed to provide a pulse for each full revolution of the test table. The first table pulse to be received after the start command is given is used to initiate pulse counting as soon as the next full 1kHz cycle is started, as described above. Counting continues until the number of table pulses received is equal to a value preset into the timing reference. The actual stop time corresponds to the end of the full 1kHz cycle in progress at the time the table pulse is received.

As stated in the ground rules initially established for this study, data recording and processing is to be done manually. Therefore, pulse counts from the gyros and accelerometers (P^G and P^A) and the timing reference ($P^{\Delta tm}$ and $P^{\Phi m}$) are read from the counters and recorded after each run (m) for the particular inertial sensors (j) selected. Data processing is performed manually using a desk calculator. However, this ground rule is currently under review and more automatic data processing (and possibly data collection) may be adopted. Use of the ISU flight computer is being considered since it would provide many desirable features.

6.2 SINGLE-AXIS TEST STAND (SATS)

The SATS must be capable of supporting the weight of the ISU and TAF, and yet retain definition of its rotary axis within several arc seconds (1σ). This is only a requirement for $w^T = \pm 2^\circ/\text{sec}$ and when $w^T = 0$, since the alignment between the bubble level coordinate frame and the rotary axis must be measured. Leveling screws are required to adjust the rotary axis with respect to the local vertical with a sensitivity of approximately $.2 \widehat{\text{min}}$.

The table rate drive must be adjustable and accurate to .5% and respond to changes in rate and stabilize within about .5 minute. The nonuniformity of the table rate (NUWT) must be such that

$$\text{NUWT} = 15 \int_0^{360^\circ/w^T} \sin(w^T t + \phi) dt \quad (\text{for } w^T \text{ in deg/sec}) \quad (6-1)$$

is less than $4.3 \widehat{\text{sec}} (1\sigma)$ (per revolution of the table) for $w^T = \pm 2^\circ/\text{sec}$ and any given value of ϕ . Assuming a maximum positive rate error over half a revolution and a maximum negative rate error over the other half, the percentage of maximum rate error to $w^T = 2^\circ/\text{sec}$ is .25%. These values are to be considered maximum permissible values and it would be very desirable to reduce them by a factor of 4 or more (see the error analysis in Section 10.5).

The test table pulse output that indicates full table rotations should be repeatable within $6 \widehat{\text{sec}} (1\sigma)$ as a maximum permissible value. A 1 to 2 $\widehat{\text{sec}}$ error would be desirable, particularly for the higher table rates for which a sufficient number of table revolutions can be achieved in a shorter time, thereby reducing the test time.

The test stand should also be provided with a means to repeatably position the test table within approximately $.5 \widehat{\text{min}}$ about the rotary axis, at a zero position determined during initial installation. It would also be useful to provide table angle indicators every 180° or better yet 90° in order to speed up the process of setting the table rate, particularly for $w^T = \pm 1, 2$ and $4^\circ/\text{sec}$. To achieve .5%, the angle indications would need be accurate only to approximately .5%.

Slip rings must be provided to provide power to the ISU and signal outputs to the support equipment.

6.3 TWO-AXIS FIXTURE (TAF)

The TAF is required to provide to the operator precise readouts of the inner and outer gimbal angles (ϕ_4 and ϕ_3 , respectively) to an accuracy of several arc seconds (1σ). Each readout is only required within approximately $\pm 2 \widehat{\text{min}}$ of the cardinal and intercardinal values and may be of any convenient form (electrical, mechanical scales, optical, etc.), consistent with rapid readout. In addition, the gimbals must be adjustable and capable of being damped quickly and secured within the accuracy requirement.

The inner gimbal shall permanently support 3 to 4 bubble levels mounted in an orthogonal fashion so as to represent the inner gimbal coordinate frame (see Fig. 5-3 and Table 5-2) within an accuracy of approximately $1 \widehat{\text{min}}$. The directions of the tops of the vials are to be defined, as well as the need for the fourth bubble level. The repeatability of nulling the bubbles shall be no worse than $1 \widehat{\text{sec}} (1\sigma)$. Whenever any bubble level is in a position that it could be nulled, there shall be a clear view of the bubble.

The inner gimbal to outer gimbal nonorthogonality should be less than several arc seconds. However, it is possible to accommodate much larger misalignments (up to approximately $20 \widehat{\text{sec}}$.) and compensate the

measured data for the resulting effects. A similar condition applies to the outer gimbal to table rotary axis nonorthogonality.

The gimbal axes must remain defined and stable within the above accuracy requirements, which implies that the entire gimbal structure must remain stable. Also implied by this is the requirement that mounting and bolting down an ISU in the TAF does not distort the bubble level coordinate frame relative to the inner gimbal and rotary axis coordinate frames. ISU mounting repeatability shall be better than $6 \widehat{\text{min}}$ (max) and the misalignment between the ISU mounting surface and inner gimbal coordinate frame should be less than $6 \widehat{\text{min}}$ (max).

The TAF structure shall not obstruct a nominally horizontal line of sight between an externally mounted autocollimator and the ISU cube normals that are nominally horizontal, for any of the cardinal or intercardinal values of ϕ_3 and/or ϕ_4 . Means shall be provided for aligning the outer gimbal axis optically with true East, within an accuracy of approximately $20 \widehat{\text{sec}}$ (1σ), by adjusting the test table angle (ϕ_2).

6.4 OPTICAL ALIGNMENT EQUIPMENT

The autocollimator shall be capable of measuring the angle in the nominally vertical plane between horizontal and a normal to the ISU cube face that is nominally horizontal, over a range of $\pm 20 \widehat{\text{min}}$. The alignment accuracy to horizontal shall be within $1 \widehat{\text{sec}}$ (1σ) and the instrument readout accuracy shall be within $1 \widehat{\text{sec}}$ (1σ). Operability shall be sufficient to allow accurate measurements to be made within approximately 6 minutes.

6.5 DATA COLLECTION SYSTEM

The primary performance requirement of the Data Collection System is to measure the elapsed time (Δt) of each run within an accuracy of $100 \mu \text{sec}$ (1σ), and preferably 10 to $20 \mu \text{sec}$, in order to reduce the calibration time at the higher rates. Furthermore, pulses are to be counted at the maximum rate of 128 k Hz for the gyros and 256 k Hz for the accelerometers. The timing requirements when the table rate w^T is to be determined are somewhat more involved due to the delay between the time a table pulse is received and a full 1 k Hz cycle starts. This delay can be as large as 1 millisecond, which is unacceptable for estimation of the scale factor error terms. A possible solution to the problem is to measure and indicate the delays both at the start and stop of pulse counting and compute the average table rate separately using a different Δt than for the gyro pulse count.

For the cases when the inertial sensor IAs are up (or down), a large number of pulses will be generated. For $w^T = 60^\circ/\text{sec}$, the total gyro count after 6 minutes of running* will be approximately 46×10^6 . Therefore, an 8 digit counter is required. For the accelerometer, the total count after 10 minutes* will be approximately 15.4×10^6 and a 8 digit counter should be adequate. When the IAs are both at 45° to the horizontal, the maximum counts will require two, 7 digit counters to be used. The fourth counter may have a greatly reduced range since the input rates and accelerations are considerably smaller.

* as specified in the operational procedure (Section 8)

7. DEVELOPMENT OF CALIBRATION EQUATIONS

The purpose of this section is to apply the accelerometer and gyro math models presented above (in Section 4) to the ISU assembly, as supported by the Two-Axis Fixture (TAF) and the Single-Axis Test Stand (SATS). The linear accelerations and angular motions imposed upon each of the inertial sensors are related to the gravitational attraction of the earth and the rotation of the SATS and the earth in terms of the SATS and TAF relative orientations. Various positions (m) of the ISU are chosen as discussed in the next section (8), and the resulting equations are then simplified by deleting terms that contribute negligible effects. Both the gyro and accelerometer equations are arranged in the following form:

$$M_j^m / \Delta t^m \equiv \dot{M}_j^m = \underline{H}_j^m \cdot \underline{Y}_j + \delta \dot{M}_j^m \quad (7-1)$$

where superscript m refers to a particular ISU test condition (orientation), j to a particular inertial sensor, and

M_j^m \equiv adjusted measurement inertial sensor
i for run m.

$\Delta t^m = t_N - t_o$ \equiv time over which measurement M is
obtained, for run m

\dot{M}_j^m \equiv average rate of M over time Δt

\underline{Y}_j \equiv column vector of calibration terms for
instrument j (defined below).

\underline{H}_j^m \equiv row vector of coefficients that relate \underline{Y}_j to \dot{M}_j^m
for a given run m and instrument j

$\delta \dot{M}_j^m$ \equiv error in measurement \dot{M}_j^m

The measurement M_j is the indicated change in the output of inertial sensor j over the time Δt , corrected (or adjusted) for known and significant inputs (such as earth rate and/or table rate and/or gravity). Errors in the measurement and correction process, as well as neglected terms, constitute $\delta \dot{M}_j^m$. Therefore, since $\underline{H}_j^m \cdot \underline{Y}_j$ represents the effect of the terms to be calibrated, Eq. (7-1) can be used as a basis for estimating the calibration terms, as described below, by neglecting $\delta \dot{M}_j^m$.

In essence, $\underline{H}_j^m \cdot \underline{Y}_j$ is a linear combination of the various calibration terms to be estimated. Different combinations are obtained by changing the test conditions (m) - (viz, table rate and ISU orientation). When the number of linearly independent combinations (or measurements M) is equal to or greater than the number of calibration terms (unknowns), sufficient information is available to solve the set of equations*, thereby making estimates of the various calibration terms. The accuracy with which this can be done is a function of the $\delta \dot{M}_j^m$ terms and the coefficients that constitute the solution to the equations. Section 10 contains a detailed error analysis using Eq. (7-1) as a starting point.

In the case of the scale factor coefficients, Eq. (7-1) is used only to estimate the effect of various scale factor error terms. A separate regression equation is used to estimate the particular terms in order to simplify the estimation processes, while simultaneously providing flexibility in the magnitude and number of instrument input rates and accelerations

* Assuming no a priori, statistical information concerning the calibration terms and/or error sources is available.

that can be included in the regression analysis. This is discussed further in Section 7.3 below.

7.1 ACCELEROMETER EQUATIONS

In the calibration test procedure presented in Section 8 it will be noted that the accelerometers are always oriented in one of these general positions (viz., IA vertical, IA horizontal (with either OA or PA nominally vertical or at 45° to the vertical) or IA at 45° to the vertical (with either OA or PA nominally horizontal). The effect of the calibration terms on the outputs of the accelerometers for each of these three positions are determined from Eq. (4-1) as follows:

For IA Vertical

$$\Delta\Phi_j^A P_j^{Am} = \int_{t_0}^{t_N} (a_{ij})_j^m dt + \Delta t^m \{ \delta V_c^{+1}, \delta V_c^{-1} \}^m + e_j^{Am} \quad (7-2)$$

where

$$\begin{aligned} \int_{t_0}^{t_N} (a_{ij})_j^m dt &\equiv \text{integral of specific forces sensed by} \\ &\quad \text{accelerometer } j \text{ for test condition } m \\ &\equiv \Delta t^m (\underline{A}_j \cdot \underline{U})_n^m \end{aligned} \quad (7-3)$$

$$\begin{aligned} P_j^{Am} &\equiv \text{pulse count out of accelerometer } j \text{ for test} \\ &\quad \text{condition } m \\ &= \sum_k C_k \end{aligned} \quad (7-4)$$

e_j^{Am} \equiv all accelerometer j errors in position m, other than those shown

and $\delta \dot{V}_c^{+1}$ and $\delta \dot{V}_c^{-1}$ are the average acceleration errors due to scale factor errors when the IA is up and down, respectively. It will be noted that the accelerometer bias (A_b) is included in $\delta \dot{V}_c^{+1}$ and $\delta \dot{V}_c^{-1}$, for two reasons. First, it was learned in the development of the estimation equations (in Section 9) that more accurate estimates of the other calibration terms would result by doing this. Second, the $\delta \dot{V}_c$ terms when estimated in this form can be used directly in the regression analysis described below (Section 7.3) for estimating the various scale factor error terms. Only the nominal value of the dot product term will be used, as identified by the subscript n. Errors due to this assumption are defined as part of e_j^{Am} and are considered in the error analysis.

For IA horizontal

$$\Delta \Phi_j^{AP} = \int_{t_0}^{t_N} (a_{ij}^m)^m dt + \Delta t^m [A_b^i + \{ -NOA(\underline{P}_j \cdot \underline{g})_n^m + NPA(\underline{O}_j^A \cdot \underline{g})_n^m \}]_j + e_j^{Am} \quad (7-5)$$

where $\int_{t_0}^{t_N} (a_{ij}^m)^m dt = 0$

$A_b^i \equiv$ accelerometer bias as modeled in accelerometer calibration equation

and NOA and NPA are the nonorthogonalities with respect to Vertical of the IA about OA and PA respectively. Note that

$(\underline{P}_j \cdot \underline{g})_n^m$ is nominally equal to g when the PA is nominally vertical, and to $g/\sqrt{2}$ when PA is nominally 45° from the vertical. Also the product $\text{NOA}(\underline{P}_j \cdot \underline{g})_n^m$ is of second order when PA is nominally horizontal, and in this case it is neglected. Similar reasoning applies to the term $\text{NPA}(\underline{O}_j^A \cdot \underline{g})_n^m$.

For IA at 45° to the Vertical

$$\begin{aligned} \Delta \Phi_j^A P_j^{Am} &= \int_{t_0}^{t_N} (a_{ij})_j^m dt + \Delta t^m \{ -\text{NOA}(\underline{P}_j \cdot \underline{g})_n^m + \text{NPA}(\underline{O}_j^A \cdot \underline{g})_n^m \} \\ &+ \{ C_{IP}(\underline{A}_j \cdot \underline{g})_n^m (\underline{P}_j \cdot \underline{g})_n^m, C_{IO}(\underline{A}_j \cdot \underline{g})_n^m (\underline{O}_j^A \cdot \underline{g})_n^m \}_j \\ &+ \{ \delta \dot{V}_c^{+.7}, \delta \dot{V}_c^{-.7} \}_j + e_j^{Am} \end{aligned} \quad (7-6)$$

where $\int_{t_0}^{t_N} (a_{ij})_j^m dt = \Delta t^m (\underline{A}_j \cdot \underline{g})_n^m$

and $\delta \dot{V}_c^{+.7}$ and $\delta \dot{V}_c^{-.7}$ are the effects of scale factor error when the IA is 45° above and below horizontal, respectively (in which case $|\underline{A}_j \cdot \underline{g}|_n = .707g$). As in the case for the IA vertical, A_b is included in $\delta \dot{V}_c^{+.7}$ and $\delta \dot{V}_c^{-.7}$. Since Eq. (7-6) applies only for the IA at 45° to vertical and either \underline{P} or \underline{O}^A horizontal, one of the two complacance terms (C_{IP}, C_{IO}) can always be neglected. Again, nominal values of the dot product terms will be used, as identified by the subscript n .

The above accelerometer calibration equations (7-2, 7-5 and 7-6) may be combined into a general form, consistent with that of Eq. (7-1), as follows:

$$\dot{M}_j^m = \underline{H}_j^{Am} \cdot \underline{Y}_j + \delta \dot{M}_j^m \quad (7-1)$$

where

$$\dot{M}_j^m = \Delta \Phi_j^A (P_j^A / \Delta t)^m - g(\underline{A}_j \cdot \underline{U})_n^m \quad (7-7)$$

$$\underline{Y}_j = [A_b^T \mid (-NOA)g \mid (NPA)g \mid \delta \dot{V}_c^{+1} \mid \delta \dot{V}_c^{-1} \mid \delta \dot{V}_c^{+.7} \mid \delta \dot{V}_c^{-.7} \mid C_{IP}g^2 \mid C_{IO}g^2]^T_j \quad (7-8)$$

$$\underline{H}_j^A = [(0)* \mid (P_j \cdot \underline{U})_n \mid (O_j^A \cdot \underline{U})_n \mid (1)* \mid (-1)* \mid (+.707)* \mid (-.707)* \mid \\ (\underline{A}_j \cdot \underline{U})_n \mid (P_j \cdot \underline{U})_n \mid (\underline{A}_j \cdot \underline{U})_n \mid (O_j^A \cdot \underline{U})_n]^m_j \quad (7-9)$$

and the asterisk (*) indicates those elements of the row matrix are plus unity only for the cases when $(\underline{A}_j \cdot \underline{U})_n =$ the value shown in parentheses. In all other cases the elements are zero. As before, nominal values of the dot product terms (as identified by the subscript n) are used and the second order effects due to this assumption are defined as part of $\delta \dot{M}_j^m$. The term $\delta \dot{M}_j^m$ is considered in the accelerometer error analysis (Section 10.4).

Appendix B includes a complete tabulation of the basic calibration equations for each of the accelerometers in each of the orientations

specified in the calibration test procedure (Section 8). These equations are used as a basis for deriving the accelerometer estimation equations in Section 9.

7.2 GYRO EQUATIONS

As is the case with the accelerometers, the gyros are always oriented in one of three general positions. These are described in Section 8 and correspond to the gyro IA parallel to the test table rotary axis, IA normal to the table axis, or IA at 45° to the vertical (with either OA or SA nominally horizontal). As described earlier, the test table axis is nominally vertical and additional inputs are introduced to the gyros during calibration runs by rotating the table at a rate w^T .

The effect of the calibration terms on the outputs of the gyros for each of the three general positions are determined from Eq. (4-2), as follows:

For IA parallel to table axis (and nominally vertical)

$$\Delta\Phi_j^G P_j^{Gm} = \int_{t_0}^{t_N} (w_i)_j^m dt + \Delta t^m [R_b^m + B_1(G_j \cdot g)_n^m + C_{II} g^2 + \{\delta\psi_c^+, \delta\psi_c^-\}^m]_j^m e_j^{Gm} \quad (7-10)$$

where

$$\int_{t_0}^{t_N} (w_i)_j^m dt \equiv \text{integral of significant rate inputs to gyro } j, \text{ with respect to inertial space, for test condition } m$$

$$= \Delta\phi_2^m (\underline{G}_j \cdot \underline{R}'_1)_n^m + \Delta t^m w_e \sin L (\underline{G}_j \cdot \underline{U})_n^m \quad (7-11)$$

$$P_j^{Gm} \equiv \text{pulse count out of gyro } j \text{ for test condition } m$$

$$= \sum_k^N C_k \quad (7-12)$$

$$\Delta\phi_2^m \equiv \text{change in table angle } \phi_2 \text{ over time } \Delta t^m$$

$$e_j^{Gm} \equiv \text{all gyro } j \text{ errors for test condition } m, \text{ other than those shown}$$

$$R'_b \equiv \text{gyro bias, as modelled in gyro calibration equations}$$

and $\dot{\delta\psi}_c^+$ and $\dot{\delta\psi}_c^-$ are the gyro rate errors due to scale factor errors when the IA is parallel to the table axis and when the table rate (w^T) is plus and minus, respectively. The effect of scale factor error when $w^T = 0$ is assumed small* and is considered as an error source. Because of the way these terms are measured and processed, the term R'_b is considered separately (unlike the case with the accelerometer in which A_b is included as part of $\dot{\delta V}_c^{+1}$, $\dot{\delta V}_c^{+.7}$, etc.) A detailed discussion of this is included in the calibration test procedure development considerations (Section 8.1). As in the case of the accelerometers, only nominal

* It is assumed that gyros available for field use have been previously calibrated to a point that when $w^T = 0$, the effect of earth rate inputs times the scale factor error at such relatively small inputs is negligible.

8.1). The integral of the second term can be significant and so it cannot be defined as part of the error e_j^{Gm} . For $w^T = 0$, both terms can be significant and so actual values of these dot products must be used instead of nominal values. Only nominal values of the other dot product terms, as identified by the subscript n, will be used. It will also be noted that substituting Eqs. (7-17 and 7-18) into Eq. (7-13) results in coefficients of NOA and NSA equal to $-\Delta\phi \frac{m}{2} (\underline{S}_j^G \cdot \underline{R}'_1)_n^m$ and $\Delta\phi \frac{m}{2} (\underline{O}_j^G \cdot \underline{R}'_1)_n^m$, respectively.

For IA at 45° to the Vertical (and $w^T = 0$)

$$\begin{aligned} \Delta\Phi_j^G P_j^{Gm} = & \int_{t_o}^{t_N} (w_{ij})^m dt + \Delta t^m [R'_b + B_I a_j^m + B_S a_s^m + B_O a_o^m + C_{II} (a_i^m) \exp 2 \\ & + C_{SS} (a_s^m) \exp 2 + C_{IS} a_i^m a_s^m + C_{IO} a_i^m a_o^m + C_{OS} a_o^m a_s^m] + e_j^{Gm} \end{aligned} \quad (7-20)$$

where

$$\int_{t_o}^{t_N} (w_{ij})^m dt = \Delta t^m w_e [(\underline{G}_j \cdot \underline{U})^m \sin L + (\underline{G}_j \cdot \underline{N})^m \cos L] \quad (7-21)$$

$$a_i^m = g(\underline{G}_j \cdot \underline{U})_n^m \quad (7-22)$$

$$a_s^m = g(\underline{S}_j^G \cdot \underline{U})_n^m \quad (7-23)$$

$$a_o^m = g(\underline{O}_j^G \cdot \underline{U})_n^m \quad (7-24)$$

As in the case for the IA normal to the table axis, the actual values of the dot products in Eq. (7-19) must be used, whereas only nominal values will be used for the other dot product terms, as identified by the subscript n.

The above gyro calibration equations (7-10, 7-13 and 7-18) may be combined into a general form, consistent with that of Eq. (7-1), as follows:

$$\dot{M}_j^m = \underline{H}_j^{Gm} \cdot \underline{Y}_j + \delta \dot{M}_j^m \quad (7-1)$$

where

$$\dot{M}_j^m = \begin{cases} [\Delta\Phi_j^G P_j^G - \Delta\phi_2^m (\underline{G}_j \cdot \underline{R}'_1)_n^m] / \Delta t^m - w_e (\underline{G}_j \cdot \underline{R}'_1)_*^m \sin L & \text{for } w^T \neq 0 \\ \Delta\Phi_j^G (P_j / \Delta t)^m - w_e [(\underline{G}_j \cdot \underline{R}'_1)_*^m \sin L + (\underline{G}_j \cdot \underline{N})_*^m \cos L] & \text{for } w^T = 0 \end{cases} \quad (7-25)$$

$$(7-26)$$

* = the subscript n for IA nominally vertical. For IA level or at 45°, the actual value of the product is used.

$$\underline{Y}_j = [R_b \mid gB_I \mid gB_S \mid gB_O \mid g^2 C_{II} \mid g^2 C_{SS} \mid g^2 C_{IS} \mid g^2 C_{IO} \mid g^2 C_{OS} \mid w^T \mid \text{NOA} \mid \mid w^T \mid \text{NSA} \mid \delta\psi_c^+ \mid \delta\psi_c^- \mid]_j^T \quad (7-27)$$

$$\underline{H}_j^{Gm} = [1 \mid (\underline{G}_j \cdot \underline{U})_m \mid (\underline{S}_j^G \cdot \underline{U})_n \mid (\underline{O}_j^G \cdot \underline{U})_n \mid (\underline{G}_j \cdot \underline{U})_n \exp 2 \mid (\underline{S}_j^G \cdot \underline{U})_n \exp 2 \mid \mid (\underline{G}_j \cdot \underline{U})_n \mid (\underline{S}_j^G \cdot \underline{U})_n \mid (\underline{G}_j \cdot \underline{U})_n \mid (\underline{O}_j^G \cdot \underline{U})_n \mid (\underline{O}_j^G \cdot \underline{U})_n \mid (\underline{S}_j^G \cdot \underline{U})_n \mid \mid -K_1 (\underline{S}_j^G \cdot \underline{R}'_1)_n \mid K_1 (\underline{O}_j^G \cdot \underline{R}'_1)_n \mid (1)** \mid (-1)** \mid]^m \quad (7-28)$$

**indicates elements = unity only for case when $(\underline{G}_j \cdot \underline{R}'_1)_n$ = the value shown in parentheses. Otherwise, elements = zero.

$$K_1 = \begin{cases} 0 & \text{for } w^T = 0 \\ +1 & \text{for } w^T = \text{plus} \\ -1 & \text{for } w^T = \text{minus} \end{cases} \quad (7-29)$$

The second order effects due to using nominal values of the dot product terms, identified by the subscript n, are defined as part of $\delta \dot{M}_j^m$. The term $\delta \dot{M}_j^m$ is considered in the gyro error analysis (Section 10.5).

Appendix B includes a complete tabulation of the basic calibration equations for each of the gyros in each of the orientations specified in the calibration test procedure (Section 8). These equations are used as a basis for deriving the gyro estimation equations in Section 9.

7.3 SCALE FACTOR ERROR COEFFICIENT EQUATIONS

In Section 4, the errors of the accelerometer and gyro outputs that are functions of the respective inputs were modeled as polynomials of the following form:

$$\delta \dot{V}_c = A_b + D_1 a_i + D_2 a_i^2 + D_3 a_i^3 \quad (\text{for each accelerometer } j) \quad (7-30)$$

$$\delta \dot{\psi}_c = R_b + Q_1 w_i + Q_2 w_i^2 \quad (\text{for each gyro } j) \quad (7-31)$$

where

$\delta \dot{V}_c \equiv$ error in indicated acceleration from accelerometer,
due to scale factor errors

$\delta \dot{\psi}_c \equiv$ error in indicated rate from gyro due to scale factor errors

$a_i \equiv$ acceleration input to accelerometer

$w_i \equiv$ rate input to gyro

and A_b and R_b are the accelerometer and gyro biases defined as constants in the scale factor error equations. The distinction between A'_b and R'_b and A_b and R_b is discussed later in this section. The A, R, D and Q coefficients are to be estimated for each inertial sensor j as part of the ISU calibration process. Although the coefficients could be included as part of the accelerometer and gyro calibration equations derived above, considerable flexibility and some improvement in accuracy is realized by using Eqs. (7-30 and 7-31). This will be demonstrated as the theory is developed below.

Assuming no a priori knowledge re: the expected values of the coefficients, at least as many pairs of input/output measurements as terms to be estimated are required to realize a solution. This is done by defining the following regression equations, based on Eqs. (7-30 and 7-31):

$$\hat{(\delta V_c)_k} = A_b + D_1(a_i)_k + D_2(a_i)_k^2 + D_3(a_i)_k^3 \quad (\text{for each accelerometer } j) \quad (7-32)$$

$$\hat{(\delta \psi_c)_k} = R_b + Q_1(w^T)_k + Q_2(w^T)_k^2 \quad (\text{for each gyro } j) \quad (7-33)$$

where $(\delta \hat{V}_c)_k$ and $(\delta \hat{\psi}_c)_k$ are estimates determined from the accelerometer and gyro calibration processes (as presented in Sections 8 and 9). The inputs $(a_i)_k$ and $(w^T)_k$ are provided by components of gravity and test table rates, respectively, averaged over Δt^m and corresponding to the various test conditions k . Note that $\delta \hat{V}_c = A_b^i$ when $a_i = 0$ and $\delta \hat{\psi}_c = R_b^i$ when $w^T = 0$. This emphasizes the definitions of A_b and R_b as being based on all a_i and w^T runs; not just those when the inputs are zero.

When more pairs of data are available than coefficients to be estimated for a given inertial sensor, filtering is possible to improve the accuracy of the estimates for that sensor. By utilizing the above regression equations, rather than incorporating them into the basic accelerometer and gyro calibration equations (7-1, 7-7 through 7-9, and 7-25 through 7-29), different amounts of data under various conditions can be handled without having to modify the original estimation equations. The regression equations are also convenient for determining just how many coefficients are significant and should be included once test data becomes available.

The detailed derivation of the scale factor estimation equations is contained in Section 9 and Appendix C.

8. CALIBRATION TEST PROCEDURE

The purpose of this section is to establish the basic procedures required to affect calibration of the ISU. Considerations and trade-offs in the development of the accelerometer and gyro calibration processes are discussed and the basic procedures are presented in sufficient detail to support the preparation of detailed step-by-step procedures. However, the procedure described in this section is considered to be an initial or interim design since certain trade-offs have yet to be made. This is particularly true concerning pre-calibration alignment and compensation for the various misalignments measured. Furthermore, it is likely that the estimation accuracy of some of the calibration terms can be improved and time to calibrate reduced by changing some of the ISU orientations and/or specifying different combinations of runs and/or using data from all inertial sensors from each run (the case if the ISU flight computer is used to collect and reduce the data). Finally, the design may have to be changed if analysis of inertial sensor test data indicates that different math models should be used.

Calibration of the ISU gyros and accelerometers may be performed at four different levels, as indicated in Table 8-1. The minimum level of calibration is designed to estimate accelerometer and gyro biases, misalignments and scale factor errors under only one set of inputs. In addition, the gyro mass unbalance terms (B_I , B_S and B_O) are determined. Six different orientations of the ISU are required and the test table is driven at $\pm 2^\circ/\text{sec}$ for some of the runs, compensation of the gyro data for

Table 8-1 The Four Levels of ISU Calibration

Minimum Calibration.

Accelerometers

$$\left. \begin{array}{l} A'_b \\ \text{MOA} \\ \text{MPA} \end{array} \right\} T^{BA}$$

$$\left. \begin{array}{l} \delta \dot{V}_c^{+1} \\ \delta \dot{V}_c^{-1} \end{array} \right\} \begin{array}{l} A_b \\ D_1, D_2 \end{array}$$

Gyros

From $w^T = 0$

From $w^T = + 2^\circ/\text{sec}$

$$\begin{array}{l} R'_b \\ B_I \\ B_S \\ B_O \end{array}$$

$$\left. \begin{array}{l} \text{MOA} \\ \text{MSA} \end{array} \right\} T^{BG}$$

$$\left. \begin{array}{l} \delta \dot{\psi}_c^+ (\text{at } +2^\circ/\text{sec}) \\ \delta \dot{\psi}_c^- (\text{at } -2^\circ/\text{sec}) \end{array} \right\} \begin{array}{l} R_b \\ Q_1, Q_2 \end{array}$$

Partial Calibration (above plus the following)

$$\left. \begin{array}{l} \delta \dot{V}_c^{+.7} \\ \delta \dot{V}_c^{-.7} \end{array} \right\} \begin{array}{l} A_b, D_1 \\ D_2, D_3 \end{array}$$

$$\begin{array}{l} C_{II} \\ C_{SS} \end{array}$$

Full Calibration (above plus the following)

$$\begin{array}{l} C_{IP} \\ C_{IO} \end{array}$$

$$\begin{array}{l} C_{IS} \\ C_{IO} \\ C_{OS} \end{array}$$

Gyro Scale Factor Calibration

Additional measurements of $\delta \dot{\psi}_c^+$ and $\delta \dot{\psi}_c^-$ are made for a variety of table rates (w^T) between ± 1 and $\pm 60^\circ/\text{sec}$, to refine the 3 gyro scale factor error coefficients (R_b , Q_1 and Q_2).

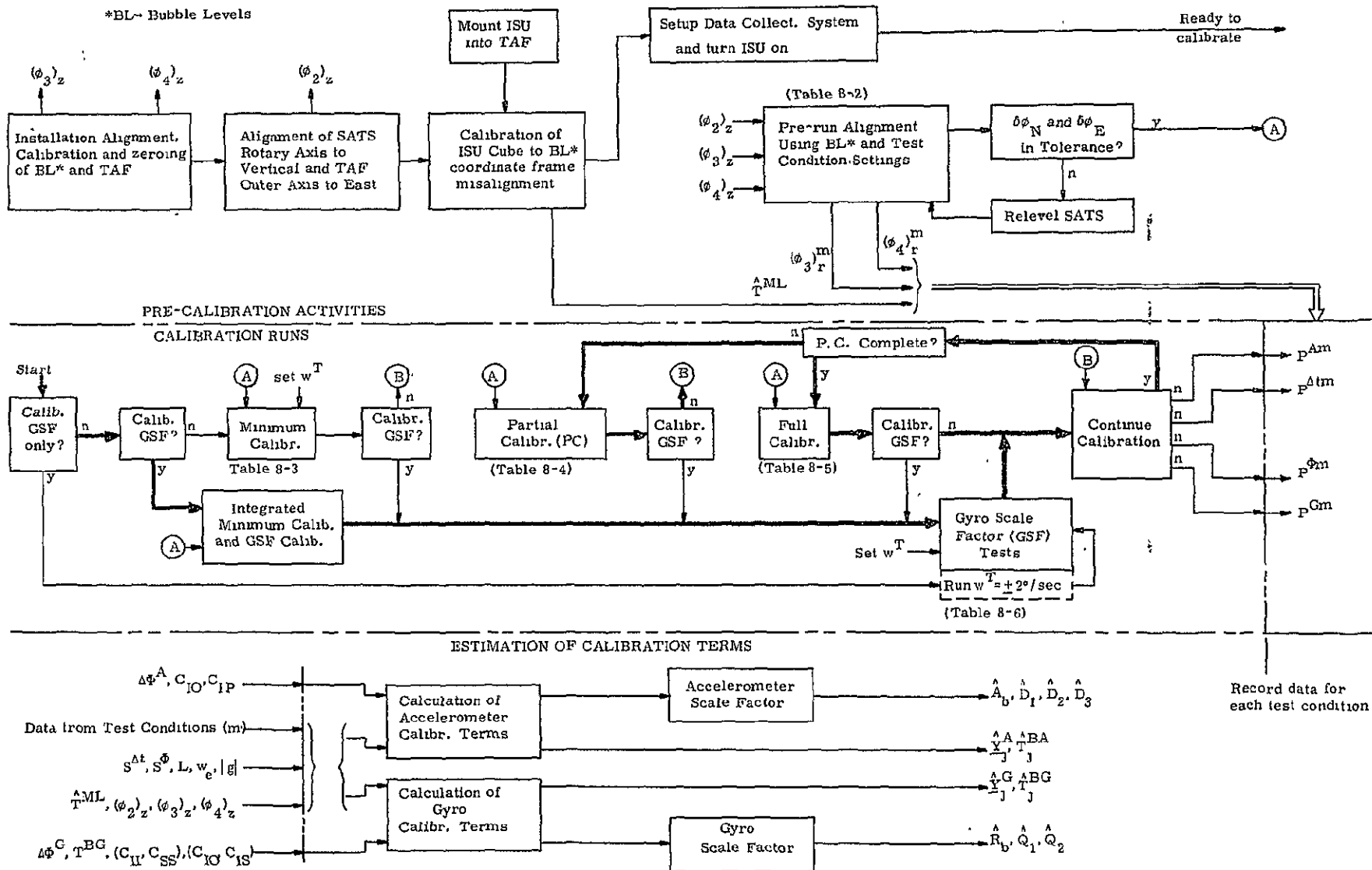
Note: A matrix format is used in the estimation of the above calibration terms, and the terms are arranged in column vectors in the order shown. The gyro terms dependent on table rates constitute the last four elements of the 13 element vector.

the C_{II} and C_{SS} terms is possible, if necessary. The partial calibration level requires an additional three ISU orientations with the sensor IAs at 45° to the vertical for a total of nine positions. This provides estimates of two additional accelerometer scale factor terms and the gyro major compliance terms C_{II} and C_{SS} . Compensation of the sensor output data for the C_{IO} , C_{IS} and C_{IP} cross compliance terms is possible, if necessary. The full level of calibration provides estimates of the cross compliance terms and requires an additional three ISU orientations, for a total of twelve positions. The fourth level of calibration provides a variety of table rates to improve the estimation accuracy of the gyro scale factor error terms.

Presentation of the operational calibration procedure is divided into three parts. The first, pre-calibration procedures, is concerned with measurements of the relationships between the ISU cube, the bubble levels, the test table rotary axis and the earth's coordinate frame. The second part, ISU orientation and calibration data collection, is concerned with the process of obtaining inertial sensor output data under the proper conditions so that the calibration terms can be estimated. The third part, processing of the data to estimate the calibration terms, is considered separately in the following section (9). Fig. 8-1 is an operational flow diagram that illustrates the total calibration procedure as described above. Details of the figure are discussed in the following sections.

Other operational procedures associated with the calibration process which are considered beyond the scope of this study, include turn-on/shut down procedures, maintenance and checkout of equipments, and initial installation and calibration of the test equipment.

Figure 8-1 Operational Flow Diagram of Total Calibration Process



8.1 DEVELOPMENT CONSIDERATIONS

The calibration test procedure was developed in accordance with the objectives and ground rules presented in the Introduction (Section 2). Additional considerations that were used in establishing the design are presented in this section and the general calibration philosophy is discussed. Although the Univac study was used as a model, the procedure evolved is different in several areas. Not only are the accelerometers different, but the test stand has only one degree of freedom, which is constrained to be vertical. This automatically required a change in certain test conditions, which necessitated further changes to provide adequate sensitivity in the estimation process.

The general calibration philosophy is to use the earth's gravity vector and test table rate capability to exercise the ISU in a variety of orientations. Having developed the propagation of these inputs (as a function of the calibration terms) to the outputs of the gyros and accelerometers (which can be measured), the terms can be estimated. The objective was to maximize the effects on the inertial sensor outputs of the calibration terms, in order to improve sensitivity of the estimation process, while minimizing the effect of various error sources. Furthermore, an attempt was made to choose test conditions* that would cause instruments outputs that were a function of only a few of the calibration terms for any one run. This has the advantage of requiring fewer runs to estimate any particular calibration term, thereby simplifying the

* and combinations of test conditions

data reduction effort and providing flexibility in determining a term without a large number of runs. It also has the advantage of minimizing the effect of random gyro drift changes between runs. For certain test conditions a calibration term not to be estimated affects the instruments outputs to an extent that compensation is required. This case occurs in two forms: in the first, errors in the knowledge of the calibration term has an insignificant effect, whereas in the second, the calibration term error may be significant.

The calibration procedures were designed to be performed in a series of groups, such that obtaining additional data would allow estimation of additional calibration terms. In the case of the gyros, the IA to cube misalignments can be determined directly from a pair of runs, as can the scale factor error at a given input rate. Once the required data for a minimum calibration has been obtained, only three additional runs are required to complete a partial calibration (see Table 8-1). A full calibration requires four more runs, as explained below.

The pre-run alignment procedure shown in Fig. 8-1 was developed with the following approach as a basis. The effect of gyro and accelerometer IA misalignments is to cause outputs that are proportional to the accelerometer IA to g nonorthogonality and the gyro IA to table rotary axis nonorthogonality^{*}, respectively. To simplify the alignment activities before each run, the bubble levels are used to determine the tilt of the

* the effect of rotary axis to vertical errors cause a negligible cross coupling of earth rate to the gyro IAs

rotary axis from g and then the TAF gimbals are positioned using the gimbal angle readouts so that the bubble levels are aligned with the rotary axis. * In this way the gyro IAs are referenced to the bubble level coordinate frame at the beginning of each run and the accelerometer output data can be compensated for changes in the rotary axis to vertical alignment, thereby also referencing the accelerometer IAs to the bubble level coordinate frame. The transformation matrix between the ISU cube and the inertial sensor IAs (which is the end result desired) is then calculated separately using the cube to bubble level calibration made at the time the ISU is installed in the TAF (as shown in Fig. 8-1 and explained in Section 8.2 below). Furthermore, compensation for earth rate coupling to the gyro IAs is accomplished using the bubble level to gyro IA transformation matrix determined above. **

Most of the calibration runs were chosen with the TAF inner gimbal axis nonvertical in order to allow use of the bubble levels in determining the rotary axis tilt from vertical. A total of 6 positions with IAs either nominally horizontal or vertical are required to perform a minimum calibration. This effectively eliminates the effect of cross compliance terms, and for the IAs vertical, the effect of IA misalignments to the ISU cube.

* this alignment is performed at assembly of the bubble levels, TAF and SATS, when the equipment is aligned, calibrated and zeroed.

** this is required for all gyro runs except those required to measure the transformation matrix itself

The gyro IA misalignments are measured by driving the test table at $\pm 2^\circ/\text{sec}$ and observing the outputs of those gyros whose IAs are nominally normal to the rotary axis (\underline{R}_1'). The process is repeated twice for each gyro; once with the OA normal to \underline{R}_1' and once with the SA normal to \underline{R}_1' . A higher rate is not recommended since rotation of a gyro about its OA at rates greater than approximately $2^\circ/\text{sec}$ will cause a potentially excessive gyroscopic torque on the gyro float about the IA, which may cause additional gyro drift rates that are significant. Lower table rates would require more run time to achieve the same calibration precision.

Data from the gyros are taken only for full revolutions of the test table, for two reasons. First, the effect of certain components of earth rate tend to cancel out over full revolutions and second, the cost of the SATS can be reduced by eliminating the requirement for a continuous, precise readout of table angle.

The partial calibration procedure is designed primarily to provide a change in accelerometer input accelerations so that the first and third order scale factor error terms can be separated. Both plus and minus 45° orientations to horizontal are chosen for each accelerometer, even though only one of these inputs would suffice, in order to minimize the potentially excessive error that may occur for inputs having the opposite sign from that chosen. The 45° orientation also is used to estimate the major gyro compliance terms.

The remaining four calibration procedures are designed to obtain data to estimate the cross compliance terms for both the gyros and

accelerometers. It is likely that the combination presented in Section 8.3 (Tables 8-3, 8-4 and 8-5), however, is not an optimum one in that the last run could probably be eliminated by choosing a different combination of test conditions. A total of six combinations were considered, all with the constraint of only observing four out of the six inertial sensor outputs for any one run. If the flight computer is made available, all six outputs could be utilized from each run and either the number of runs could be reduced or the precision of calibration term estimation could be improved.

8.2 PRE-CALIBRATION OPERATIONAL PROCEDURE

There are many ways that the precalibration alignment measurements can be made. As mentioned earlier, the method described in this section should be considered only illustrative of the type of measurements required since detailed trade-off studies have not yet been performed. Regardless of which specific method is adopted, the requirements of the precalibration alignment procedures can be divided into the following four major categories, as illustrated in Fig. 8-1:

- alignment and calibration of the bubble levels (which are located on the inner gimbal of the TAF) to the inner gimbal axis and to the SATS rotary axis (\underline{R}'_1), including zeroing of the TAF readouts ϕ_3 and ϕ_4 . This is normally done during test equipment installation and checked periodically thereafter depending upon the stability characteristics of the TAF and SATS.

- alignment of the SATS rotary axis to vertical and the TAF outer gimbal axis to East. The alignment to vertical consists of a nominal physical orientation of the rotary axis using leveling screws and then a precise measurement of the residual misalignment (for the scheme considered in this section). Depending upon the particular operational procedure finally adopted, it may be necessary to physically reduce the residual misalignment to a negligible amount. Alignment to East is done by adjusting the test table angle (ϕ_2).
- Calibration of the ISU optical cube to the bubble level coordinate frame, in the form of precise measurements of the misalignments. This measurement must be made every time the ISU is mounted in the TAF.
- Alignment of the ISU relative to the SATS rotary axis and the earth's coordinate system immediately prior to each run (m). For the scheme considered in this section, this is done using the bubble levels and TAF gimbal readouts to physically orient the ISU and measure certain critical misalignments.

In addition to these precalibration alignment procedures, it is necessary to set up the data collection system, turn the ISU on, etc., before an actual calibration run can be initiated. The operational requirements of each of the above precalibration procedures is discussed next, and

in conjunction with the hardware characteristics presented in Section 6, form the basis for the support equipment errors used in the system error analysis of Section 10. Again, the particular method described here is only illustrative of the measurements and accuracies required since other variations are feasible and have yet to be included in the calibration trade-off analysis.

The initial alignment, calibration and zeroing of the bubble levels, TAF and SATS are done at the time of test equipment installation. The process consists of mechanically adjusting the bubble levels so that they represent the TAF inner gimbal coordinate frame (I) (see Fig. 5-3 and Table 5-2). This may be done by noting the TAF gimbal angle changes as the bubble levels are nulled for various orientations of the TAF. Ideally, the bubble levels should be either parallel or perpendicular to the inner gimbal axis. The inner gimbal angle (ϕ_4) is zeroed such that the L_2 bubble level is parallel to the outer gimbal axis. The outer gimbal angle (ϕ_3) is zeroed such that the inner gimbal axis is parallel to the rotary axis. The values of the TAF gimbal angles when the bubble levels are normal to the rotary axis are labeled $(\phi_3)_z$ and $(\phi_4)_z$ and are recorded. Nonorthogonality checks between the ϕ_2 , ϕ_3 and ϕ_4 axes are recommended to assure acceptable performance, and if compensation is to be applied in the data processing equations, the nonorthogonalities must be measured and recorded.

The alignment of the SATS rotary axis to vertical is accomplished by using the leveling screws, as indicated by the TAF gimbal angle changes required to null the bubble levels when the test table is rotated 180°.

Alignment of the TAF outer gimbal axis to East is accomplished using the autocollimator and adjusting the test table angle (ϕ_2). A separate survey is required to establish East, as a reference for the autocollimator. The device for indicating this position of the table is secured and this angle of the table is labeled $(\phi_2)_z$.

Calibration of the ISU cube to bubble level coordinate frame misalignment is performed each time the ISU is mounted within the TAF. The procedure is to place each of the three bubble levels in the nominally horizontal position, in sequence. In each instance, the bubble level is nulled by adjusting ϕ_3 and ϕ_4 . With the autocollimator referenced to level, the angle the visible ISU cube face makes with respect to level is measured. This angle is then a measure of the misalignment between the bubble level pointing in the direction of the autocollimator and the ISU cube face observed. The process is repeated for each bubble level, and assuming the ISU cube faces are all orthogonal, all six elements of the bubble level to mirror coordinate frame* transformation matrix (T^{ML}) are established. It is estimated that approximately 1.5 hours will be required to mount the ISU, setup the autocollimator and calibrate the ISU cube/bubble level misalignments. This is based on the following time allocation.

* i. e., ISU cube

• Mount ISU	15 minutes
• Setup autocollimator and level	20
• Perform optical measurements (3 times)	45
• 4 minutes to index ISU	
• 6 minutes to measure	
• <u>5</u> minutes to complete records	
15 minutes per ISU position	80 minutes = 1.33 hrs.

An additional estimated 15 minutes is required to set up the data collection system, turn the ISU on and prepare to start the calibration runs.

The alignment of the ISU prior to each calibration run (m) is performed using the bubble levels and the TAF gimbal angle readouts. However, since the alignment procedure is part of the operational calibration procedure, it will be explained in detail in the next section (8.3). In Fig. 8-1, the procedure is shown as a precalibration activity, but separate from the other alignment procedures because it is repeated for each test condition (m).

8.3 CALIBRATION OPERATIONAL PROCEDURE

An operational flow diagram of the calibration procedure is illustrated in Fig. 8-1. The various options are indicated, and the heavy line represents the one that would normally be followed if all four levels of ISU calibration (as listed in Table 8-1) were to be performed. Although the pre-run alignment procedure is included as a precalibration activity, it

is required before each run (m), except for the Gyro Scale Factor (GSF) tests.

The pre-run alignment procedure is designed to properly orientate the ISU relative to the SATS rotary axis and the earth's coordinate system, immediately prior to each run. The five step procedure is outlined in Table 8-2 and provides a way to compensate for short term tilts of the rotary axis from vertical. If the physical tilt is excessive (say greater than $.3 \text{ min}$), the releveing procedure is initiated, as described in Section 8.2, in order to minimize errors in the gyro output data. At the end of the procedure, the bubble levels are normal to the rotary axis and the misalignment of the rotary axis to vertical is known. The latter is necessary for compensation of the accelerometer output data.

The detailed operational test procedures to perform the four levels of ISU calibration, as listed in Table 8-1, are contained in Tables 8-3 through 8-6. The tables are organized to indicate the ISU orientation required for each test condition (m); both in terms of directions of each inertial sensor coordinate frame and the corresponding SATS and TAF gimbal angle indications. The time estimated to set up each run is tabulated. Also tabulated are the data to be collected* and the elapsed time (Δt^m) of each run. The runs within any one table may be made in any order; however, data taken with $w^T = \pm 2^\circ/\text{sec}$ provides misalignment information that may be helpful in subsequent runs.

*The G_j and A_j column headings refer to the particular gyro and accelerometer pulse outputs to be counted, $\Delta\phi_2$ refers to the test table pulse output, and TAF refers to ϕ_3, ϕ_4 gimbal angle readouts.

ϕ_2	ϕ_3	ϕ_4	Procedure ⁽¹⁾
$(\phi_2)_z$	90	0	1. Position TAF to pre-run align orientation
$(\phi_2)_z$	$(\phi_3)_r^m$	$(\phi_4)_r^m$	2. Null the two bubble levels that are horizontal, by adjusting ϕ_3 and ϕ_4 . Record the gimbal readouts as $(\phi_3)_r^m$ and $(\phi_4)_r^m$.
			3. Check for excessive tilt of rotary axis ⁽²⁾ .
			4. If either $(\delta\phi_E)^m$ or $(\delta\phi_N)^m$ is greater than .3 m̄in, relevel SATS, as described in Section 8.2, and repeat step 2 above.
$(\phi_2)_z$	$(\phi_3)_z^m$	$(\phi_4)_z^m$	5. Index ISU by positioning the TAF gimbals as follows: $(\phi_3)_z^m = (\phi_3)_n^m + \text{value of } \phi_3 \text{ from zeroing process}$ $(\phi_4)_z^m = (\phi_4)_n^m + \text{value of } \phi_4 \text{ from zeroing process}$ <p>where subscript n refers to the nominal value.</p>

Notes: (1) The ISU should not be rotated about any axis at a rate greater than 60°/sec, during any of the positioning procedures, in order to prevent gyro loop saturation.

(2) Check for tilt ($\delta\phi_E$ and $\delta\phi_N$) out-of-tolerance by computing

$$(\delta\phi_E)^m = (\phi_3)_z - (\phi_3)_r^m$$

$$(\delta\phi_N)^m = (\phi_4)_z + (\phi_4)_r^m$$

Table 8-2 Pre-Run Alignment and ISU Indexing Procedures

Perform the following after completing the pre-calibration procedure.

m	Inst. No. J	Gyro		Accel.			
		i o s	i o p	i o s	i o p		
4 ↓	1	U	S	D	S	W	
	2	W	D	S	W	U	N
	3	S	D	E	S	D	E

5 ↓	1	E	U	S	W	U	N
	2	N	W	U	N	E	D
	3	U	W	S	U	W	S

6 ↓	1	E	S	D	W	S	U
	2	U	W	S	U	E	N
	3	S	W	D	S	W	D

1 ↓	1	S	D	E	N	D	W
	2	W	N	D	E	W	U
	3	D	N	E	D	N	E
2 ↓	1	E	N	U	W	N	D
	2	D	W	N	U	D	S
	3	N	W	U	N	W	U
3 ↓	1	D	N	E	U	N	W
	2	W	U	N	E	W	S
	3	N	U	E	N	U	E

Data Collection				m	$\phi_2 \cdot w^T$ deg., °/sec.	ϕ_3 deg.	ϕ_4 deg.	Operation		Setup Time min.	Run	
G_z	A_j	$\Delta\phi_2$	TAF					Step	Description		Δt^m min.	$\Delta\phi_2$ rev.
#1	all	✓	✓	6	0 _z	90 _r	0 _r	1.1	Pre-run align.	8		
				4	↓	90 _z	90 _z	1.2	Index ISU	4		
				↓	↓	↓	↓	1.3	Collect Data	-	5	
all	✓	✓	✓	42 ⁺	+2°/sec.	↓	↓	2.1	Set w ^T	6		
				↓	↓	↓	↓	2.2	Collect Data	-	6	+2
all	✓	✓	✓	42 ⁻	-2°/sec.	↓	↓	3.1	Set w ^T	6		
				↓	↓	↓	↓	3.2	Collect Data	-	6	-2
#3	all	✓	✓	6	0 _z	90 _r	0 _r	4.1	Pre-run align.	8		
				5	↓	0 _z	0 _z	4.2	Index ISU	4		
				↓	↓	↓	↓	4.3	Collect Data	-	5	
all	✓	✓	✓	52 ⁺	+2°/sec.	↓	↓	5.1	Set w ^T	6		
				↓	↓	↓	↓	5.2	Collect Data	-	6	+2
all	✓	✓	✓	52 ⁻	-2°/sec.	↓	↓	6.1	Set w ^T	6		
				↓	↓	↓	↓	6.2	Collect Data	-	6	-2
#2	all	✓	✓	6	0 _z	90 _r	0 _r	7.1	Pre-run align.	8		
				↓	↓	90 _z	0 _z	7.2	No index reqd.	-		
				↓	↓	↓	↓	7.3	Collect Data	-	5	
all	✓	✓	✓	62 ⁺	+2°/sec.	↓	↓	8.1	Set w ^T	6		
				↓	↓	↓	↓	8.2	Collect Data	-	6	+2
all	✓	✓	✓	62 ⁻	-2°/sec.	↓	↓	9.1	Set w ^T	6		
				↓	↓	↓	↓	9.2	Collect Data	-	6	-2
1,2	1,3	✓	✓	6	0 _z	90 _r	0 _r	10.1	Pre-run align.	8		
				1	↓	180 _z	90 _z	10.2	Index ISU	4		
				↓	↓	↓	↓	10.3	Collect Data	-	10	
1,3	2,3	✓	✓	6	0 _z	90 _r	0 _r	11.1	Pre-run align.	8		
				2	↓	270 _z	0 _z	11.2	Index ISU	4		
				↓	↓	↓	↓	11.3	Collect Data	-	10	
2,3	1,2	✓	✓	6	0 _z	90 _r	0 _r	12.1	Pre-run align.	8		
				3	↓	270 _z	90 _z	12.2	Index ISU	4		
				↓	↓	↓	↓	12.3	Collect Data	-	10	
Subtotal										104	81 minutes	
										1.73	1.35 hours	

Minimum Calib. 3:08 hours

Pre-Calib. 1.58

Total 4.57 hours

$(\phi_3)_r = 90_r$ = actual value of ϕ_3 to be recorded from Pre-run Alignment using Bubble Levels when $(\phi_3)_n = 90^\circ$

$(\phi_3)_z = 90_z$ = 90° + value of ϕ_3 from zeroing process.

Similarly for $(\phi_4)_r$, $(\phi_4)_z$ and other nominal values of ϕ_3 and ϕ_4

Table 8-3 Operational Test Procedure for Minimum Calibration

Perform a Minimum Calibration plus the following

m	Inst. No. j	Gyro		Accel.		Data Collection				m	ϕ_2^w deg. °/sec.	ϕ_3 deg.	ϕ_4 deg.	Operation		Setup Time min.	Run			
		i	o	s	i	o	p	G _j	A _j					$\Delta\phi_2$	TAF		Step	Description	Δt^m min.	$\Delta\phi_2$ rev.
7 ↓	1	DS	US	W	UN	US	E				6	O _z	90 _r	O _r	13.1	Pre-run align.	8			
	2	E	UN	US	E	DS	DN				7	O _z	45 _z	270 _z	13.2	Index ISU	4			
	3	US	UN	W	US	UN	W	1,3	1,3		↓	↓	↓	↓	13.3	Collect Data	-	10	-	
8 ↓	1	UE	S	DE	DW	S	UW				6	O _z	90 _r	O _r	14.1	Pre-run Align.	8			
	2	UW	DW	S	UW	UE	N				8	O _z	90 _z	45 _z	14.2	Index ISU	4			
	3	S	DW	DE	S	DW	DE	1,2	1,2		↓	↓	↓	↓	14.3	Collect Data	-	10	-	
9 ↓	1	E	DN	UN	W	DN	DS				6	O _z	90 _r	O _r	15.1	Pre-run Align.	8			
	2	DS	W	DN	DS	E	US				9	O _z	225 _z	O _z	15.2	Index ISU	4			
	3	DN	W	UN	DN	W	UN	2,3	2,3		↓	↓	↓	↓	15.3	Collect Data	-	10	-	
Minimum Calibration																36	30			
Subtotal																140	111	minutes		
Partial Calibration																2.33	1.85	hours		
Pre-Calibration																4.18		hours		
Total																1.58		hours		
Total																5.8		hours		

$(\phi_3)_r = 90_r$ = actual value of ϕ_3 to be recorded from
Pre-run Alignment using Bubble Levels, when $(\phi_3)_n = 90^\circ$
 $(\phi_3)_z = 90_z = 90^\circ +$ value of ϕ_3 from zeroing process.
 Similarly for $(\phi_4)_r$, $(\phi_4)_z$ and other nominal values of ϕ_3 and ϕ_4 .

Table 8-4 Operational Test Procedure for Partial Calibration

Perform a Partial Calibration plus the following

m	Inst. No. j	Gyro		Accel.		Data Collection				m	ϕ_2^w deg. °/sec.	ϕ_3 deg.	ϕ_4 deg.	Operation		Setup Time min.	Run			
		i	o	s	i	o	p	G _j	A _j					$\Delta\phi_2$	TAF		Step	Description	Δt^m min.	$\Delta\phi_2$ rev.
10 ↓	1	DN	DS	E	US	DS	E				6	O _z	90 _r	O _r	16.1	Pre-run align.	8			
	2	E	US	DS	E	DN	UN				10	O _z	135 _z	270 _z	16.2	Index ISU	4			
	3	DS	US	W	DS	US	W	all	1,3		↓	↓	↓	↓		Collect Data	4	2x10	-	
11 ↓	1	UE	N	UW	DW	N	DE				6	O _z	90 _r	O _r	17.1	Pre-run align.	8			
	2	DE	DW	N	DE	UE	S				11	O _z	270 _z	315 _z	17.2	Index ISU	4			
	3	N	DW	UW	N	DW	UW	all	all		↓	↓	↓	↓	17.3	Collect Data	4	2x10	-	
12 ↓	1	E	DS	DN	W	DS	US				6	O _z	90 _r	O _r	18.1	Pre-run align.	8			
	2	US	W	DS	US	E	UN				12	O _z	135 _z	O _z	18.2	Index ISU	4			
	3	DS	W	DN	DS	W	DN	all	all		↓	↓	↓	↓	18.3	Collect Data	4	2x10	-	
13 ↓	1	DE	S	DW	UW	S	UE				6	O _z	90 _r	O _r	19.1	Pre-run align.	8			
	2	UE	UW	S	UE	DE	N				13	O _z	90 _z	315 _z	19.2	Index ISU	4			
	3	S	UW	DW	S	UW	DW	2,3	#2		↓	↓	↓	↓	19.3	Collect Data	-	10	-	
Partial Calibration																60	70			
Subtotal																140	111	minutes		
Full Calibration																200	181	minutes		
Pre-Calibration																3.33	3.02	hours		
Total																6.35		hours		
Total																1.58		hours		
Total																7.9		hours		

$(\phi_3)_r = 90_r$ = actual value of ϕ_3 to be recorded from
Pre-run Alignment using Bubble Levels when $(\phi_3)_n = 90^\circ$
 $(\phi_3)_z = 90_z = 90^\circ +$ value of ϕ_3 from zeroing process.
 Similarly, for $(\phi_4)_r$, $(\phi_4)_z$ and other nominal values of ϕ_3 and ϕ_4 .

Table 8-5 Operational Test Procedure for Full Calibration

8-6a. Detailed Procedures

m	Inst. No. j	Gyro i o s	Data Collect		m	ϕ_2, w^T	ϕ_3	ϕ_4	Operation	Setup Time min	Run			
			G	$\Delta\phi_2$		deg, °/sec					deg	deg	Δt^m	$\Delta\phi_2$
													min	rev
4 ↓ ↓	1	U S E			4	0 _n	90 _Z	90 _Z	Index ISU	4				
			/		↓	↓	↓	↓	Collect data	-	5	-		
	2	W D S			43 ⁺	+1°/sec			Set w ^T	6				
			#1	✓	↓	↓	↓	↓	Collect data	-	6	+1		
	3	S D E			43 ⁻	-1°/sec			Set w ^T	6				
			#1	✓	↓	↓	↓	↓	Collect data	-	6	-1		
					44 ⁺	+4°/sec			Set w ^T	3				
	#1	✓	↓	↓	↓	↓	↓	Collect data	-	6	+4			
				44 ⁻	-4°/sec			Set w ^T	3					
#1	✓	↓	↓	↓	↓	↓	Collect data	-	6	-4				

continue for $w^T = \pm 8, \pm 20$ and $\pm 60^\circ/\text{sec}$ ($m=45^+, 45^-, 46^+, 46^-, 47^+, 47^-$)

m	j	i o s
5	1	E U S
↓	2	N W U
↓	3	U W S

		5	0 _n	0 _Z	0 _Z	Index ISU	4		
/		↓	↓	↓	↓	Collect data	-	5	-
		53 ⁺	+1°/sec			Set w ^T	6		
#3	✓	↓	↓	↓	↓	Collect data	-	6	+1
		53 ⁻	-1°/sec			Set w ^T	6		
#3	✓	↓	↓	↓	↓	Collect data	-	6	-1

continue for $w^T = \pm 4, \pm 8, \pm 20$ and $\pm 60^\circ/\text{sec}$ ($m=54^+, 54^-, 55^+, 55^-, 56^+, 56^-, 57^+, 57^-$)

m	j	i o s
6	1	E S D
↓	2	U W S
↓	3	S W D

		6	0 _n	90 _Z	0 _Z	Index ISU	4		
/		↓	↓	↓	↓	Collect data	-	5	-
		63 ⁺	+1°/sec			Set w ^T	6		
#2	✓	↓	↓	↓	↓	Collect data	-	6	+1
		63 ⁻	-1°/sec			Set w ^T	6		
#2	✓	↓	↓	↓	↓	Collect data	-	6	-1

continue for $w^T = \pm 4, \pm 8, \pm 20$ and $\pm 60^\circ/\text{sec}$ ($m=64^+, 64^-, 65^+, 65^-, 66^+, 66^-, 67^+, 67^-$)

8-6b. Calculation of Time Required to Calibrate

Procedure	Index ISU	Table Rate (w^T), deg/sec						1 Gyro		3 Gyros	
		0	± 1	± 4	± 8	± 20	± 60	min	hr	min	hr
Setup	4	-	12	6	4	4	4	32	.53		1.59
Run	-	5	12	12	12	12	12	65	1.08		3.24
Totals	4	5	24	18	16	16	16	97	1.6		4.8

If $w^T = \pm 2^\circ/\text{sec}$ has not been run (as part of other calibration tests), must add an additional .4 hr per gyro.

Table entries are times required to perform the operations indicated.

Table 8-6 Operational Test Procedure for Gyro Scale Factor Error Calibration

The "Pre-run align" and "Index ISU" procedures referred to in the tables are as discussed above and summarized in Table 8-2. The "Set w^T " procedure is the process of adjusting the test table rate drive to the w^T value indicated.

This is done by checking the time required for the table to rotate through a known angle (90°, 180° or 360°, depending upon the table readouts provided). If the rate is not within $\pm .5\%$ of the desired value, the rate drive is readjusted and the timing process repeated. The data collection system is described in Sections 6.1 and 6.5.

The operational test procedure for performing a minimum calibration is specified in Table 8-3. A total of 12 runs for 6 different orientations of the ISU are required to collect the necessary data. This includes operating the test table at plus and minus 2°/sec for each of 3 of the ISU positions. An estimated 3.1 hours is required to complete the runs, which in addition to 1.58 hours to perform the precalibration activities*, requires a total of 4.7 hours to calibrate.

To perform a partial calibration, an additional 3 runs for 3 ISU orientations at 45° to the vertical are required, as indicated in Table 8-4. This consumes an additional 1.1 hours which when combined with the 4.7 hours for the minimum calibration, requires a total of 5.8 hours to complete a partial calibration of the ISU.

* as determined in Section 8.2

The additional procedures to perform a full calibration are specified in Table 8-5. The new ISU positions are also at 45° to the vertical since the cross compliance terms are to be estimated. Each of the first 3 runs are repeated twice since data from all inertial sensors are required; yet only 4 outputs can be processed at any one time. The additional data is required to avoid excessive sensitivity in the estimation of the calibration terms. Test condition No. 13 is required to provide additional data from accelerometer No. 2 in order to estimate one of the cross compliance terms. It is likely that a different combination of test conditions could eliminate the need for the extra run, particularly if data from each inertial sensor could be collected for each run (the case, for example, if the flight computer were to be used to collect data). As shown in Table 8-5, an additional 2.1 hours is required to collect the data. Combining this with the 5.8 hours for a partial calibration, a total of 7.9 hours is required to complete a full calibration of the ISU.

Table 8-6 specifies the procedures and times required to operate the test table at various rates between $\pm 1^\circ/\text{sec}$ and $\pm 60^\circ/\text{sec}$, in order to provide data for the gyro scale factor error regression analysis discussed in Sections 7.3 and 9.3. The rates listed are only suggestions and more or less data may be taken depending upon time available and number of samples desired to be included. A total of 4.8 hours is required to run 5 pairs of plus and minus rates for each gyro. If only gyro scale factor calibration is desired, $w^T = \pm 2^\circ/\text{sec}$ is also required (at .4 hr. per gyro) and the total calibration time becomes 6.0 hours.

If gyro scale factor calibration is to be done in conjunction with the other calibration runs, it is recommended that they be combined, as

indicated in Fig. 8-1. In this way, the first 2 steps in each of the test condition runs $m = 4, 5$ and 6 in Table 8-6 can be eliminated, since they are already performed as part of the minimum calibration (see Table 8-3). Therefore, only 4.4 hours is required in addition to the times listed in Tables 8-3, 8-4 or 8-5 to perform the calibrations indicated plus a full range gyro scale factor calibration.

9. ESTIMATION OF CALIBRATION TERMS

The purpose of this section is to derive the equations to be used in estimating the calibration terms. The algorithms presented are based on making a least squares fit to the data obtained whenever more measurements are used compared to the number of terms to be estimated. When the number of measurements and terms to be estimated are equal, the least squares equations degenerate into a deterministic solution. The pre-calibration calibrations are also presented.

Both the accelerometer and gyro calibration equations are arranged in the following form; as shown in Section 7:

$$\underline{M}_j^m / \Delta t^m \equiv \dot{\underline{M}}_j^m = \underline{H}_j^m \cdot \underline{Y}_j + \delta \dot{\underline{M}}_j^m \quad (7-1) \text{ and } (9-1)$$

in which the various terms are defined by Eqs. (7-7), (7-8), and (7-9) for the accelerometers and Eqs. (7-25) through (7-29) for the gyros. Tables B-2 through B-7 in Appendix B contain the results of applying the calibration equations to each test condition (m) for each inertial sensor. The equations are organized in the following matrix form:

$$\dot{\underline{M}}_j = \underline{H}_j \underline{Y}_j \quad (9-2)$$

where

$$\underline{H}_j \equiv \text{a matrix whose rows are the } \underline{H}_j^m \text{ of Eq. (9-1), for the various test conditions (m)} \quad (9-3)$$

and

$$\dot{\underline{M}}_j \equiv \text{a column vector whose elements are the } \dot{\underline{M}}_j^m \text{ from Eq. (9-1)} \quad (9-4)$$

The matrix H_j can assume various dimensions, depending upon the measurements (M) used and the calibration terms in the vector \underline{Y} that propagate into M . For the case when H_j contains the same or more rows than columns, and $(H_j^T H_j)$ is nonsingular, it can be shown that the least squares solution of Eq. (9-2) is as follows:

$$\hat{\underline{Y}}_j = (H_j^T H_j)^{-1} H_j^T M_j \quad (9-5)$$

where $\hat{\underline{Y}}_j$ is the estimated value of \underline{Y}_j . This equation was applied to the calibration equations in Tables B-2 through B-7, for the test conditions specified in the various calibration procedures of Tables 8-3, 8-4 and 8-5. Results are presented in Appendix C and discussed in Sections 9.2 and 9.3.

In the case of the scale factor error coefficients, defined in Eqs. (7-32) and 7-33) of Section 7.3, the general least squares solution is as follows:

$$\hat{C}_0 = (F_4 Z_0 - F_2 Z_2) / (K F_4 - F_2^2) \quad (9-6)$$

$$\hat{C}_1 = (F_6 Z_1 - F_4 Z_3) / (F_2 F_6 - F_4^2) \quad (9-7)$$

$$\hat{C}_2 = (K Z_2 - F_2 Z_0) / (K F_4 - F_2^2) \quad (9-8)$$

$$\hat{C}_3 = (F_2 Z_3 - F_4 Z_1) / (F_2 F_6 - F_4^2) \quad (9-9)$$

where the C's correspond to the respective A_b , D, R_b and Q coefficients in Eqs. (7-32) and (7-33) and the F and Z terms are functions of the inertial sensor inputs and indicated outputs. These terms are defined below for the accelerometers and gyros. The term K is the number of data samples used in the least squares fit. The above equations are based on the assumption that inputs to the inertial sensors occur in equal and opposite pairs (e. g. , $\pm g/\sqrt{2}$ for the accelerometers and $\pm 4^\circ/\text{sec}$ for the gyros, as well as other pairs of inputs). The equations also assume that A'_b and R'_b are used, corresponding to zero input to the accelerometer and gyro, respectively.

The estimated inertial sensor misalignments transformation matrices \hat{T}^{BA} and \hat{T}^{BG} are determined from the estimated accelerometer and gyro nonorthogonalities, as contained in the \hat{Y} vectors of the calibration estimation equations. However, these \hat{Y} elements are the misalignments between the IAs of the inertial sensors and the bubble level coordinate frame (\hat{T}^{AL} and \hat{T}^{GL}), as discussed in Appendix B (following Eq. B-7); and not the misalignments between the IAs and the ISU cube (mirrors) which are elements of the desired \hat{T}^{BA} and \hat{T}^{BG} matrices. Having measured the elements of T^{ML} , as described above under the pre-calibration calculations (Section 9.1), the \hat{T}^{BA} and \hat{T}^{BG} matrices can be determined as follows:

$$\hat{T}^{BA} = T^{BM} T^{ML} (\hat{T}^{AL})^{-1} \quad (9-10)$$

and

$$\hat{T}^{BG} = T^{BM} T^{ML} (\hat{T}^{GL})^{-1} \quad (9-11)$$

where T^{BM} and T^{ML} are given in Eq. (B-6) and T^{AL} and T^{GL} are composed of the estimated nonorthogonalities of the three accelerometers and three gyros with respect to the bubble level coordinate frame. The various matrices are defined in Table 9-1 and are expanded in the following sections to estimate the elements of T^{BA} and T^{BG} , the transformation matrices ultimately desired.

<u>Matrix</u>	<u>Description of Transformation Matrix</u>
T^{ML}	misalignment of ISU cube (mirror) coordinate frame relative to bubble level coordinate frame; elements defined in Eqs. (B-6) and (9-18).
T^{BM}	definition of body axes in terms of ISU Cube (mirror) coordinate frame
T^{AL}	misalignment of coordinate frame defined by IAs of the accelerometers relative to the bubble level coordinate frame; elements of matrix are NOA and NPA for each accelerometer
T^{GL}	misalignment of coordinate frame defined by IAs of the gyros relative to the bubble level coordinate frame; elements of matrix are NOA and NSA for each gyro
T^{BA}	matrix used to transform accelerations sensed along IAs of the accelerometers into accelerations in the body axes coordinate frame; elements of matrix are MOA and MPA for each accelerometer
T^{BG}	matrix used to transform rates sensed about IAs of the gyros into rates about the body axes coordinate frame; elements of matrix are MOA and MSA for each gyro

Table 9-1 Transformation Matrices Used to Calculate Inertial Sensor to ISU Cube Misalignments

9.1 PRE-CALIBRATION CALCULATIONS

Calculations in this category consist of processing data obtained before the actual calibration runs are made. The calibration procedure was arranged such that only two calculations had to be made before each run, to determine the tilt of the test table rotary axis from vertical to assure that it was not excessive. The other calculations are involved in determining the bubble level to ISU cube transformation matrix (T^{ML}).

The calculations to determine the tilt of the rotary axis are presented in Table 8-2 and repeated as follows:

$$(\delta\phi_E)^m = (\phi_3)_Z^m - (\phi_3)_R^m \quad (9-12)$$

$$(\delta\phi_N)^m = (\phi_4)_Z^m + (\phi_4)_R^m \quad (9-13)$$

where

$$(\phi_3)_Z^m \equiv (\phi_3)_N^m + \text{value of } \phi_3 \text{ from zeroing process} \quad (9-14)$$

$$(\phi_4)_Z^m \equiv (\phi_4)_N^m + \text{value of } \phi_4 \text{ from zeroing process} \quad (9-15)$$

$$(\phi_3)_R^m \equiv \text{TAF outer gimbal readout when bubble levels are nulled in the pre-run align orientation, just prior to run (m)} \quad (9-16)$$

$$(\phi_4)_R^m \equiv \text{TAF inner gimbal readout when bubble levels are nulled in the pre-run align orientation*, just prior to run (m)} \quad (9-17)$$

* the pre-run align orientation is when $\phi_3 \approx 90^\circ$, $\phi_4 \approx 0^\circ$, as discussed in Section 8.3 and Table 8-2.

and subscript n refers to the nominal values of $(\phi_3)^m$ and $(\phi_4)^m$ for run (m). The values of ϕ_3 and ϕ_4 from the zeroing process are those values that align the bubble levels with respect to the rotary axis. The $\delta\phi_E$ and $\delta\phi_N$ terms are used in the accelerometer estimation equations, as shown below.

The transformation matrix (T^{ML}) contains 6 elements, 3 of which are independent and must be measured separately. This is done using the bubble levels and the autocollimator at the time of TSU mounting as explained in Section 8.2. The T^{ML} matrix is defined in Eq. (B-6) and Table B-1 and repeated as follows:

$$T^{ML} = \begin{bmatrix} -\underline{M}_{13} \cdot \underline{L}_1 & 1 & \underline{M}_{11} \cdot \underline{L}_3 \\ \underline{M}_{22} \cdot \underline{L}_1 & -\underline{M}_{21} \cdot \underline{L}_2 & 1 \\ -1 & -\underline{M}_{33} \cdot \underline{L}_2 & \underline{M}_{32} \cdot \underline{L}_3 \end{bmatrix} \quad (\text{B-6)-and (9-18)}$$

in which the elements are defined in the form $\underline{M}_{ab} \cdot \underline{L}_c$ = nonorthogonality of \underline{M}_a about \underline{L}_b with respect to \underline{L}_c , measured about the positive \underline{L}_b axis in accordance with the right-hand rule. The matrix elements are determined from the following transformation equation:

$$T^{ML} = T^{MS} T^{SE} (T^{LE})^{-1} \quad (9-19)$$

where the transformations are defined in Table 9-2. The bubble levels

<u>Matrix</u>	<u>Description of Transformation Matrix</u>
T^{ML}	misalignment of ISU cube (mirror) coordinate frame relative to bubble level coordinate frame; elements defined in Eqs. (B-6) and (9-18).
T^{MS}	matrix of measurements of ISU cube, expressed in autocollimator coordinate frame
T^{SE}	matrix relating autocollimator coordinate frame relative to earth coordinates (specifically to vertical); assumed equal to the identity matrix when the autocollimator is leveled.
T^{LE}	matrix representing bubble level coordinate frame relative to earth coordinates (specifically to vertical); assumed equal to the identity matrix when the bubble levels are nulled

Table 9-2 Transformation Matrices Used in Alignment of ISU Cube and Bubble Level Coordinate Frame

and autocollimator are adjusted relative to vertical such that T^{SE} and T^{LE} are essentially equal to identity matrices. Therefore, the autocollimator to ISU cube measurements provide elements of T^{ML} directly. As mentioned above, only 3 measurements are required since the coordinate frames are essentially orthogonal and therefore the following relationships exist:

$$-M_{21} \cdot L_2 = M_{11} \cdot L_3 \quad (9-20)$$

$$-M_{13} \cdot L_1 = -M_{33} \cdot L_2 \quad (9-21)$$

$$M_{32} \cdot L_3 = M_{22} \cdot L_1 \quad (9-22)$$

Thus all elements of T^{ML} in Eq. (9-18) are determined.

9.2 ACCELEROMETER CALIBRATION ESTIMATION EQUATIONS

The calibration estimation equation [Eq. (9-5)] was applied to the accelerometer calibration equations in Tables B-2, B-3 and B-4 to provide the accelerometer calibration estimation equations. The results are tabulated in matrix form in Tables C-1, C-2 and C-3 of Appendix C for the minimum, partial and full levels of calibration respectively. It will be noted that the equations do not include compensations to be applied to the \dot{M} measurements in order to account for gravity coupling due to significant misalignments and tilt of the rotary test table axis from

vertical. These corrections can be specified when the final pre-calibration alignment scheme is defined. Compensation for C_{IO} and C_{IP} in the partial calibration estimation equations is shown in Table C-2.

The accelerometer scale factor error estimation equations were determined from Eqs. (9-6) through (9-9), using the $\hat{\delta \dot{V}}$ estimates from the accelerometer calibration equations (viz., $\hat{\delta \dot{V}}_c^{+1}$, $\hat{\delta \dot{V}}_c^{-1}$, $\hat{\delta \dot{V}}_c^{+.7}$, $\hat{\delta \dot{V}}_c^{-.7}$) and the term A'_b . The results are tabulated in Table C-4 of Appendix C.

The elements of the T^{BA} transformation matrix, which are a function of the misalignments of the IAs of the accelerometers relative to the ISU cube, are computed using Eq. (9-10) as a basis. The matrix T^{AL} in Eq. (9-10) is composed of the estimated nonorthogonalities (in $\underline{\hat{Y}}_1^A$, $\underline{\hat{Y}}_2^A$ and $\underline{\hat{Y}}_3^A$ from Tables C-1, C-2 and C-3), as follows:

$$T^{AL} = \begin{bmatrix} \hat{NPA}_1 & -1 & -\hat{NOA}_1 \\ \hat{NOA}_2 & \hat{NPA}_2 & 1 \\ 1 & -\hat{NPA}_3 & \hat{NOA}_3 \end{bmatrix} \quad (9-23)$$

Upon inverting T^{AL} , and writing T^{BA} in terms of the inertial sensor misalignments to be estimated (viz., \hat{MOA} and \hat{MPA}), Eq. (9-10) is expanded to yield:

$$\hat{T}^{BA} = \begin{bmatrix} -1 & -\hat{M}OA_1 & +\hat{M}PA_1 \\ \hat{M}PA_2 & 1 & -\hat{M}OA_2 \\ -\hat{M}PA_3 & -\hat{M}OA_3 & 1 \end{bmatrix} = \begin{bmatrix} 1 & 0 & 0 \\ 0 & 1 & 0 \\ 0 & 0 & -1 \end{bmatrix} \hat{T}^{ML} \begin{bmatrix} -\hat{N}PA_3 & -\hat{N}OA_3 & 1 \\ -1 & -\hat{N}OA_1 & +\hat{N}PA_1 \\ \hat{N}PA_2 & 1 & -\hat{N}OA_2 \end{bmatrix} \quad (9-24)$$

Upon performing the multiplications indicated and equating corresponding elements in the resulting matrices, the elements of \hat{T}^{BA} are computed as follows:

$$\hat{M}OA_1 = \hat{N}OA_1 - \underline{M}_{11} \hat{L}_3 \quad (9-25)$$

$$\hat{M}PA_1 = \hat{N}PA_1 - \underline{M}_{13} \hat{L}_1 \quad (9-26)$$

$$\hat{M}OA_2 = \hat{N}OA_2 - \underline{M}_{22} \hat{L}_1 \quad (9-27)$$

$$\hat{M}PA_2 = \hat{N}PA_2 + \underline{M}_{21} \hat{L}_2 \quad (9-28)$$

$$\hat{M}OA_3 = \hat{N}OA_3 + \underline{M}_{32} \hat{L}_3 \quad (9-29)$$

$$\hat{M}PA_3 = \hat{N}PA_3 + \underline{M}_{33} \hat{L}_2 \quad (9-30)$$

9.3 GYRO CALIBRATION ESTIMATION EQUATIONS

The gyro rate errors due to scale factor errors and the gyro misalignments are calculated in a deterministic fashion as implied in the first four rows of the calibration equations tabulated in Tables B-5, B-6 and B-7. In this way a minimum number of runs are required to estimate the terms and the calculations are relatively simple. The results are tabulated in Table C-5.

The remaining gyro calibration terms in \underline{Y}^G are computed by applying the least squares equation [Eq. (9-5)] to the gyro calibration equations in Tables B-5, B-6 and B-7. The results are tabulated in matrix form in Tables C-6, C-7 and C-8 of Appendix C for the minimum, partial and full levels of calibration, respectively. It will be noted that the equations do not include compensations to be applied to the \dot{M} measurements in order to account for earth rate coupling due to NOA and NSA, the elements of $(T^{GM}_T^{ML})$. These corrections can be specified in detail when the final pre-calibration alignment scheme is defined. Compensation for C_{II} and C_{SS} in the minimum calibration estimation equations is shown in Table C-6 and a similar approach is used in Table C-7 to compensate for C_{IO} and C_{IS} in the partial calibration estimation equations.

The gyro scale factor error estimation equations were determined from Eqs. (9-6) through (9-8), using the $\hat{\delta\dot{\psi}}_c$ estimates from Table C-5, (viz., $\hat{\delta\dot{\psi}}_c^+$, $\hat{\delta\dot{\psi}}_c^-$ pairs for various table rates w^T) and R'_b as estimated in \underline{Y}^G . Since a third order term is not modeled for the gyro, the F_6 term

in Eqs. (9-7) and (9-8) can be allowed to approach infinity (which eliminates the third order term) and the resulting estimation equations are as tabulated in Table C-9 of Appendix C. If the third order term is desired, the F_6 term is retained, and Eq. (9-9) provides the desired estimate (note that \hat{Q}_1 in this case would be given by Eq. (9-7)).

The elements of the \hat{T}^{BG} transformation matrix, which are a function of the misalignments of the IAs of the gyros relative to the ISU cube, are computed using Eq. (9-10) as a basis. The matrix \hat{T}^{GL} in Eq. (9-10) is composed of the estimated nonorthogonalities from Table C-5, as follows:

$$\hat{T}^{GL} = \begin{bmatrix} \hat{NSA}_1 & 1 & \hat{NOA}_1 \\ -\hat{NOA}_2 & -\hat{NSA}_2 & 1 \\ 1 & -\hat{NSA}_3 & \hat{NOA}_3 \end{bmatrix} \quad (9-31)$$

Upon inverting \hat{T}^{GL} , and writing \hat{T}^{BG} in terms of the inertial sensor misalignments to be estimated (viz., \hat{MOA} and \hat{MSA}), Eq. (9-11) is expanded to yield

$$\hat{T}^{BG} = \begin{bmatrix} 1 & -\hat{MOA}_1 & -\hat{MSA}_1 \\ \hat{MSA}_2 & 1 & \hat{MOA}_2 \\ \hat{MSA}_3 & -\hat{MOA}_3 & 1 \end{bmatrix} = \begin{bmatrix} 1 & 0 & 0 \\ 0 & 1 & 0 \\ 0 & 0 & -1 \end{bmatrix} \hat{T}^{ML} \begin{bmatrix} \hat{NSA}_3 & -\hat{NOA}_3 & 1 \\ 1 & -\hat{NOA}_1 & -\hat{NSA}_1 \\ \hat{NSA}_2 & 1 & \hat{NOA}_2 \end{bmatrix} \quad (9-32)$$

Upon performing the multiplications indicated and equating corresponding elements in the resulting matrices, the elements of \hat{T}^{BG} are computed as follows:

$$\hat{M}OA_1 = \hat{N}OA_1 - \underline{\hat{M}}_{11} \cdot \hat{L}_3 \quad (9-33)$$

$$\hat{M}SA_1 = \hat{N}SA_1 + \underline{\hat{M}}_{13} \cdot \hat{L}_1 \quad (9-34)$$

$$\hat{M}OA_2 = \hat{N}OA_2 + \underline{\hat{M}}_{22} \cdot \hat{L}_1 \quad (9-35)$$

$$\hat{M}SA_2 = \hat{N}SA_2 - \underline{\hat{M}}_{21} \cdot \hat{L}_2 \quad (9-36)$$

$$\hat{M}OA_3 = \hat{N}OA_3 + \underline{\hat{M}}_{32} \cdot \hat{L}_3 \quad (9-37)$$

$$\hat{M}SA_3 = \hat{N}SA_3 + \underline{\hat{M}}_{33} \cdot \hat{L}_2 \quad (9-38)$$

10. ERROR ANALYSIS

10.1 GENERAL FORM OF ERROR EQUATIONS

The error analysis of the calibration process is based on the general form of the calibration equation developed in Section 7. Eq. (7-1) defines the relationships between the various calibration terms (\underline{Y}) and adjusted measurements (\dot{M}), based on the average of the inertial sensor outputs over the calibration run time (Δt). The sensor outputs are compensated for significant and known inputs to the instruments such that

$$\dot{M}_j^m = \underline{H}_j^m \cdot \underline{Y}_j + \delta \dot{M}_j^m \quad (7-1) \& (10-1)$$

where $\delta \dot{M}_j^m$ is the total of all errors in the quantity \dot{M}_j^m . The error analysis consists of identifying all of the significant error sources that contribute to $\delta \dot{M}_j^m$ and then determining the effect this has on the precision with which the calibration terms can be estimated. Since the terms are estimated using Eq. (9-5), the problem is to determine the effect of $\delta \dot{M}_j^m$ on $\hat{\underline{Y}}_j$ in Eq. (9-5).

The errors are all assumed to be random variables with zero means. The analysis is generally performed on a statistical basis in terms of variances. Following this approach, it can be shown that the covariance of errors in the estimation of the calibration terms is given by the following matrix equation:

$$E[\hat{\underline{Y}} \cdot \hat{\underline{Y}}^T]_j = (\underline{H}^T \underline{H})_j^{-1} \underline{H}_j^T E[\delta \dot{\underline{M}} \cdot \delta \dot{\underline{M}}^T]_j \underline{H}_j (\underline{H}^T \underline{H})_j^{-1} \quad (10-2)$$

where

$$\begin{aligned}
 \underline{\delta \dot{M}}_j &= \text{column vector of errors } \delta \dot{M}^m \text{ for instrument } j \\
 E[\underline{\delta \dot{M}} \cdot \underline{\delta \dot{M}}^T] &\equiv \text{expected value of the matrix of error correlations} \\
 &= \text{error covariance matrix of } \underline{\dot{M}}_j, \text{ composed of} \\
 &\quad e_{ss}^m \text{ elements, the sum squared errors in } \delta \dot{M}_j^m; \\
 &\quad \text{assumed to be a diagonal matrix}
 \end{aligned} \tag{10-3}$$

$$\begin{aligned}
 E[\underline{\hat{Y}} \cdot \underline{\hat{Y}}^T]_j &\equiv \text{error covariance matrix of } \underline{\hat{Y}}_j; \text{ in which the} \\
 &\quad \text{square root of the diagonal elements are the} \\
 &\quad \text{standard errors (SE) of each of the estimated} \\
 &\quad \text{calibration terms in } \underline{\hat{Y}}_j
 \end{aligned} \tag{10-4}$$

and H_j is defined in Eq. (9-3) as a matrix whose rows are the H_j^m of Eq. (9-1), for the various test conditions (m). The error analysis now becomes a matter of defining $E[\underline{\delta \dot{M}} \cdot \underline{\delta \dot{M}}^T]_j$ for each gyro and each accelerometer.

The inertial sensor error sources ($\delta \dot{M}^m$) are identified by taking partial derivatives of the general calibration equation (7-1), as defined for the accelerometers by Eqs. (7-7) thru (7-9) and for the gyros by Eqs. (7-25) thru (7-29). Errors in the compensation corrections within the \dot{M} calculations, as given by Tables B-2 thru B-7, C-2, C-6 and C-7, must also be considered. The general categories of the error sources are associated with inertial sensor output pulse counting, sampling time, IA, OA, SA and PA orientation errors, environmental acceleration and rate effects (viz., linear and rotational vibration of the test stand), inertial sensor noise (internal and rebalance loop effects), compensation errors, second order terms and other neglected error sources. Additional error sources in the calibration of the gyros are due to test stand rate errors.

In the case of determining \hat{T}^{BA} and \hat{T}^{BG} , using Eqs. (9-24) thru (9-30) and (9-32) thru (9-38) respectively, errors in measuring the elements of \hat{T}^{ML} must be included to determine the errors in estimating the misalignments between the inertial sensor IAs and the body axes.

10.2 PRE-CALIBRATION ALIGNMENT ERRORS

One of the errors in this category is associated with the measurement of T^{ML} . Since details of the procedures have not yet been defined the error analysis of this portion of the calibration procedure must be postponed. The effect of the errors, however, is not difficult to incorporate later since they occur at the end of the analysis, in the determination of \hat{T}^{BA} and \hat{T}^{BG} as shown in Eqs. (9-25) thru (9-30) and (9-33) thru (9-38), respectively.

The effect of errors in T^{ML} on compensation for earth rate coupling in the gyro calibration process are of second order and completely negligible. The accelerometer calibration process does not use T^{ML} compensation, except as noted above in the computation of \hat{T}^{BA} .

Pre-calibration alignment errors due to use of the bubble levels and indexing of the ISU have not been defined in detail pending final definition of the pre-calibration alignment procedure and significant error sources. The primary effect is expected to be associated with compensation of the accelerometer output for $\delta\phi_E$ and $\delta\phi_N$ changes. ISU indexing precision will also affect the accuracy with which the gyro nonorthogonality terms can be estimated.

10.3 ENVIRONMENTAL ERROR SOURCES

The effect of test stand base motion is to cause extraneous rates and accelerations to be sensed by the gyros and accelerometers. The analysis is patterned after that in the UNIVAC study as pointed out in the ground rules (Section 2.3), and the significant error sources are:

$$\Delta\phi_n \equiv \text{change in } \delta\phi_N \text{ and } \delta\phi_E \text{ (the derivative of this } (\Delta\dot{\phi}_n) \text{ is also considered an error source)}$$
$$a_v \equiv \text{vibration acceleration, assumed to be isotropic in all directions}$$

These errors are specified in terms of power spectral densities (PSDs) as shown in Figs. 10-1 and 10-2*. The PSDs are approximated for computational purposes as shown in Tables 10-1 and 10-2**. It is noted in Table 10-1 that there are several apparent inconsistencies between Table 10-1 and Fig. 10-1. Since a ground rule of the analysis was to use the results of the UNIVAC study (Ref. 4), this was done as shown in Appendices E and F. Generally, a conservative approach was taken. The discrepancies should be resolved, however, since the error source is significant (for both the gyros and accelerometers) and the expected calibration precision is directly influenced.

Since the effect of $\Delta\phi_n$ on the accelerometer output is particularly critical, as discussed in Section D.1 of Appendix D, the bubble level compensation procedure presented in Sections 8.2 and 8.3 is specified. The objective is to attenuate the low frequency portion of the $\Delta\phi_n$ spectrum. In

*These PSD's are as listed in Ref. (4), Figs. 3-3 and 3-4, which in turn were reproduced from those presented in Ref. (8), Fig. 1-1.

**The approximations are as listed in Ref. (4), Tables A-3 and A-2.

accordance with the ground rules of Section 2.3, the UNIVAC analyses was used. On page 2-17 of Ref. 4, the following two models were proposed to characterize the use of bubble level compensation:

- (1) The rotational noise spectrum, PSD ($\Delta\phi_n$), was reduced to zero below a frequency corresponding to a 50 minute period.
- (2) The rotational noise spectrum, PSD ($\Delta\phi_n$), was assumed to be the squared modulus of a first order transfer function having an RMS noise in $\Delta\phi_n$ of 4.5 $\widehat{\text{sec}}$ and a half-power frequency of 10^{-2} Hz, corresponding to a 1.7 minute period.

The results on the accelerometer output using these assumptions are plotted in Fig. E-5, as reproduced from Fig. 2-5 on Ref. 4. Model #1 yields unsatisfactory performance and would imply that compensation is required more often than every 50 minutes. Model #2 is more compatible with the calibration precision goals and is used in the error analysis. A preliminary analysis has indicated that the true model may be one that slopes to zero as the frequency decreases from that corresponding to the averaging time. Because of the critical nature of the error source, it is recommended that further analyses be conducted.

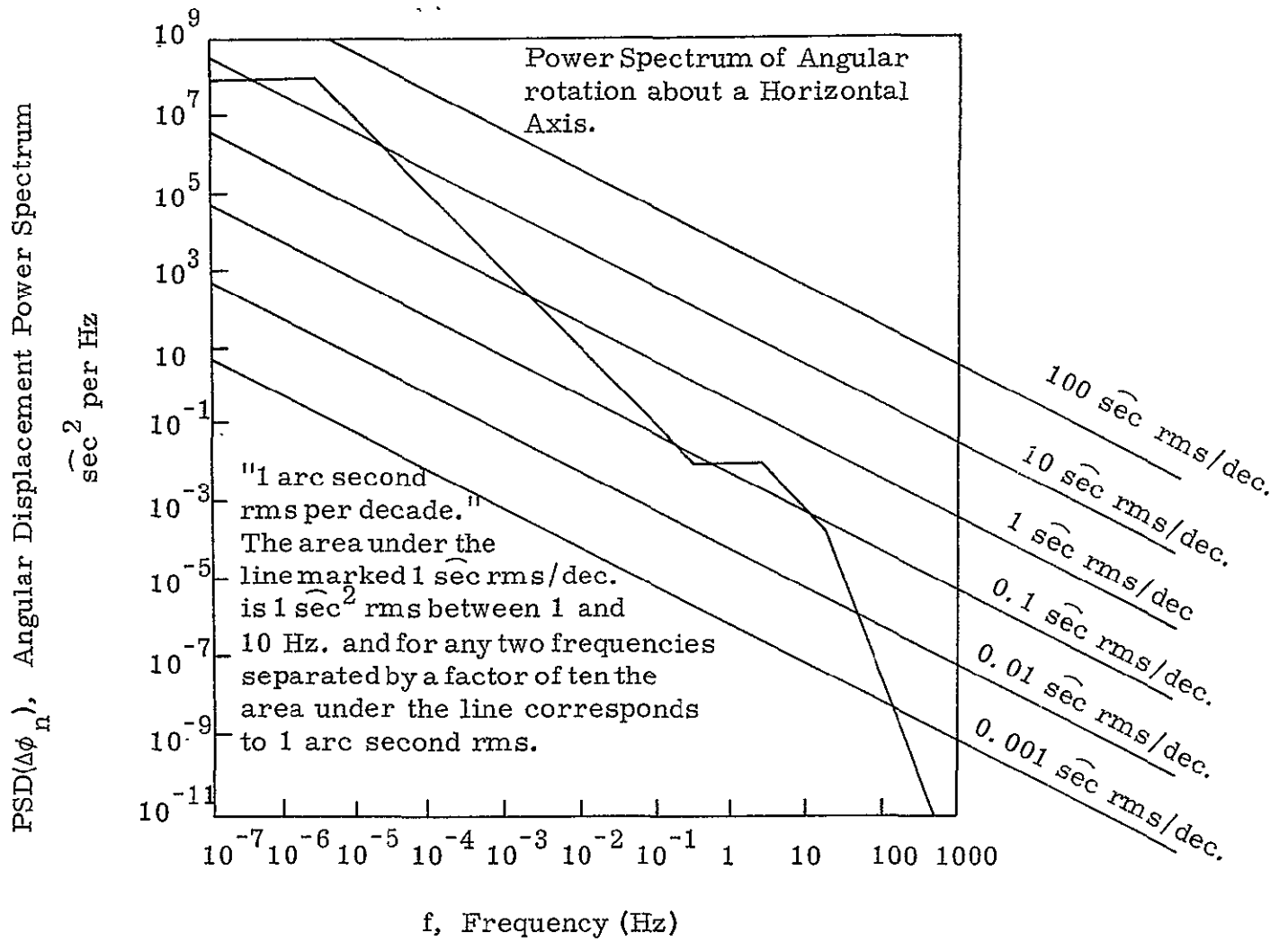


Figure 10-1 Representative Angular Vibration and Base Motion of Test Stand

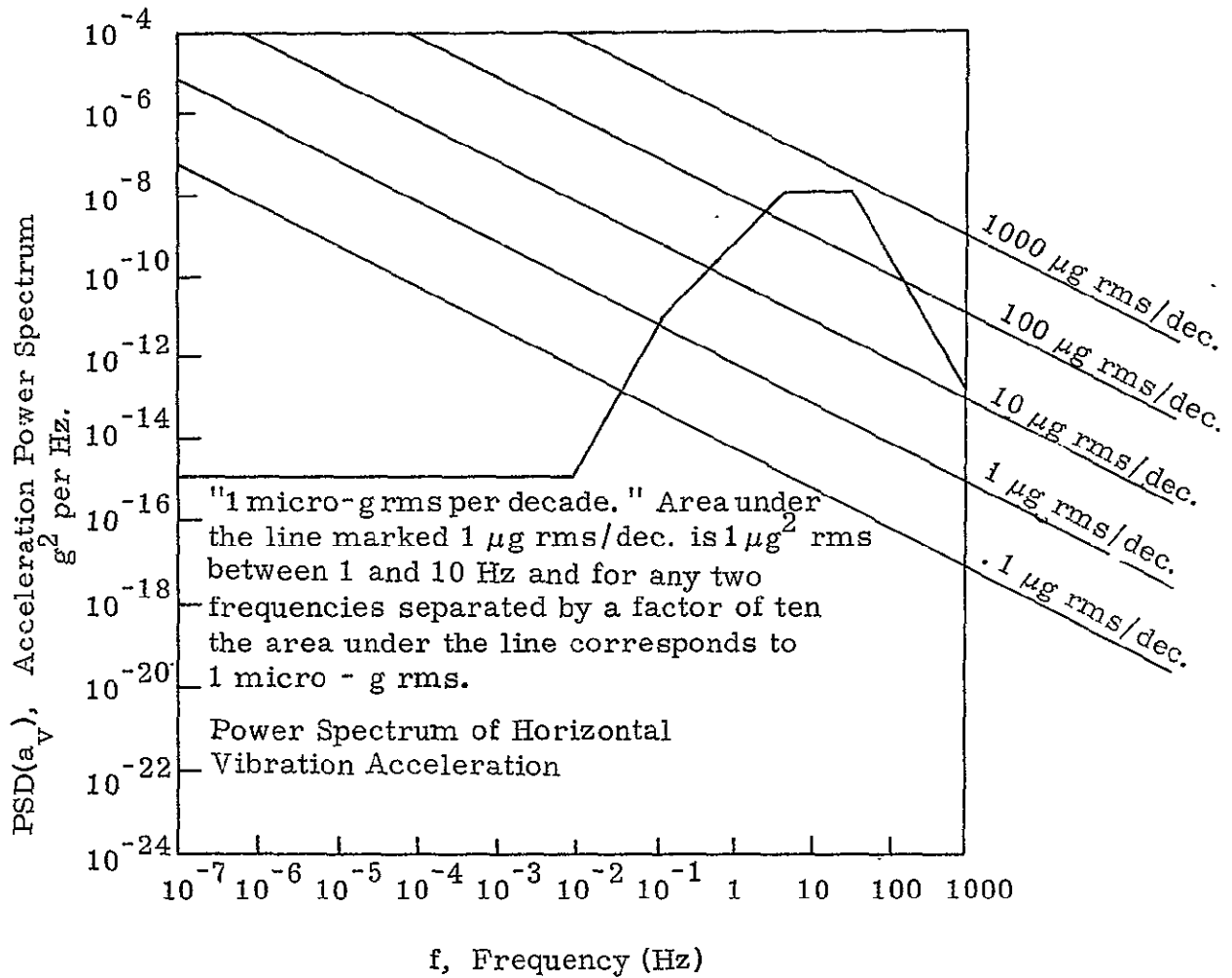


Figure 10-2 Representative Linear Vibration of Test Stand

Table 10-1 Approximation of Test Stand Angular Vibration PSD

f (Hz)	PSD ($\Delta\phi_n$)	
	rad ² /Hz	sec ² /Hz
0. to 5×10^{-6}	9.42×10^{-4}	4.0×10^7
5×10^{-6} to .317	$2.345 \times 10^{-4} f^{-2}$	$9.95 \times 10^6 f^{-2}$
.317 to 3.17	2.345×10^{-13}	10^{-2}
3.17 to 15.7	$2.345 \times 10^{-12} f^{-2}$	$9.95 \times 10^{-2} f^{-2}$
above 15.7	$1.022 \times 10^{-8} f^{-5}$	$4.34 \times 10^2 f^{-5}$

Notes:

- (1) This table was derived from Table A-2 of Ref. (4) by removing the earth rate coefficient of PSD ($\Delta\phi_n$).
- (2) The second and third lines of the table are as listed in Ref. (4) even though the values do not correspond to those in Fig. 10-1. This is discussed in the text (Section 10.3)

Table 10-2 Approximation of Test Stand Linear Vibration PSD

f (Hz)	PSD(a_v), g^2 /Hz
0 to 10^{-2}	10^{-15}
10^{-2} to 10^{-1}	10^{-11}
10^{-1} to 1	10^{-9}
1 to 10^{2*}	10^{-8}
10^2 to 10^3	10^{-11}
above 10^3	0

* This was listed as 10^3 in Table A-3 of Ref. (4).

10.4 ACCELEROMETER ERROR ANALYSIS

10.4.1 Error Sensitivities

The accelerometer error sources were identified as described in Section 10.1. The detailed error sources considered are tabulated in Table 10-3, including 1σ values of the magnitudes of the errors. It is noted in the table that pre-calibration alignment error sources are to be determined, as discussed in the previous sections (10.2 and 10.3).

The effect of these error sources on the accelerometer output (i. e., components of $\delta\dot{M}^m$) are considered in detail in Appendix E for each test condition (m). Each component of $\delta\dot{M}^m$ is related to the error sources of Table 10-3 as shown in Tables E-1 and E-2. The actual propagation of the errors is shown in Table E-1, for accelerometer #1, and Table E-2 is a summary of the numerical calculations used to determine the accelerometer error covariance matrix elements for each test condition (m).

Appendix E also contains plots of the effect on $\delta\dot{M}$ of each potentially significant error source (see Figs. E-1 thru E-6). Use of these plots is discussed in Appendix E. Fig. E-1 graphically shows the estimation precision goals stated in Table 4-3 and provides a basis for determining acceptable levels of the various error sources, as described in Appendix E. The critical error source is shown in Table E-2 to be the cross-coupling of gravity due to rotation of the test stand base ($\Delta\phi_n$). The errors listed are for the case when bubble levels are used. Detailed discussions of errors associated with bubble level compensation are contained in Sections 10.2, 10.3 and D.1. Fig. E-5 shows the final effect on $\delta\dot{M}$, as a function of run time (Δt).

TABLE 10-3 ACCELEROMETER ERROR SOURCES CONSIDERED

<u>ERROR. NO.</u>	<u>ERROR SOURCE</u>	<u>SYMBOL</u>	<u>1 σ VALUE</u>
1	Compensation for C_{IO}	δC_{IO}	(1)
2	Compensation for C_{IP}	δC_{IP}	(1)
3	Compensation for magnitude of g (effect of error is correlated)	δg	.3 μg
4	Compensation for ISU cube to bubble level misalignment (for calculating \hat{T}^{BA})	$\delta(\underline{B} \cdot \underline{L})$	(2)
5	Compensation for $\{\delta \phi_E, \delta \phi_N\}$		(2)
6	Error in setting bubble level to null	$(\underline{L} \cdot \underline{V})$	1 $\widehat{\text{sec}}$
7	TAF ϕ_3 positioning error	$\delta \phi_3$	(2)
8	TAF ϕ_4 positioning error	$\delta \phi_4$	(2)
9	Nonorthogonality of ϕ_3 and ϕ_4 axes	MO3'	(2)
10	Nonorthogonality of ϕ_3 and ϕ_4 axes	MR3'	(2)
11	Misalignment of IA to body axes (cube)	MIA ⁽³⁾	5/3 $\widehat{\text{min.}}$
12	Misalignment of OA to body axes (cube)	$(\underline{O}^A \cdot \underline{B})$	10/3 $\widehat{\text{min.}}$
13	Misalignment of PA to body axes (cube)	$(\underline{P} \cdot \underline{B})$	10/3 $\widehat{\text{min.}}$
14	Misalignment of body axis to bubble level	$(\underline{B} \cdot \underline{L})$	10.4/3 $\widehat{\text{min.}}$
15	Effect of uncompensated C_{IP}	C_{IP}	10 μg
16	Effect of uncompensated C_{IO}	C_{IO}	10 μg
17	Sampling time error	$\delta(\Delta t)$	100 $\mu \text{ sec}$
18	Quantization	q^A	$\frac{.0025 \sqrt{2}}{\sqrt{12}}$ fps
19	Accelerometer internal random noise	$e_{nr}^A dt$	negligible
20	Accelerometer rebalance loop noise	e_{nreb}^A	included with #18

TABLE 10-3 ACCELEROMETER ERROR SOURCES CONSIDERED
(Cont.)

<u>ERROR NO.</u>	<u>ERROR SOURCE</u>	<u>SYMBOL</u>	<u>1 σ VALUE</u>
21	Angular base motion of test stand, about level axes	$\Delta\phi_n$	See Section 10.3
22	Linear vibration of test stand(in all directions)	a_v	See Figure 10-2

Negligible Error Sources

- $Q_{IP} w_p w_i$
- Compliance (other than C_{IO} and C_{IP})
- Rotational cross-coupling
- Cross-coupling of accelerations along OA
- Second order terms (except as listed above)

Notes: (1) These error sources are assumed negligible for this analysis, pending results from laboratory tests

(2) Values for these error sources are to be determined once the pre-calibration alignment scheme is specified in detail

(3) $MIA \equiv (MOA^2 + MPA^2)^{1/2}$

The error covariance matrix elements derived in Table E-2 were used in Eq. (10-2) to determine the expected precision (i. e., standard error) with which each accelerometer calibration term can be estimated. This is considered in the next section.

10.4.2 Expected Accelerometer Calibration Precision

The error covariance matrix elements required to perform the error analysis using Eq. (10-2) are derived in Table E-2 and summarized in Table 10-4. The H matrix required in Eq. (10-2) is given for each accelerometer in Tables B-2, B-3 and B-4 by selecting the appropriate rows according to the measurements used in the estimation equation being analyzed (see Tables C-1, C-2 and C-3). The results of the accelerometer error analysis are summarized in Table 10-4.

Generally the estimation precision goal is met, except for $\delta \dot{V}_c^{-.7}$ for accelerometer #3 which is 32% over the goal. It should be mentioned that not all error sources have been included, as discussed in Sections 10.2 and 10.3, pending final definition of the pre-calibration alignment procedure.

The effect of δg (equal to $3\mu g$) is included in the $\delta \dot{V}_c$ terms, taking into account the fact that the error is correlated between the various $\delta \dot{M}$. The error propagates one-to-one for $\delta \dot{V}_c^{+1}$ and $\delta \dot{V}_c^{-1}$ and by $1/\sqrt{2}$ for $\delta \dot{V}_c^{+.7}$ and $\delta \dot{V}_c^{-.7}$. The error has no effect on the other calibration terms.

The precision of the Minimum and Partial Calibration processes are essentially the same as that shown in Table 10-4, which is for the Full Accelerometer Calibration Process. In the case of Partial Calibration,

TABLE 10-4 EXPECTED ACCELEROMETER CALIBRATION PRECISION

Calibration Term Estimated	Units	Precision Goal	Standard Error(SE) of \underline{y} in Accel. #			
			#1(z)	#2(x)	#3(y)	#1(all data)
\hat{A}_b	μg	8.3	3.96	3.76	3.98	2.41
$-(NOA) g$	μg	TBD	6.43	5.35	3.72	2.91
$(NPA) g$	μg	TBD	3.59	3.76	6.62	3.40
$\hat{\delta V}_C^{+1}$	μg	8.3	3.02	3.02	3.02	3.02
$\hat{\delta V}_C^{-1}$	μg	8.3	3.02	3.02	3.02	3.02
$\hat{\delta V}_C^{+.7}$	μg	8.3	3.28	3.28	11.00	2.77
$\hat{\delta V}_C^{-.7}$	μg	8.3	3.28	6.70	2.77	2.77
\hat{C}_{IP}	$\mu g/g^2$	TBD	10.39	8.63	6.35	5.43
\hat{C}_{IO}	$\mu g/g^2$	TBD	7.14	7.02	12.28	5.98

Square Root of Error Covariance
Diagonal Elements

	#1	#2	#3	#1(all)
m	$\sqrt{e_{ss}^m}$	$\sqrt{e_{ss}^m}$	$\sqrt{e_{ss}^m}$	$\sqrt{e_{ss}^m}$
4	.63	6.2	6.2	.63
5	6.2	6.2	.63	6.2
6	6.2	.63	6.2	6.2
1	5.00	-	.54	5.00
2	-	.54	5.00	5.00
3	.54	5.00	-	.54
7	3.56	-	3.56	3.56
8	3.56	3.56	-	3.56
9	-	3.56	3.56	5.00
10	3.56	-	3.56	3.56
11	3.56	3.56	5.00	3.56
12	5.0	3.56	3.56	5.0
13	-	3.56	-	-

compensation for C_{IO} and C_{IP} is required. Errors in this compensation will only cause additional errors in $\hat{\delta V}_c^{+.7}$ and $\hat{\delta V}_c^{-.7}$ that are equal to $.5g^2 \delta C_{IO}$ and $.5g^2 \delta C_{IP}$.

Included in Table 10-4 is a column that indicates the expected calibration precision assuming all data available is utilized. This was done only for accelerometer #1 to illustrate the potential improvement that is possible. However, it does not necessarily follow that more data (i. e., measurements \hat{M}) will always yield better results. Since the least squares estimation algorithm is not optimum, it is possible that an additional measurement can have a relatively large error associated with it that can propagate through the weighting coefficients (of Appendix C) so as to cause certain terms to be estimated with less accuracy. A weighted least square algorithm would provide weighting coefficients that could avoid this problem. It is possible that the relatively large error associated with $\hat{\delta V}_c^{+.7}$ for accelerometer #3 could be reduced in this manner. A study of this approach is recommended.

The precision with which T^{BA} can be estimated is dependent upon the measurement accuracy of T^{ML} , as well as $SE(\hat{NOA})$ and $SE(\hat{NPA})$ as indicated by Eqs. (9-25) thru (9-30). The error propagation is one-to-one. From Table 10-4,

$$.7 \widehat{\text{sec}} \quad SE\{\hat{NOA}, \hat{NPA}\} < 1.4 \widehat{\text{sec}} \quad (10-5)$$

which is within the precision goal of $1.7 \widehat{\text{sec}}$. To meet this goal, $SE(T^{ML})$ must be $< 1.0 \widehat{\text{sec}}$.

10.5 GYRO ERROR ANALYSIS

10.5.1 Error Sensitivities

The gyro error sources were identified as described in Section 10.1. The detailed error sources considered are tabulated in Table 10-5, including 1σ values of the magnitudes of the errors. It is noted in the table that pre-calibration alignment error sources are to be determined, as discussed in the previous sections (10.2 and 10.3).

The effect of these error sources on the gyro output (i. e. , components of $\delta\dot{M}^m$) are considered in detailed in Appendix F for each test condition (m). Each component of $\delta\dot{M}^m$ is related to the error sources of Table 10-5 as shown in Tables F-1 and F-2. The actual propagation of the errors is shown in Table F-1, for gyro #1, and Table F-2 is a summary of the numerical calculations used to determine the gyro error covariance matrix elements for each test condition (m).

Appendix F also contains plots of the effect on $\delta\dot{M}$ of each potentially significant error source (see Figs. F-1 thru F-8). Use of these plots is discussed in Appendix F. Figs. F-1 thru F-3 graphically show the estimation precision goals stated in Table 4-5 and provides a basis for determining acceptable levels of the various error sources, as described in Appendix F. The critical error sources are shown in Table F-2 to be the angular rate of vibration of the test stand ($\Delta\dot{\phi}_n$) and the nonuniform table rate error (NUWT). Very little can be done economically with the former, other than perhaps to provide a more massive foundation for the test stand, whereas the later error may be reduced by a better quality table rate drive. For the gyro scale factor tests, the largest error source is the test table rotary angle

TABLE 10-5 GYRO ERROR SOURCES CONSIDERED

<u>ERROR NO.</u>	<u>ERROR SOURCE</u>	<u>SYMBOL</u>	<u>1 σ VALUE</u>
1	Compensation for C_{II}	$\delta \dot{C}_{II}$	(1)
2	Compensation for C_{SS}	δC_{SS}	(1)
3	Compensation for C_{IO}	δC_{IO}	(1)
4	Compensation for C_{IS}	δC_{IS}	(1)
5	Compensation for ISU cube to bubble level misalignment (for calculating \hat{T}^{BG})	$\delta(\underline{B} \cdot \underline{L})$	(2)
6	Compensation for earth rate coupling through $T^{GM}T^{ML}$	$\delta(\underline{G} \cdot \underline{L})$	$< .5/3 \widehat{\text{min.}}$
7	Bubble level coordinate frame to table axis misalignment.	$(\underline{L} \cdot \underline{R}')$	(2)
8	Nonorthogonality of ϕ_3 and ϕ_4 axes	$MO3'$	(2)
9	Nonorthogonality of ϕ_3 and ϕ_2 axes	$MR3'$	(2)
10	TAF ϕ_3 positioning error	$\delta\phi_3$	(2)
11	TAF ϕ_4 positioning error	$\delta\phi_4$	TBD(2)
12	Scale factor error at earth rate	δQ_e	200/3 ppm
13	Azimuth misalignment of bubble level coordinate frame to East	$(\underline{L} \cdot \underline{N})$	20 $\widehat{\text{sec}}$
14	Misalignment of gyro IA to body axes(cube)	$MIA^{(3)}$	5/3 $\widehat{\text{min.}}$

TABLE 10-5 GYRO ERROR SOURCES CONSIDERED
(cont.)

<u>ERROR NO.</u>	<u>ERROR SOURCE</u>	<u>SYMBOL</u>	<u>1 σ VALUE</u>
15	Misalignment of gyro SA to body axes about IA	$(\underline{S}^G \cdot \underline{B})$	10/3 $\widehat{\text{min}}$
16	Misalignment of body axes to bubble level	$(\underline{B} \cdot \underline{L})$	10.4/3 $\widehat{\text{min}}$.
17	Effect of uncompensated B_I	(B_I)	1.5 $^\circ$ /hr/g
18	Effect of uncompensated B_S	B_S	1.5 $^\circ$ /hr/g
19	Tilt of test table axis about East	$\delta\phi_E$.2 $\widehat{\text{min}}$.
20	Nonuniform table rate	NUWT	3.7 $\widehat{\text{sec}}$
21	Tilt of test table axis about North	$\delta\phi_N$.2 $\widehat{\text{min}}$
22	Distance of gyro along normal to table axis	m	10 inches
23	Sampling time error	$\delta(\Delta t)$	100 μsec
24	Uncertainty of test table angle read out	$\delta(\Delta\phi_2)$	6 $\widehat{\text{sec}}$
25	Quantization	q^G	See Note (4)
26	Gyro random noise	\dot{e}_{nr}^G	See Table 4-6
27	Gyro rebalance loop noise	\dot{e}_{nreb}^G	Included in #25
28	Angular vibration of test stand base, about level axis	$\Delta\phi_n$	See Fig. 10-1
29	Angular test stand rate about level axis	$\dot{\Delta\phi}_n$	See Fig. D-17
30	Error in setting table rate	$\delta(w^T)$.5%

TABLE 10-5 GYRO ERROR SOURCES CONSIDERED

(cont.)

Negligible Error Sources

- Linear environmental vibration
- Error in setting bubble level to null
- Second order terms (except as listed above)

- Notes:
- (1) These error sources are assumed negligible for this analysis, pending results from laboratory tests
 - (2) Values for these error sources are to be determined once the pre-calibration alignment scheme is specified in detail
 - (3) $MIA = (MOA^2 + MSA^2)^{1/2}$
 - (4) $q_i^G = .844 \widehat{\text{sec}}$ for $|w_i| < 30^\circ/\text{sec.}$ and $1.688 \widehat{\text{sec}}$ for $30 < |w_i| < 60^\circ/\text{sec.}$

output error ($\delta(\Delta\phi_2)$) with misalignment of the gyro IA parallel to the rotary axis as the next largest. Both of these errors could be reduced without much trouble, if desired. Use of the bubble levels has little effect on the gyro calibration precision (other than in measuring T^{ML}).

The error covariance matrix elements derived in Table F-2 were used in Eq. (10-2) to determine the expected precision (i. e., standard error) with which each gyro calibration term can be estimated. This is considered in the next section.

10.5.2 Expected Gyro Calibration Precision

The error covariance matrix elements required to perform the error analysis using Eq. (10-2) are derived in Table F-2 and summarized in Table 10-6. The H matrix required in Eq. (10-2) is given for each gyro in Tables B-5, B-6 and B-7 by selecting the appropriate rows according to the measurements used in the estimation equation being analyzed (see Tables C-7, C-8 and C-9). The results of the gyro error analysis are summarized in Table 10-6.

Generally, the estimation precision goal is essentially met* for the bias and g sensitive terms, except B_I for gyro #2 which is about 50% over the goal. For the major compliance terms, the errors are from 30% to 62% over but probably are only significant for the C_{II} term of the Z gyro (#1), since the IAs and SAs are all nominally level for the other two gyros when in flight. If all the measurements (i. e., 2 extra samples) are used,

* within approximately 20% of the goal

TABLE 10-6 EXPECTED GYRO CALIBRATION PRECISION

Calibration Term Estimated	Units	Precision Goal	Standard Error(SE) of \underline{Y} in Gyro #			
			#1(z)	#2(x)	#3(y)	#1(all data)
\hat{R}_b	mdh	7.0	8.52	7.42	7.77	7.03
\hat{B}_I	mdh/g	7.0	6.30	10.33	6.02	2.78
\hat{B}_S	mdh/g	7.0	8.54	7.45	7.29	8.54
\hat{B}_O	mdh/g	7.0	8.54	7.74	6.38	6.96
\hat{C}_{II}	mdh/g ²	8.3	13.46	13.93	10.90	8.15
\hat{C}_{SS}	mdh/g ²	8.3	11.66	10.75	11.00	10.83
\hat{C}_{IS}	mdh/g ²	8.3	17.26	19.07	16.05	14.90
\hat{C}_{IO}	mdh/g ²	8.3	17.23	15.21	14.98	12.93
\hat{C}_{OS}	mdh/g ²	8.3	20.45	29.34	20.82	17.09

Square Root of Error Covariance
Diagonal Elements

m	#1	#2	#3	#1(all)
	$\sqrt{e_{SS}^m}$	$\sqrt{e_{SS}^m}$	$\sqrt{e_{SS}^m}$	$\sqrt{e_{SS}^m}$
4	2.8	11.4	11.4	2.8
5	11.4	11.4	2.8	11.4
6	11.4	2.8	11.4	11.4
1	12.4	12.4	-	12.4
2	12.4	-	12.4	12.4
3	-	12.4	12.4	2.7
7	8.9	-	8.9	8.9
8	8.9	8.9	-	8.9
9	-	8.9	8.9	12.3
10	8.9	12.3	8.9	8.9
11	8.9	8.9	12.3	8.9
12	12.3	8.9	8.9	12.3
13	-	8.9	12.3	-

the goal can be met, as shown in Table 10-6. In the case of the cross compliance terms, the errors are from 80 to 150% over and in the case of C_{SS} for the #2 gyro (x), 250% over. The estimation precision goals can probably be relaxed for the cross compliance terms since gravity effects will yield only second order errors under normal flight conditions, and in the worst case, when the ISU is tilted 45° from the nominally level position the resulting rate errors propagate at half the values shown in Table 10-6. Although not all error sources have been included (viz., those associated with the pre-calibration alignment procedure), they are not anticipated to alter the results of Table 10-6 significantly. They are important, however, in the estimation precision of \hat{T}^{BG} , which is discussed below.

The precision of the Minimum and Partial Calibration processes are approximately the same as that shown in Table 10-4, which is for the Full Gyro Calibration process. In the case of Minimum Calibration, compensation for C_{II} and C_{SS} is required. Errors in this compensation will only cause additional errors in R_b and B_I that are equal to $.5\delta C_{SS}$ and $(.5\delta C_{SS} + \delta C_{II})$, respectively. The total error should be about the same as that shown in Table 10-6. The B_S and B_O terms are not affected at all. In the case of Partial Calibration, compensation for C_{IO} and C_{IS} is required. Errors in this compensation propagate at 40% into the estimation of the \hat{B}_I and \hat{C}_{II} terms, and is expected to cause a slight degradation in estimation precision compared to that of a Full Calibration. The other terms are unaffected.

Included in Table 10-6 is a column that indicates the expected calibration precision assuming all data available is utilized. This was done only for gyro #1 to illustrate the potential improvement that is possible. However, it does not necessarily follow that more data

(i. e., measurements \dot{M}) will always yield better results. Since the least squares estimation algorithm is not optimum, it is possible that an additional measurement can have a relatively large error associated with it that can propagate through the weighting coefficients (of Appendix C) so as to cause certain terms to be estimated with less accuracy. A weighted least square algorithm would provide weighting coefficients that could avoid this problem. It is possible that the relatively large errors associated with B_I , C_{II} and C_{OS} for gyro #2 and C_{II} for gyro #1 could be reduced in this manner. A study of this approach is recommended.

The precision with which T^{BG} can be estimated is dependent upon the measurement accuracy of T^{ML} , as well as $SE(\hat{NOA})$ and $SE(\hat{NSA})$ as indicated by Eqs. (9-33) thru (9-38). The error propagation is one-to-one. The precision with which NOA and NSA can be estimated is determined using the estimation equations in Table C-5 and the $\delta\dot{M}$ errors given in Table F-2 for $m = 41, 51$ and 61 and $|W^T| = 2^\circ/\text{sec}$. The results are as follows:

$$SE \{ \hat{NOA}, \hat{NSA} \} = \frac{11.13 \times 10^{-3}}{\pi [2 - (-2)] / 360} = .32 \widehat{\text{sec}} \quad (10-6)$$

The error in knowing W^T has an insignificant effect in Eq. (10-6). Considering errors in aligning the bubble levels to the test table rotary axis, and errors in the measurement of T^{ML} , a total of $(1.7^2 - .32^2)^{1/2} = 1.6 \widehat{\text{sec}}$ (1σ) can be allocated to these measurements and yet meet the estimation precision goal of $1.7 \widehat{\text{sec}}$ (1σ).

In the case of the gyro scale factor error estimate, the errors propagate one-to-one as shown in Table C-5. From Table F-2, for $m = 72, 82,$ and $92,$

$$SE(\hat{\psi}_c) = \delta\dot{M} = 18.6 \text{ mdh for } W^T = \pm 2^\circ/\text{sec} \quad (10-7)$$

for any of the three gyros. This is within the precision goal of 62 mdh, as shown in Fig. F-2.

11. CONCLUSIONS

The following conclusions are drawn from the studies made:

1. The calibration system and procedure developed in this study can be used in the laboratory as well as under field conditions.
2. The calibration can be performed within an 8 hour period, providing a minimum number of gyro scale factor rates are used.
3. Accelerometer calibration precision is generally within the goals specified.
4. Gyro calibration precision is generally equal to the goals specified, except the B_I term of gyro #2 (which is 13 mdh/g, rather than 7 mdh/g).
5. Estimation precision of the compliance terms is worse than that for the basic terms, but probably of acceptable level for the accelerometers and marginal to probably acceptable for the gyros.
6. The additional runs required to estimate the cross compliance terms generally have only a minor affect on the precision with which the other terms can be estimated.
7. Errors in the knowledge of $|g|$ affect only the accelerometer scale factor terms.
8. The data sampling error ($\delta(\Delta t)$) is critical for the gyros, but not the accelerometers.
9. The angular vibration ($\Delta\phi_n$) is critical for the accelerometers and the angular vibration rate ($\Delta\dot{\phi}_n$) is critical for the gyros.

10. Using data from additional runs to improve precision of estimates does not always yield the desired results, depending upon the errors associated with the additional measurements.
11. The hardware requirements to support the total calibration process are considered to be feasible technically and economically. The alignment accuracy of the ISU and TAF gimbals before each run, however, are yet to be specified in final detail.

12. RECOMMENDATIONS

It is recommended that development of the calibration procedure continue along the lines currently being followed since most objectives are basically being met. However, the design can very likely be improved, if deemed necessary, by considering a different combination of test conditions. The primary results of this would be to reduce test time and possibly improve estimation precision. Alternatively, estimation precision requirements should be reviewed to determine if any can be relaxed, particularly for the gyro cross compliance terms.

Another way to provide significant improvements in the design is to consider using weighted least squares, particularly for estimation of the scale factor error coefficients. This is recommended since instances of reduced calibration precision for certain terms were experienced in this study upon using additional data, due to the relative errors of the various measurements. This effect would be eliminated using weighted least squares estimation algorithms, and may provide significant improvements in calibration precision and/or reduce test time with little effect on computational complexity.

It is also recommended that the resolution of the test table pulse output (for $\Delta\phi_2$) be improved from $6 \widehat{\text{sec}} (1\sigma)$ to approximately 1 to 2 $\widehat{\text{sec}}$, along with reducing the sampling time error from 100 μsec to about 10 μsec . If the nonuniformity of table rate (NUWT) can be held better than 4.3 $\widehat{\text{sec}}/\text{rev}$ (as defined in Eq. (6-1)), gyro calibration precision can be further improved significantly. Reduction much less than $\sim 2 \widehat{\text{sec}}/\text{rev}$ is not warranted, however, assuming the other errors remain as shown in this report.

It is believed that the pre-calibration alignment procedure proposed is basically sound and is an improvement over previously used methods. It is recommended that development of the method be continued along the lines proposed, and that the associated procedures and error analysis be updated accordingly. Similarly, final details of the data collection system require definition.

The "base-line" design proposed herein should be reviewed to determine what changes are desired, if any, to provide a more "balanced" design (i. e., tradeoffs between the various equipment performance requirements, calibration run times, alternate procedures, etc.). Not only is the error analysis useful in doing this, but consideration should be given to the revisions associated with use of the flight computer to collect and reduce the data, assuming a final decision is made along these lines.

It is recommended that the error analysis be revised to reflect more final consideration of the various error sources. Also analysis of the final precision in estimating T^{BA} and T^{GA} should be performed, as well as that of the scale factor error coefficients. This would include analysis of errors to be identified once the final pre-calibration alignment procedures are finalized.* The effect of errors in compensation for compliance terms in the Minimum and Partial Calibration procedures should also be refined.

It is strongly recommended that the apparent inconsistencies of the environmental models and associated error analysis in the Univac study be resolved and the analyses in this report corrected accordingly. Not only is

* Such as compensation for $\delta\phi_N$ and $\delta\phi_E$, gimbal nonorthogonalities, gimbal angle readout nonlinearities, etc.

the environmental angular motion particularly critical, but an initial investigation has indicated a better analytical approach that will more realistically determine the effect of bubble level compensation.

Finally, it is recommended that the centrifugal acceleration analysis be refined to reflect a more precise value of the moment arm (m) of the gyros from the SATS rotary axis. This effect on the gyro scale factor error coefficients is potentially significant at the higher table rates.

13. REFERENCES

1. "Operational Alignment and Calibration of a Strapdown Inertial Guidance System", D. O. Benson, Jr., W. H. Fincke, H. J. Rome, D. E. Lev, DRC Report E-1863U (Interim Scientific Report for NASA Electronics Research Center), Aug. 1969.
2. "Definition of Calibration Task", W. H. Fincke, DRC letter report E-1891U to NASA Electronics Research Center, Aug. 29, 1969
3. "Strapdown Calibration and Alignment Study: Volume 1- Development Document", UNIVAC Federal Systems Division prepared for Electronics Research Center, NASA (NAS-12-577), 1968.
4. "Strapdown Calibration and Alignment Study: Volume 2 - Procedural and Parametric Trade-off Analyses Document", UNIVAC Federal Systems Division, prepared for Electronics Research Center, NASA (NAS 12-577), 1968.
5. "Strapdown Calibration and Alignment Study: Volume 3 - Laboratory Procedures Manual", UNIVAC Federal Systems Division, prepared for Electronics Research Center, NASA (NAS 12-577), 1968.
6. "Axis Definitions for CH-46C Helicopter and Inertial Sensing Unit", A. H. Lipton, memorandum, NASA-ERC, January 3, 1969.
7. "GG334 Gas Bearing Gyro, Technical Description ASD-3", Honeywell Aeronautical Division, Minneapolis, November 28, 1966.
8. "Design of a Precision Tilt and Vibration Isolation System", H. Weinstock, NASA TR R-281, ERC, March 1968.
9. "The Mechanization of a Strapdown Inertial System Based on Time-Modulated Torquing", A. E. Scoville and J. Yamson, United Aircraft Corporate Systems Center Report.

APPENDIX A
DEVELOPMENT OF ACCELEROMETER MATH MODEL

The purpose of this appendix is to document the salient errors associated with a pendulum type of accelerometer under the condition of vigorous linear and angular case motions. Detailed derivations are not presented, rather the error sources are stated and categorized.

The performance equation for a pendulous accelerometer (Fig. A-1) can be evolved by writing a moment equation about the accelerometer output axis, thus,

$$I_o (\ddot{\theta}_o + \dot{\omega}_o) = -D\dot{\theta}_o - K\theta_o + T_u + \Sigma T_{OA} \quad (A-1)$$

where I_o , D , and K are the moment of inertia, damping constant and spring constant, respectively and θ_o is the pickoff angle on the output axis. The spring constant in pulse-rebalanced instruments is the result of torquing the float so as to null the float error angle. T_u denotes the uncertainty torques, while ΣT_{OA} represents the sum of all remaining kinematic and gravity related torques. This last term can be separated as follows:

$$\Sigma T_{OA} = \Sigma T_{\substack{\text{linear} \\ \text{accel.}}} + \Sigma T_{\text{(gyroscopic)}} + \Sigma T_{\substack{\text{rotational} \\ \text{accel.}}} \quad (A-2)$$

Using small angle approximations, the component of output-axis torque due to linear accelerations in the absence of mass unbalance and gimbal deformations is

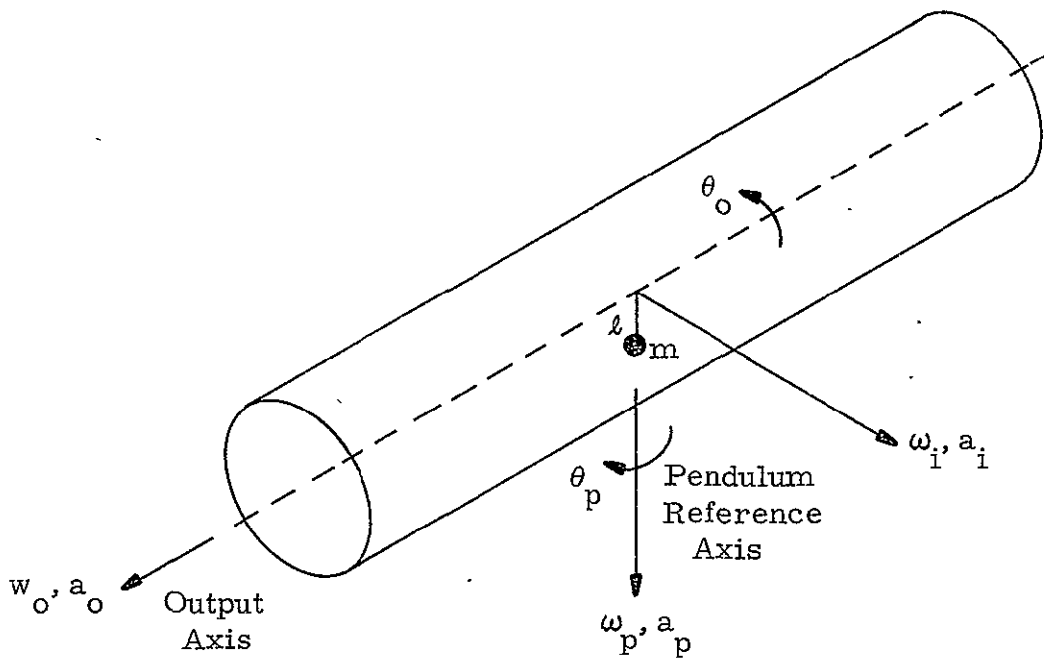


Figure A-1 Pendulous Accelerometer Axis System

$$m\ell (a_i + \theta a_p) \quad (A-3)$$

Torques arising from mass unbalance and (kinematically produced) girder deflections are expressed as linear and quadratic terms in the three carrier accelerations. Here we lump them as one compliance term,

$$M_c(a_i, a_o, a_p) \quad (A-4)$$

and breakout the compliance of the pendulous axis as the following separate term:

$$-\theta a_o = (C_{IO} a_i) a_o \quad (A-5)$$

The dominant gyroscopic torque is

$$(I_p - I_i) w_p w_i \quad (A-6)$$

while that due to rotational acceleration is

$$m\ell^2 \theta (w_p^2 - w_i^2 - w_o^2) \quad (A-7)$$

Using these relationships Eq. (A-1) can be rewritten as

$$\begin{aligned} I_o \ddot{\theta}_o + D \dot{\theta}_o + K \theta_o &= m\ell (a_i + \theta a_p) - I_o w_o + (I_p - I_i) w_p w_i + C_{IO} a_i a_o \\ &+ m\ell^2 \theta (w_p^2 - w_i^2 - w_o^2) + T_c(a_i, a_o, a_p) + T_u \end{aligned} \quad (A-8)$$

We now define the equation of motion of an ideal accelerometer as

$$I_o \ddot{\theta}_I + D\dot{\theta}_I + K\theta_I = m\ell a_i \quad (A-9)$$

Denoting the difference in angular response of these two instruments as

$$e_\theta = \theta_o - \theta_I \quad (A-10)$$

yields

$$\begin{aligned} I_o \ddot{e}_\theta + D\dot{e}_\theta + Ke_o = m\ell \theta a_p - I_o w_o + (I_p - I_i)w_p w_i + C_{IO} a_i a_o \\ + m\ell^2 \theta (w_p^2 - w_i^2 - w_o^2) + T_c(a_i, a_o, a_p) + T_u \end{aligned} \quad (A-11)$$

The corresponding steady-state error is

$$\begin{aligned} e_\theta = \frac{1}{K} \left(m\ell \left(\frac{m\ell a_i}{K} \right) a_p - I_o w_o + (I_p - I_i)w_p w_i + C_{IO} a_i a_o \right. \\ \left. + m\ell^2 \left(\frac{m\ell a_i}{K} \right) (w_p^2 - w_i^2 - w_o^2) + T_c(a_i, a_o, a_p) + T_u \right) \end{aligned} \quad (A-12)$$

where we have used the relationship

$$\theta_o \approx \theta_I \approx \frac{m\ell}{K} a_i \quad (A-13)$$

Converting the angle error to an acceleration error by multiplying by K/ml yields

$$e_a = \frac{ml}{K} a_i a_p \quad (\text{cross-coupling or vibropendulous error})$$

$$- \frac{I_o}{ml} \dot{w}_o \quad (\text{OA rotation error})$$

$$+ \frac{(I_p - I_i)}{ml} w_p w_i \quad (\text{anisoinertia or dynamic unbalance error})$$

$$+ C_{IO} a_i a_o \quad (\text{compliance of pendulous axis})$$

$$+ \frac{ml^2}{K} a_i (w_p^2 - w_i^2 - w_o^2) \quad (\text{rotational cross-coupling error})$$

$$+ \frac{T_c(a_i, a_o, a_p)}{ml} \quad (\text{compliance error - not including } C_{IO})$$

$$+ \frac{T_u}{ml} \quad (\text{uncertainty error, including bias term})$$

$$+ \left(\delta \frac{ml}{K} \right) a_i \quad (\text{scale factor error})$$

(A-14)

The last term displays the dominant effect of an error in knowledge of the instrument scale factor, ml/K .

APPENDIX B
TABULATION OF CALIBRATION EQUATIONS

In Section 7, it was shown that both the accelerometer and gyro calibration equations could be arranged in the following form:

$$\underline{M}_j^m / \Delta t^m \equiv \dot{\underline{M}}_j^m = \underline{H}_j^m \cdot \underline{Y}_j + \delta \dot{\underline{M}}_j^m \quad (7-1 \text{ and B-1})$$

in which the various terms are defined by Eqs. (7-7) (7-8) and (7-9) for the accelerometers and Eqs. (7-25) through (7-29) for the gyros. The purpose of this appendix is to apply these equations to each inertial sensor for each test condition (m) specified in the calibration procedure (Section 8). These equations are then used as a basis for deriving the calibration term estimation equations in Section 9, as well as the error analysis in Section 10.

The first step is to determine the relationships (i. e., transformation matrices) between each inertial sensor coordinate frame and the "environment" (i. e., \underline{g} , \underline{w}_e and \underline{w}^T). The transformation matrices are defined in terms of the unit vectors that define the coordinate frames, as follows:

$$\begin{bmatrix} \underline{B}_1 \\ \underline{B}_2 \\ \underline{B}_3 \end{bmatrix} = T^{BE} \begin{bmatrix} \underline{E}_1 \\ \underline{E}_2 \\ \underline{E}_3 \end{bmatrix} = T^{BE} \begin{bmatrix} \underline{U} \\ \underline{E} \\ \underline{N} \end{bmatrix} \quad (B-2)$$

where a multiplication of the k^{th} row of the 3x3 transformation matrix T^{BE} with the \underline{E}_k column represents \underline{B}_k expressed in the \underline{E}_k frame. For example, a vector \underline{w}_e known in the \underline{E}_k frame can be expressed in the \underline{B} frame by computing the dot product of both sides of Eq. (B-2), as follows:

$$\begin{bmatrix} \underline{w}_e \cdot \underline{B}_1 \\ \underline{w}_e \cdot \underline{B}_2 \\ \underline{w}_e \cdot \underline{B}_3 \end{bmatrix} = T^{\text{BE}} \begin{bmatrix} \underline{w}_e \cdot \underline{U} \\ \underline{w}_e \cdot \underline{E} \\ \underline{w}_e \cdot \underline{N} \end{bmatrix} = T^{\text{BE}} \begin{bmatrix} w_e \sin L \\ 0 \\ w_e \cos L \end{bmatrix} \quad (\text{B-3})$$

and

$$\underline{w}_e \cdot \underline{B}_1 = \text{component of } \underline{w}_e \text{ along } \underline{B}_1 = w_e \sin L (\underline{B}_1 \cdot \underline{U}) + 0 (\underline{B}_1 \cdot \underline{E}) + w_e \cos L (\underline{B}_1 \cdot \underline{N}) \quad (\text{B-4})$$

where $(\underline{B}_1 \cdot \underline{U})$, $(\underline{B}_1 \cdot \underline{E})$ and $(\underline{B}_1 \cdot \underline{N})$ are the first row elements of T^{BE} . The components of \underline{w}_e along \underline{B}_2 and \underline{B}_3 are computed similarly. In this appendix, the components of \underline{g} , \underline{w}_e and \underline{w}^{T} along the inertial sensor axes are determined for each test condition (m), using the above approach.

The test conditions are defined in terms of the TAF gimbal angles (ϕ_3 and ϕ_4), the SATS rotary angle (ϕ_2), and the test table rate (w^{T}). In addition, the following four angles are included in the transformation matrices in anticipation of their possible use in the estimation equations:

$\delta\phi_N$	vertical tilt error of the rotary axis about North
$\delta\phi_E$	vertical tilt error of the rotary axis about East
MR3'	Nonorthogonality between the TAF outer gimbal axis and the test table rotary axis, measured about the \underline{R}_3' axis
MO3'	nonorthogonality between the TAF inner and outer gimbal axes, measured about the \underline{O}_3' axis

The transformation matrices relating the "environment" and the ISU body axes are as follows:

T^{BRm} \equiv rotary axes to body axes transformation matrix

T^{BEm} \equiv earth axes to body axes transformation matrix

where

$$T^{BEm} = T^{BRm} T^{R'Em}$$

(B-5)

$$T^{BRm} = T^{BM} T^{ML} T^{LI} T^{IOM} T^{OO'} T^{O'Rm} T^{RR'} \quad (B-6)$$

$$= \begin{bmatrix} 1 & 0 & 0 \\ 0 & 1 & 0 \\ 0 & 0 & -1 \end{bmatrix} \begin{bmatrix} -\underline{M}_{13} \cdot \underline{L}_1 & 1 & \underline{M}_{11} \cdot \underline{L}_3 \\ \underline{M}_{22} \cdot \underline{L}_1 & -\underline{M}_{21} \cdot \underline{L}_2 & 1 \\ -1 & -\underline{M}_{33} \cdot \underline{L}_2 & \underline{M}_{32} \cdot \underline{L}_3 \end{bmatrix} \begin{bmatrix} 1 & 0 & 0 \\ 0 & 1 & 0 \\ 0 & 0 & 1 \end{bmatrix}$$

T^{BM}
 T^{ML}
 T^{LI}

$$\begin{bmatrix} 0 & 1 & 0 \\ C\phi_4 & 0 & -S\phi_4 \\ -S\phi_4 & 0 & -C\phi_4 \end{bmatrix} \begin{bmatrix} 1 & MO3' & 0 \\ -MO3' & 1 & 0 \\ 0 & 0 & 1 \end{bmatrix} \begin{bmatrix} 0 & 1 & 0 \\ C\phi_3 & 0 & -S\phi_3 \\ -S\phi_3 & 0 & -C\phi_3 \end{bmatrix} \begin{bmatrix} 1 & MR3' & 0 \\ -MR3' & 1 & 0 \\ 0 & 0 & 1 \end{bmatrix}$$

T^{IOM}
 $T^{OO'}$
 $T^{O'Rm}$
 $T^{RR'}$

$$T^{R'Em} = T^{R'Tm} T^{TF} T^{FE} \quad (B-7)$$

$$= \begin{bmatrix} 0 & 1 & 0 \\ C\phi_2 & 0 & -S\phi_2 \\ -S\phi_2 & 0 & -C\phi_2 \end{bmatrix} \begin{bmatrix} 0 & 1 & 0 \\ 1 & 0 & -\delta\phi_E \\ -\delta\phi_E & 0 & -1 \end{bmatrix} \begin{bmatrix} 1 & \delta\phi_N & 0 \\ -\delta\phi_N & 1 & 0 \\ 0 & 0 & 1 \end{bmatrix}$$

$T^{R'Tm}$
 T^{TF}
 T^{FE}

and the various transformation matrices are defined in Table B-1 and the coordinate frames in Tables 5-1 and 5-2. Fig. 5-3 contains an illustration of the various coordinate frames. The elements of the T^{ML} matrix represent the ISU optical cube to bubble level misalignments that are measured when the ISU is mounted within the TAF. In the derivation here, these elements are set equal to zero since the misalignment terms in the \underline{Y} vectors are defined relative to the bubble level coordinate frame (L). The way in which these terms are introduced is shown in Section 9.

The nominal transformations from the body axes to the inertial sensor coordinate frames are based on the axes orientations illustrated in Fig. 5-2, and are expressed in matrix form, as follows:

$$\begin{bmatrix} \underline{A} \\ \underline{O}^A \\ \underline{P} \end{bmatrix}_1 = \begin{bmatrix} -1 & 0 & 0 \\ 0 & 0 & 1 \\ 0 & 1 & 0 \end{bmatrix} \underline{B} \quad (\text{B-8}) \quad \begin{bmatrix} \underline{G} \\ \underline{O}^G \\ \underline{S}^G \end{bmatrix}_1 = \begin{bmatrix} 1 & 0 & 0 \\ 0 & 0 & 1 \\ 0 & -1 & 0 \end{bmatrix} \underline{B} \quad (\text{B-11})$$

$$\begin{bmatrix} \underline{A} \\ \underline{O}^A \\ \underline{P} \end{bmatrix}_2 = \begin{bmatrix} 0 & 1 & 0 \\ 1 & 0 & 0 \\ 0 & 0 & -1 \end{bmatrix} \underline{B} \quad (\text{B-9}) \quad \begin{bmatrix} \underline{G} \\ \underline{O}^G \\ \underline{S}^G \end{bmatrix}_2 = \begin{bmatrix} 0 & 1 & 0 \\ -1 & 0 & 0 \\ 0 & 0 & 1 \end{bmatrix} \underline{B} \quad (\text{B-12})$$

$$\begin{bmatrix} \underline{A} \\ \underline{O}^A \\ \underline{P} \end{bmatrix}_3 = \begin{bmatrix} 0 & 0 & 1 \\ -1 & 0 & 0 \\ 0 & -1 & 0 \end{bmatrix} \underline{B} \quad (\text{B-10}) \quad \begin{bmatrix} \underline{G} \\ \underline{O}^G \\ \underline{S}^G \end{bmatrix}_3 = \begin{bmatrix} 0 & 0 & 1 \\ -1 & 0 & 0 \\ 0 & -1 & 0 \end{bmatrix} \underline{B} \quad (\text{B-13})$$

<u>Matrix</u>	<u>Description of Angle(s) that Characterizes Transformation</u>
T^{FE}	misalignment of test table rotary axis about North ($\delta\phi_N$)
T^{TF}	misalignment of test table rotary axis about East ($\delta\phi_E$)
$T^{R'T}$	rotation of test table about rotary axis (ϕ_2); zero value corresponds to TAF outer gimbal axis (ϕ_3 axis) pointing East
$T^{RR'}$	nonorthogonality between rotary axis and ϕ_3 axis (MR3')
$T^{O'R}$	rotation of TAF outer gimbal about ϕ_3 axis (ϕ_3); zero value is when TAF inner gimbal axis (ϕ_4 axis) and rotary axis are parallel to each other
$T^{OO'}$	nonorthogonality between TAF ϕ_3 and ϕ_4 axes (MO3')
T^{IO}	rotation of TAF inner gimbal about ϕ_4 axis (ϕ_4); zero value corresponds to the \underline{L}_2 bubble level aligned parallel to the ϕ_3 axis.
T_n^{LI}	nominal relationship between bubble level and inner gimbal coordinate frames - misalignments assumed to be negligible
T^{ML}	misalignment of ISU cube (mirror) coordinate frame relative to bubble level coordinate frame; elements of the form $\underline{M}_{ab} \underline{L}_c$ = nonorthogonality of \underline{M}_a about \underline{L}_b with respect to \underline{L}_c , measured about the positive \underline{L}_a axis that is normal to \underline{L}_b and \underline{L}_c
T^{BM}	definition of body axes in terms of ISU cube (mirror) coordinate frame

Table B-1 Transformation Matrices Relating Body Axes to Earth Coordinates

At this point all the transformations required to relate the "environment" coordinate frames to the inertial sensors axes has been defined.

The next step is to define the "environment" as vectors in an appropriate coordinate frame, as follows:

$$\underline{g} = \begin{bmatrix} g \\ 0 \\ 0 \end{bmatrix} \quad \text{in the earth coordinate frame (E)} \quad (\text{B-14})$$

$$\underline{w}_e = \begin{bmatrix} w_e \sin L \\ 0 \\ w_e \cos L \end{bmatrix} \quad \text{in the earth coordinate frame (E)} \quad (\text{B-15})$$

$$\underline{w}^T = \begin{bmatrix} T \\ w \\ 0 \\ 0 \end{bmatrix} \quad \text{in the rotary axes coordinate frame (R')} \quad (\text{B-16})$$

The above "environment vectors", transformation matrices, and inertial sensor calibration equations were combined as indicated by Eqs. (B-3) and (B-4), using a digital computer. The elements of the \underline{H}_j^{Am} and \underline{H}_j^{Gm} row matrices were determined for each inertial sensor, for each of the test conditions (m) (assuming $\delta \dot{M} = 0$). The results were organized in matrix form and are summarized in Tables B-2 through B-4 for the accelerometers and Tables B-5 through B-7 for the gyros, in which products of small quantities have been neglected. Errors that are not compensated for in the computation of \dot{M} , or that are not negligible, are considered in the error analysis (Section 10) as part of the $\delta \dot{M}$ term.

In the case of the gyros, the runs for which the test table was rotating are tabulated separately, at the bottom of each table. These runs are combined with each other and other runs, as shown at the top of each table. This is done to separate out certain calibration terms and simplify the estimation calculations. When other table rates (w^T) are used, as indicated in Table 8-6, the same six equations at the bottom of each table are used, substituting the new values of m for those shown. Rates other than $w^T = \pm 2^\circ/\text{sec}$ are used only in the estimation of the gyro scale factor error coefficients (\hat{R}_b , \hat{Q}_1 and \hat{Q}_2), as discussed in Section 9 and Appendix C.

Although the w^{T+} and w^{T-} values for a given test condition m are nominally equal and opposite, the errors in setting w^T are sufficiently large to warrant using the actual (i. e., measured) values of w^T , as indicated in Tables B-5, B-6, and B-7. The compensation terms that are functions of NOA and NSA should be computed after NOA and NSA have been estimated. The terms can be estimated from T^{GM} T^{ML} , providing T^{GM} is assumed known within approximately 15 to $30 \widehat{\text{sec}} (1\sigma)$.

Table B-2 Accelerometer No. 1 Calibration Equations

$$\begin{array}{c}
 \left[\begin{array}{c}
 \Delta\Phi(P^A/\Delta t)^4 + g \\
 \Delta\Phi(P^A/\Delta t)^5 \\
 \Delta\Phi(P^A/\Delta t)^6 \\
 \Delta\Phi(P^A/\Delta t)^1 + 0 \\
 \Delta\Phi(P^A/\Delta t)^2 \\
 \frac{10^6}{g} \Delta\Phi(P^A/\Delta t)^3 - g \\
 \Delta\Phi(P^A/\Delta t)^7 - g/\sqrt{2} \\
 \Delta\Phi(P^A/\Delta t)^8 + g/\sqrt{2} \\
 \Delta\Phi(P^A/\Delta t)^9 \\
 \Delta\Phi(P^A/\Delta t)^{10} - g/\sqrt{2} \\
 \Delta\Phi(P^A/\Delta t)^{11} + g/\sqrt{2} \\
 \Delta\Phi(P^A/\Delta t)^{12} \\
 \Delta\Phi(P^A/\Delta t)^{13} - g/\sqrt{2}
 \end{array} \right]
 \end{array}
 =
 \begin{array}{c}
 \left[\begin{array}{c}
 \dot{M}^4 \\
 \dot{M}^5 \\
 \dot{M}^6 \\
 \dot{M}^1 \\
 \dot{M}^2 \\
 \dot{M}^3 \\
 \dot{M}^7 \\
 \dot{M}^8 \\
 \dot{M}^9 \\
 \dot{M}^{10} \\
 \dot{M}^{11} \\
 \dot{M}^{12} \\
 \dot{M}^{13}
 \end{array} \right]
 =
 \begin{array}{c}
 \left[\begin{array}{cccccccc}
 0 & 0 & 0 & 0 & 1 & 0 & 0 & 0 \\
 1 & 0 & 1 & 0 & 0 & 0 & 0 & 0 \\
 1 & +1 & 0 & 0 & 0 & 0 & 0 & 0 \\
 1 & 0 & -1 & 0 & 0 & 0 & 0 & 0 \\
 1 & -1 & 0 & 0 & 0 & 0 & 0 & 0 \\
 0 & 0 & 0 & 1 & 0 & 0 & 0 & 0 \\
 0 & 0 & .7 & 0 & 0 & 1 & 0 & 0 \\
 0 & +.7 & 0 & 0 & 0 & +1 & 0 & -.5 \\
 1 & -.7 & -.7 & 0 & 0 & 0 & 0 & 0 \\
 0 & 0 & -.7 & 0 & 0 & 1 & 0 & 0 \\
 0 & -.7 & 0 & 0 & 0 & 0 & 1 & .5 \\
 1 & +.7 & -.7 & 0 & 0 & 0 & 0 & 0 \\
 1 & +.7 & 0 & 0 & 0 & 0 & 1 & .5
 \end{array} \right]
 \end{array}
 \begin{array}{c}
 \left[\begin{array}{c}
 A'_b \\
 -4.85 \text{ NOA} \\
 4.85 \text{ NPA} \\
 \delta \dot{V}_c^{+1} \\
 \delta \dot{V}_c^{-1} \\
 \delta \dot{V}_c^{+.7} \\
 \delta \dot{V}_c^{-.7} \\
 C_{IP} g^2 \\
 C_{IO} g^2
 \end{array} \right]
 \end{array}
 \begin{array}{c}
 j=1 \\
 j=1 \\
 j=1
 \end{array}$$

- Notes: (1) g = magnitude of gravity at location of SATS (to the 4th decimal place)
- (2) Units of \dot{M} are μg
- (3) Matrix elements shown as .7 are actually equal to $1/\sqrt{2}$
- (4) Units of NOA and NPA are $\widehat{\text{sec}}$

Table B-3 Accelerometer No. 2 Calibration Equations

$$\begin{aligned}
 & \frac{10^6}{g} \begin{bmatrix} \Delta\Phi(P^A/\Delta t)^4 \\ \Delta\Phi(P^A/\Delta t)^5 \\ \Delta\Phi(P^A/\Delta t)^6 - g \\ \Delta\Phi(P^A/\Delta t)^1 + 0 \\ \Delta\Phi(P^A/\Delta t)^2 + g \\ \Delta\Phi(P^A/\Delta t)^3 + 0 \\ \Delta\Phi(P^A/\Delta t)^7 + 0 \\ \Delta\Phi(P^A/\Delta t)^8 - g/\sqrt{2} \\ \Delta\Phi(P^A/\Delta t)^9 + g/\sqrt{2} \\ \Delta\Phi(P^A/\Delta t)^{10} + 0 \\ \Delta\Phi(P^A/\Delta t)^{11} + g/\sqrt{2} \\ \Delta\Phi(P^A/\Delta t)^{12} - g/\sqrt{2} \\ \Delta\Phi(P^A/\Delta t)^{13} - g/\sqrt{2} \end{bmatrix} \equiv \begin{bmatrix} \dot{M}^4 \\ \dot{M}^5 \\ \dot{M}^6 \\ \dot{M}^1 \\ \dot{M}^2 \\ \dot{M}^3 \\ \dot{M}^7 \\ \dot{M}^8 \\ \dot{M}^9 \\ \dot{M}^{10} \\ \dot{M}^{11} \\ \dot{M}^{12} \\ \dot{M}^{13} \end{bmatrix} = \begin{bmatrix} 1 & 0 & +1 & 0 & 0 & 0 & 0 & 0 & 0 & 0 \\ 1 & -1 & 0 & 0 & 0 & 0 & 0 & 0 & 0 & 0 \\ 0 & 0 & 0 & 1 & 0 & 0 & 0 & 0 & 0 & 0 \\ 1 & +1 & 0 & 0 & 0 & 0 & 0 & 0 & 0 & 0 \\ 0 & 0 & 0 & 0 & +1 & 0 & 0 & 0 & 0 & 0 \\ 1 & 0 & -1 & 0 & 0 & 0 & 0 & 0 & 0 & 0 \\ 1 & -.7 & -.7 & 0 & 0 & 0 & 0 & 0 & 0 & 0 \\ 0 & 0 & +.7 & 0 & 0 & +1 & 0 & 0 & +.5 & 0 \\ 0 & +.7 & 0 & 0 & 0 & 0 & +1 & -.5 & 0 & 0 \\ 1 & +.7 & -.7 & 0 & 0 & 0 & 0 & 0 & 0 & 0 \\ 0 & 0 & +.7 & 0 & 0 & 0 & +1 & 0 & -.5 & 0 \\ 0 & +.7 & 0 & 0 & 0 & 1 & 0 & +.5 & 0 & 0 \\ 0 & 0 & -.7 & 0 & 0 & 1 & 0 & 0 & -.5 & 0 \end{bmatrix} \begin{bmatrix} A'_b \\ -4.85 \text{ NOA} \\ 4.85 \text{ NPA} \\ \delta \dot{V}_c^{+1} \\ \delta \dot{V}_c^{-1} \\ \delta \dot{V}_c^{+.7} \\ \delta \dot{V}_c^{-.7} \\ C_{IP} g^2 \\ C_{IO} g^2 \end{bmatrix} \quad j=2 \quad j=2 \quad j=2
 \end{aligned}$$

- Notes: (1) g = magnitude of gravity at location of SATS (to the 4th decimal place)
 (2) Units of \dot{M} are μg
 (3) Matrix elements shown as .7 are actually equal to $1/\sqrt{2}$
 (4) Units of NOA and NPA are $\widehat{\text{sec}}$.

Table B-4 Accelerometer No. 3 Calibration Equations

$$\frac{10^6}{g} \begin{bmatrix} \Delta\Phi(P^A/\Delta t)^4 \\ \Delta\Phi(P^A/\Delta t)^5 - g \\ \Delta\Phi(P^A/\Delta t)^6 \\ \Delta\Phi(P^A/\Delta t)^1 + g \\ \Delta\Phi(P^A/\Delta t)^2 + 0 \\ \Delta\Phi(P^A/\Delta t)^3 + 0 \\ \Delta\Phi(P^A/\Delta t)^7 - g/\sqrt{2} \\ \Delta\Phi(P^A/\Delta t)^8 + 0 \\ \Delta\Phi(P^A/\Delta t)^9 + g/\sqrt{2} \\ \Delta\Phi(P^A/\Delta t)^{10} + g/\sqrt{2} \\ \Delta\Phi(P^A/\Delta t)^{11} + 0 \\ \Delta\Phi(P^A/\Delta t)^{12} + g/\sqrt{2} \\ \Delta\Phi(P^A/\Delta t)^{13} \end{bmatrix} \equiv \begin{bmatrix} \dot{M}^4 \\ \dot{M}^5 \\ \dot{M}^6 \\ \dot{M}^1 \\ \dot{M}^2 \\ \dot{M}^3 \\ \dot{M}^7 \\ \dot{M}^8 \\ \dot{M}^9 \\ \dot{M}^{10} \\ \dot{M}^{11} \\ \dot{M}^{12} \\ \dot{M}^{13} \end{bmatrix} = \begin{bmatrix} 1 & 0 & -1 & 0 & 0 & 0 & 0 & 0 & 0 & 0 \\ 0 & 0 & 0 & 1 & 0 & 0 & 0 & 0 & 0 & 0 \\ 1 & -1 & 0 & 0 & 0 & 0 & 0 & 0 & 0 & 0 \\ 0 & 0 & 0 & 0 & +1 & 0 & 0 & 0 & 0 & 0 \\ 1 & 1 & 0 & 0 & 0 & 0 & 0 & 0 & 0 & 0 \\ 1 & 0 & 1 & 0 & 0 & 0 & 0 & 0 & 0 & 0 \\ 0 & 0 & .7 & 0 & 0 & 1 & 0 & 0 & .5 & 0 \\ 1 & -.7 & -.7 & 0 & 0 & 1 & 0 & 0 & 0 & 0 \\ 0 & .7 & 0 & 0 & 0 & 0 & 1 & -.5 & 0 & 0 \\ 0 & 0 & .7 & 0 & 0 & 0 & 1 & 0 & -.5 & 0 \\ 1 & .7 & -.7 & 0 & 0 & 0 & 0 & 0 & 0 & 0 \\ 0 & -.7 & 0 & 0 & 0 & 0 & 1 & .5 & 0 & 0 \\ 1 & -.7 & .7 & 0 & 0 & 0 & 0 & 0 & 0 & 0 \end{bmatrix} \begin{bmatrix} A'_b \\ -4.85 \text{ NOA} \\ 4.85 \text{ NPA} \\ \delta \dot{V}_c^{+.1} \\ \delta \dot{V}_c^{-.1} \\ \delta \dot{V}_c^{+.7} \\ \delta \dot{V}_c^{-.7} \\ C_{IP}g^2 \\ C_{IO}g^2 \end{bmatrix} \quad j=3 \quad j=3 \quad j=3$$

- Notes: (1) g = magnitude of gravity at location of SATS (to the 4th decimal place)
 (2) Units of \dot{M} are μg
 (3) Matrix elements shown as .7 are actually equal to $1/\sqrt{2}$
 (4) Units of NOA and NPA are $\text{s}\ddot{e}c$

$\begin{bmatrix} \dot{M}^{52+} - \dot{M}^{55} \\ \dot{M}^{52-} - \dot{M}^{55} \\ (\dot{M}^{42+} - \dot{M}^{42-})/2 \\ (\dot{M}^{62+} - \dot{M}^{62-})/2 \\ [(\dot{M}^{42+} + \dot{M}^{42-}) - c^{42+} \text{NSA}]/2 \\ \Delta\Phi(P^G/\Delta t)^5 - w_e \sin L \\ [(\dot{M}^{62+} + \dot{M}^{62-}) - c^{62+} \text{NOA}]/2 \\ \Delta\Phi(P^G/\Delta t)^1 + w_e \sin L \\ \Delta\Phi(P^G/\Delta t)^2 + 0 \\ \Delta\Phi(P^G/\Delta t)^3 + w_e \cos L \\ \Delta\Phi(P^G/\Delta t)^7 + w_e (\cos L - \sin L)/\sqrt{2} \\ \Delta\Phi(P^G/\Delta t)^8 + 0 \\ \Delta\Phi(P^G/\Delta t)^9 + (w_e \sin L)/\sqrt{2} \\ \Delta\Phi(P^G/\Delta t)^{10} + w_e (\cos L + \sin L)/\sqrt{2} \\ \Delta\Phi(P^G/\Delta t)^{11} + 0 \\ \Delta\Phi(P^G/\Delta t)^{12} + (w_e \sin L)/\sqrt{2} \\ \Delta\Phi(P^G/\Delta t)^{13} + 0 \end{bmatrix}$ <p style="text-align: center;">j=3</p>	$\begin{bmatrix} \dot{M}^{82+} \\ \dot{M}^{82-} \\ \dot{M}^{41} \\ \dot{M}^{61} \\ \dot{M}^{40} \\ \dot{M}^5 \\ \dot{M}^{60} \\ \dot{M}^1 \\ \dot{M}^2 \\ \dot{M}^3 \\ \dot{M}^7 \\ \dot{M}^8 \\ \dot{M}^9 \\ \dot{M}^{10} \\ \dot{M}^{11} \\ \dot{M}^{12} \\ \dot{M}^{13} \end{bmatrix}$ <p style="text-align: center;">j=3</p>	<table border="0" style="width: 100%; border-collapse: collapse;"> <tr> <td style="width: 70%;"></td> <td style="width: 5%;"></td> <td style="width: 10%; text-align: center;">○</td> <td style="width: 15%; border-left: 1px dashed black; border-right: 1px dashed black; padding: 0 5px;"> <table border="0" style="width: 100%; border-collapse: collapse;"> <tr><td style="border-right: 1px dashed black; padding: 0 5px;">1</td><td style="padding: 0 5px;">0</td></tr> <tr><td style="border-right: 1px dashed black; padding: 0 5px;">0</td><td style="padding: 0 5px;">1</td></tr> </table> </td> </tr> <tr> <td style="border-top: 1px dashed black;"></td> <td style="border-top: 1px dashed black;"></td> <td style="border-top: 1px dashed black; text-align: center;">○</td> <td style="border-top: 1px dashed black; border-left: 1px dashed black; border-right: 1px dashed black; padding: 0 5px;"> <table border="0" style="width: 100%; border-collapse: collapse;"> <tr><td style="border-right: 1px dashed black; padding: 0 5px;">0</td><td style="padding: 0 5px;">c⁴²⁻</td></tr> <tr><td style="border-right: 1px dashed black; padding: 0 5px;">c⁶²⁻</td><td style="padding: 0 5px;">0</td></tr> </table> </td> </tr> <tr> <td style="border-bottom: 1px dashed black;"></td> <td style="border-bottom: 1px dashed black;"></td> <td style="border-bottom: 1px dashed black; text-align: center;">○</td> <td style="border-bottom: 1px dashed black; border-left: 1px dashed black; border-right: 1px dashed black; padding: 0 5px;"> <table border="0" style="width: 100%; border-collapse: collapse;"> <tr><td style="border-right: 1px dashed black; padding: 0 5px;">1</td><td style="padding: 0 5px;">0</td></tr> <tr><td style="border-right: 1px dashed black; padding: 0 5px;">0</td><td style="padding: 0 5px;">1</td></tr> </table> </td> </tr> </table> <p style="text-align: center;">j=3</p>			○	<table border="0" style="width: 100%; border-collapse: collapse;"> <tr><td style="border-right: 1px dashed black; padding: 0 5px;">1</td><td style="padding: 0 5px;">0</td></tr> <tr><td style="border-right: 1px dashed black; padding: 0 5px;">0</td><td style="padding: 0 5px;">1</td></tr> </table>	1	0	0	1			○	<table border="0" style="width: 100%; border-collapse: collapse;"> <tr><td style="border-right: 1px dashed black; padding: 0 5px;">0</td><td style="padding: 0 5px;">c⁴²⁻</td></tr> <tr><td style="border-right: 1px dashed black; padding: 0 5px;">c⁶²⁻</td><td style="padding: 0 5px;">0</td></tr> </table>	0	c ⁴²⁻	c ⁶²⁻	0			○	<table border="0" style="width: 100%; border-collapse: collapse;"> <tr><td style="border-right: 1px dashed black; padding: 0 5px;">1</td><td style="padding: 0 5px;">0</td></tr> <tr><td style="border-right: 1px dashed black; padding: 0 5px;">0</td><td style="padding: 0 5px;">1</td></tr> </table>	1	0	0	1								
		○	<table border="0" style="width: 100%; border-collapse: collapse;"> <tr><td style="border-right: 1px dashed black; padding: 0 5px;">1</td><td style="padding: 0 5px;">0</td></tr> <tr><td style="border-right: 1px dashed black; padding: 0 5px;">0</td><td style="padding: 0 5px;">1</td></tr> </table>	1	0	0	1																											
1	0																																	
0	1																																	
		○	<table border="0" style="width: 100%; border-collapse: collapse;"> <tr><td style="border-right: 1px dashed black; padding: 0 5px;">0</td><td style="padding: 0 5px;">c⁴²⁻</td></tr> <tr><td style="border-right: 1px dashed black; padding: 0 5px;">c⁶²⁻</td><td style="padding: 0 5px;">0</td></tr> </table>	0	c ⁴²⁻	c ⁶²⁻	0																											
0	c ⁴²⁻																																	
c ⁶²⁻	0																																	
		○	<table border="0" style="width: 100%; border-collapse: collapse;"> <tr><td style="border-right: 1px dashed black; padding: 0 5px;">1</td><td style="padding: 0 5px;">0</td></tr> <tr><td style="border-right: 1px dashed black; padding: 0 5px;">0</td><td style="padding: 0 5px;">1</td></tr> </table>	1	0	0	1																											
1	0																																	
0	1																																	
$\begin{bmatrix} \Delta\Phi(P^G/\Delta t)^{42+} - w_e \cos L \\ \Delta\Phi(P^G/\Delta t)^{42-} - w_e \cos L \\ [(\Delta\Phi P^G - 3600S^\phi P^\phi)/\Delta t]^{52+} - w_e \sin L \\ [(\Delta\Phi P^G - 3600S^\phi P^\phi)/\Delta t]^{52-} - w_e \sin L \\ \Delta\Phi(P^G/\Delta t)^{62+} \\ \Delta\Phi(P^G/\Delta t)^{62-} \end{bmatrix}$ <p style="text-align: center;">j=3</p>	$\begin{bmatrix} \dot{M}^{42+} \\ \dot{M}^{42-} \\ \dot{M}^{52+} \\ \dot{M}^{52-} \\ \dot{M}^{62+} \\ \dot{M}^{62-} \end{bmatrix}$ <p style="text-align: center;">j=3</p>	<table border="0" style="width: 100%; border-collapse: collapse;"> <tr> <td style="width: 70%;"></td> <td style="width: 5%;"></td> <td style="width: 10%; text-align: center;">○</td> <td style="width: 15%; border-left: 1px dashed black; border-right: 1px dashed black; padding: 0 5px;"> <table border="0" style="width: 100%; border-collapse: collapse;"> <tr><td style="border-right: 1px dashed black; padding: 0 5px;">0</td><td style="padding: 0 5px;">w⁴²⁺</td><td style="padding: 0 5px;">0</td><td style="padding: 0 5px;">0</td></tr> <tr><td style="border-right: 1px dashed black; padding: 0 5px;">0</td><td style="padding: 0 5px;">w⁴²⁻</td><td style="padding: 0 5px;">0</td><td style="padding: 0 5px;">0</td></tr> <tr><td style="border-right: 1px dashed black; padding: 0 5px;">1</td><td style="padding: 0 5px;">0</td><td style="padding: 0 5px;">1</td><td style="padding: 0 5px;">0</td></tr> <tr><td style="border-right: 1px dashed black; padding: 0 5px;">1</td><td style="padding: 0 5px;">0</td><td style="padding: 0 5px;">1</td><td style="padding: 0 5px;">0</td></tr> <tr><td style="border-right: 1px dashed black; padding: 0 5px;">1</td><td style="padding: 0 5px;">0</td><td style="padding: 0 5px;">0</td><td style="padding: 0 5px;">1</td></tr> <tr><td style="border-right: 1px dashed black; padding: 0 5px;">1</td><td style="padding: 0 5px;">0</td><td style="padding: 0 5px;">0</td><td style="padding: 0 5px;">0</td></tr> <tr><td style="border-right: 1px dashed black; padding: 0 5px;">1</td><td style="padding: 0 5px;">0</td><td style="padding: 0 5px;">0</td><td style="padding: 0 5px;">0</td></tr> </table> </td> </tr> </table> <p style="text-align: center;">j=3</p>			○	<table border="0" style="width: 100%; border-collapse: collapse;"> <tr><td style="border-right: 1px dashed black; padding: 0 5px;">0</td><td style="padding: 0 5px;">w⁴²⁺</td><td style="padding: 0 5px;">0</td><td style="padding: 0 5px;">0</td></tr> <tr><td style="border-right: 1px dashed black; padding: 0 5px;">0</td><td style="padding: 0 5px;">w⁴²⁻</td><td style="padding: 0 5px;">0</td><td style="padding: 0 5px;">0</td></tr> <tr><td style="border-right: 1px dashed black; padding: 0 5px;">1</td><td style="padding: 0 5px;">0</td><td style="padding: 0 5px;">1</td><td style="padding: 0 5px;">0</td></tr> <tr><td style="border-right: 1px dashed black; padding: 0 5px;">1</td><td style="padding: 0 5px;">0</td><td style="padding: 0 5px;">1</td><td style="padding: 0 5px;">0</td></tr> <tr><td style="border-right: 1px dashed black; padding: 0 5px;">1</td><td style="padding: 0 5px;">0</td><td style="padding: 0 5px;">0</td><td style="padding: 0 5px;">1</td></tr> <tr><td style="border-right: 1px dashed black; padding: 0 5px;">1</td><td style="padding: 0 5px;">0</td><td style="padding: 0 5px;">0</td><td style="padding: 0 5px;">0</td></tr> <tr><td style="border-right: 1px dashed black; padding: 0 5px;">1</td><td style="padding: 0 5px;">0</td><td style="padding: 0 5px;">0</td><td style="padding: 0 5px;">0</td></tr> </table>	0	w ⁴²⁺	0	0	0	w ⁴²⁻	0	0	1	0	1	0	1	0	1	0	1	0	0	1	1	0	0	0	1	0	0	0
		○	<table border="0" style="width: 100%; border-collapse: collapse;"> <tr><td style="border-right: 1px dashed black; padding: 0 5px;">0</td><td style="padding: 0 5px;">w⁴²⁺</td><td style="padding: 0 5px;">0</td><td style="padding: 0 5px;">0</td></tr> <tr><td style="border-right: 1px dashed black; padding: 0 5px;">0</td><td style="padding: 0 5px;">w⁴²⁻</td><td style="padding: 0 5px;">0</td><td style="padding: 0 5px;">0</td></tr> <tr><td style="border-right: 1px dashed black; padding: 0 5px;">1</td><td style="padding: 0 5px;">0</td><td style="padding: 0 5px;">1</td><td style="padding: 0 5px;">0</td></tr> <tr><td style="border-right: 1px dashed black; padding: 0 5px;">1</td><td style="padding: 0 5px;">0</td><td style="padding: 0 5px;">1</td><td style="padding: 0 5px;">0</td></tr> <tr><td style="border-right: 1px dashed black; padding: 0 5px;">1</td><td style="padding: 0 5px;">0</td><td style="padding: 0 5px;">0</td><td style="padding: 0 5px;">1</td></tr> <tr><td style="border-right: 1px dashed black; padding: 0 5px;">1</td><td style="padding: 0 5px;">0</td><td style="padding: 0 5px;">0</td><td style="padding: 0 5px;">0</td></tr> <tr><td style="border-right: 1px dashed black; padding: 0 5px;">1</td><td style="padding: 0 5px;">0</td><td style="padding: 0 5px;">0</td><td style="padding: 0 5px;">0</td></tr> </table>	0	w ⁴²⁺	0	0	0	w ⁴²⁻	0	0	1	0	1	0	1	0	1	0	1	0	0	1	1	0	0	0	1	0	0	0			
0	w ⁴²⁺	0	0																															
0	w ⁴²⁻	0	0																															
1	0	1	0																															
1	0	1	0																															
1	0	0	1																															
1	0	0	0																															
1	0	0	0																															

Notes: (1) $w^T = S^\phi P^\phi / \Delta t$ (deg/sec)

(2) $c^{m+} = \pi(w^{T+} + w^{T-})^m / 360$ (deg/hr sec)

(3) $c^m = \pi(w^{T+} - w^{T-})^m / 360$ (deg/hr sec)

(4) Matrix elements shown as .7 are actually equal to $1/\sqrt{2}$

Table B-7 Gyro No. 3 Calibration Equations

APPENDIX C
CALIBRATION ESTIMATION EQUATIONS

This appendix summarizes the accelerometer and gyro calibration estimation equations for each of the four levels of calibration (minimum, partial, full and scale factor error).

C.1 EQUATIONS FOR ESTIMATING CALIBRATION TERMS ASSOCIATED WITH THE ACCELEROMETERS

Tables C-1, C-2 and C-3 contain the accelerometer calibration estimation equations for the minimum, partial and full calibrations, respectively. Each table presents the equations for each accelerometer. The M_j^m terms, which are functions of the accelerometer pulse count (P^A), run time (Δt), accelerometer scale factor ($\Delta\Phi^A$) and magnitude of gravity (g), are computed as indicated in Tables B-2, B-3 and B-4. The number of calculations can very likely be reduced for manual data reduction by expressing certain calibration terms as functions of other calibration terms.

The accelerometer scale factor error estimation equations are contained in Table C-4, both in general form and for the data obtained in Tables C-2 and C-3. These equations are applied separately to each accelerometer (j).

The calculations for determining the ${}^A T^B$ matrix are listed in Section 9.2 (Eqs. 9-25 through 9-30).

C. 2 EQUATIONS FOR ESTIMATING CALIBRATION TERMS ASSOCIATED WITH THE GYROS

Tables C-6, C-7 and C-8 contain the gyro calibration estimation equations for the minimum, partial and full calibrations, respectively. Each table presents the equations for each gyro. The M_j^m terms, which are functions of the gyro pulse count (P^G), run time (Δt), gyro scale factor ($\Delta\Phi^G$), test table pulse count (P^Φ) and scale factor (S^Φ), earth rate (w_e) and latitude (L), are computed as indicated in Tables B-5, B-6 and B-7. The number of calculations can very likely be reduced for manual data reduction by expressing certain calibration terms as functions of other calibration terms.

The gyro scale factor error estimation equations are contained in Table C-9, in which the $\hat{\delta\psi}_c^+$ and $\hat{\delta\psi}_c^-$ terms are determined as shown in Table C-5. The calculations to determine the T^{BG} matrix elements are listed in Section 9.3 (Eqs. 9-33 through 9-38), in which the \hat{NOA} and \hat{NSA} terms are computed as shown in Table C-5. It will be noted from Eq. (9-31) that the \hat{NOA} , \hat{NSA} pairs are the estimated misalignments of the gyro IAs relative to the bubble level coordinate frame.

TABLE C-1 ACCELEROMETER MINIMUM CALIBRATION ESTIMATION

EQUATIONS

Accelerometer #1

$$\begin{bmatrix} \hat{A}'_b \\ -(\hat{NOA})g \\ (\hat{NPA})g \\ \hat{\delta \dot{V}}_c^{+1} \\ \hat{\delta \dot{V}}_c^{-1} \end{bmatrix}_{j=1} = \begin{bmatrix} 0 & .5 & 0 & .5 & 0 \\ 0 & -.5 & 1 & -.5 & 0 \\ 0 & .5 & 0 & -.5 & 0 \\ 0 & 0 & 0 & 0 & 1 \\ 1 & 0 & 0 & 0 & 0 \end{bmatrix}_{j=1} \begin{bmatrix} \dot{M}^4 \\ \dot{M}^5 \\ \dot{M}^6 \\ \dot{M}^1 \\ \dot{M}^3 \end{bmatrix}_{j=1}$$

Accelerometer #2

$$\begin{bmatrix} \hat{A}'_b \\ -(\hat{NOA})g \\ (\hat{NPA})g \\ \hat{\delta \dot{V}}_c^{+1} \\ \hat{\delta \dot{V}}_c^{-1} \end{bmatrix}_{j=2} = \begin{bmatrix} .5 & 0 & 0 & 0 & .5 \\ .5 & -1 & 0 & 0 & .5 \\ .5 & 0 & 0 & 0 & -.5 \\ 0 & 0 & 1 & 0 & 0 \\ 0 & 0 & 0 & 1 & 0 \end{bmatrix}_{j=2} \begin{bmatrix} \dot{M}^4 \\ \dot{M}^5 \\ \dot{M}^6 \\ \dot{M}^2 \\ \dot{M}^3 \end{bmatrix}_{j=2}$$

Accelerometer #3

$$\begin{bmatrix} \hat{A}'_b \\ -(\hat{NOA})g \\ (\hat{NPA})g \\ \hat{\delta \dot{V}}_c^{+1} \\ \hat{\delta \dot{V}}_c^{-1} \end{bmatrix}_{j=3} = \begin{bmatrix} 0 & 0 & .5 & 0 & .5 \\ 0 & 0 & -.5 & 0 & .5 \\ -1 & 0 & .5 & 0 & .5 \\ 0 & 1 & 0 & 0 & 0 \\ 0 & 0 & 0 & 1 & 0 \end{bmatrix}_{j=3} \begin{bmatrix} \dot{M}^4 \\ \dot{M}^5 \\ \dot{M}^6 \\ \dot{M}^1 \\ \dot{M}^2 \end{bmatrix}_{j=3}$$

- The \dot{M}_j^m terms are computed as indicated in Tables B-2, B-3 and B-4.
- Not shown are compensations for rotary axis tilt error (from vertical).

TABLE C-2 ACCELEROMETER PARTIAL CALIBRATION ESTIMATION EQUATIONS

Accelerometer #1

$$\begin{bmatrix} \hat{A}_b^i \\ -(\hat{NOA})g \\ -(\hat{NPA})g \\ \delta \hat{V}_c^{+1} \\ \delta \hat{V}_c^{-1} \\ \delta \hat{V}_c^{+.7} \\ \delta \hat{V}_c^{-.7} \end{bmatrix}_{j=1} = \begin{bmatrix} 0 & .5 & 0 & .5 & 0 & 0 & 0 \\ 0 & -.5 & 1 & -.5 & 0 & 0 & 0 \\ 0 & .5 & 0 & -.5 & 0 & 0 & 0 \\ 0 & 0 & 0 & 0 & 1 & 0 & 0 \\ 1 & 0 & 0 & 0 & 0 & 0 & 0 \\ 0 & -.354 & 0 & .354 & 0 & 1 & 0 \\ 0 & .354 & -.707 & .354 & 0 & 0 & 1 \end{bmatrix}_{j=1} \begin{bmatrix} \dot{M}^4 \\ \dot{M}^5 \\ \dot{M}^6 \\ \dot{M}^1 \\ \dot{M}^3 \\ \dot{M}^7 - .5g^2 C_{IO} \\ \dot{M}^8 + .5g^2 C_{IP} \end{bmatrix}_{j=1}$$

Accelerometer #2

$$\begin{bmatrix} \hat{A}_b^i \\ -(\hat{NOA})g \\ (\hat{NPA})g \\ \delta \hat{V}_c^{+1} \\ \delta \hat{V}_c^{-1} \\ \delta \hat{V}_c^{+.7} \\ \delta \hat{V}_c^{-.7} \end{bmatrix}_{j=2} = \begin{bmatrix} .5 & 0 & 0 & 0 & .5 & 0 & 0 \\ .5 & -1 & 0 & 0 & .5 & 0 & 0 \\ .5 & 0 & 0 & 0 & -.5 & 0 & 0 \\ 0 & 0 & 1 & 0 & 0 & 0 & 0 \\ 0 & 0 & 0 & 1 & 0 & 0 & 0 \\ -.354 & 0 & 0 & 0 & .354 & 1 & 0 \\ -.354 & .707 & 0 & 0 & -.354 & 0 & 1 \end{bmatrix}_{j=2} \begin{bmatrix} \dot{M}^4 \\ \dot{M}^5 \\ \dot{M}^6 \\ \dot{M}^2 \\ \dot{M}^3 \\ \dot{M}^8 - .5g^2 C_{IO} \\ \dot{M}^9 + .5g^2 C_{IP} \end{bmatrix}_{j=2}$$

TABLE C-2 ACCELEROMETER PARTIAL CALIBRATION ESTIMATION
EQUATIONS (Cont.)

Accelerometer #3

$$\begin{bmatrix} \hat{A}'_b \\ -(\hat{NOA})g \\ (\hat{NPA})g \\ \hat{\delta V}_c^{+.1} \\ \hat{\delta V}_c^{-.1} \\ \hat{\delta V}_c^{+.7} \\ \hat{\delta V}_c^{-.7} \end{bmatrix}_{j=3} = \begin{bmatrix} 1 & 0 & .5 & 0 & .5 & 0 & 0 \\ 0 & 0 & -.5 & 0 & .5 & 0 & 0 \\ -1 & 0 & .5 & 0 & .5 & 0 & 0 \\ 0 & 1 & 0 & 0 & 0 & 0 & 0 \\ 0 & 0 & 0 & 1 & 0 & 0 & 0 \\ .7 & 0 & -.354 & 0 & -.354 & 1 & 0 \\ 0 & 0 & .354 & 0 & -.354 & 0 & 1 \end{bmatrix}_{j=3} \begin{bmatrix} \dot{M}^4 \\ \dot{M}^5 \\ \dot{M}^6 \\ \dot{M}^1 \\ \dot{M}^2 \\ \dot{M}^7 -.5g^2 C_{IO} \\ \dot{M}^9 +.5g^2 C_{IP} \end{bmatrix}_{j=3}$$

* The \dot{M}_j^m terms are computed as indicated in Tables B-2, B-3 and B-4.

* Not shown are compensations for rotary axis tilt error (from vertical).

TABLE C-3 ACCELEROMETER FULL CALIBRATION ESTIMATION EQUATIONS

Accelerometer #1

$$\begin{bmatrix}
 \hat{A}'_{b \ \hat{a}} \\
 -(NOA)g \\
 (NPA)g \\
 \hat{\delta V}_c^{+.1} \\
 \hat{\delta V}_c^{-.1} \\
 \hat{\delta V}_c^{+.7} \\
 \hat{\delta V}_c^{-.7} \\
 C_{IP}^{\hat{a}} \\
 C_{IO}^{\hat{a}}
 \end{bmatrix}
 =
 \begin{bmatrix}
 0 & .517 & -.058 & .459 & 0 & 0 & 0 & 0 & 0 & .082 \\
 0 & -.435 & +.779 & -.656 & 0 & 0 & 0 & 0 & 0 & .313 \\
 0 & .459 & .139 & -.401 & 0 & 0 & 0 & 0 & 0 & -.197 \\
 0 & 0 & 0 & 0 & 1 & 0 & 0 & 0 & 0 & 0 \\
 1 & 0 & 0 & 0 & 0 & 0 & 0 & 0 & 0 & 0 \\
 0 & 0 & 0 & 0 & 0 & .5 & 0 & .5 & 0 & 0 \\
 0 & 0 & 0 & 0 & 0 & .0 & .5 & 0 & .5 & 0 \\
 0 & -.615 & 1.101 & -.928 & 0 & 0 & -1 & 0 & 1 & .442 \\
 0 & -.649 & -.198 & .568 & 0 & +1 & 0 & -1 & 0 & .279
 \end{bmatrix}
 \begin{bmatrix}
 \dot{M}^4 \\
 \dot{M}^5 \\
 \dot{M}^6 \\
 \dot{M}^1 \\
 \dot{M}^3 \\
 \dot{M}^7 \\
 \dot{M}^8 \\
 \dot{M}^{10} \\
 \dot{M}^{11} \\
 \dot{M}^{12}
 \end{bmatrix}$$

$j=1$ $j=1$ $j=1$

Accelerometer #2

$$\begin{bmatrix}
 \hat{A}'_{b \ \hat{a}} \\
 -(NOA)g \\
 (NPA)g \\
 \hat{\delta V}_c^{+.1} \\
 \hat{\delta V}_c^{-.1} \\
 \hat{\delta V}_c^{+.7} \\
 \hat{\delta V}_c^{-.7} \\
 C_{IP}^{\hat{a}} \\
 C_{IO}^{\hat{a}}
 \end{bmatrix}
 =
 \begin{bmatrix}
 .5 & .125 & 0 & 0 & .375 & -.088 & .088 & -.088 & .088 & 0 \\
 -.5 & .625 & 0 & 0 & -.125 & .265 & -.265 & .265 & -.265 & 0 \\
 -.5 & .125 & 0 & 0 & .375 & -.088 & .088 & -.088 & +.088 & 0 \\
 0 & 0 & 1 & 0 & 0 & .0 & 0 & 0 & 0 & 0 \\
 0 & 0 & 0 & 1 & 0 & 0 & 0 & 0 & 0 & 0 \\
 0 & -.088 & 0 & 0 & -.088 & .437 & .063 & -.063 & +.063 & .5 \\
 -.707 & .442 & 0 & 0 & .265 & .187 & .313 & .687 & .313 & -.5 \\
 .707 & -.354 & 0 & 0 & -.354 & .250 & .750 & -.750 & -1.250 & 1 \\
 .707 & -.354 & 0 & 0 & -.354 & -.750 & -.250 & .250 & -.250 & 1
 \end{bmatrix}
 \begin{bmatrix}
 \dot{M}^4 \\
 \dot{M}^5 \\
 \dot{M}^6 \\
 \dot{M}^2 \\
 \dot{M}^3 \\
 \dot{M}^8 \\
 \dot{M}^9 \\
 \dot{M}^{11} \\
 \dot{M}^{12} \\
 \dot{M}^{13}
 \end{bmatrix}$$

$j=2$ $j=2$ $j=2$

TABLE C-3 ACCELEROMETER FULL CALIBRATION ESTIMATION EQUATIONS (Cont.)

Accelerometer #3

$$\begin{bmatrix}
 \hat{A}_b \\
 \text{-(NOA)g} \\
 \text{(NPA)g} \\
 \hat{\delta V}_c^{+.1} \\
 \hat{\delta V}_c^{.-1} \\
 \hat{\delta V}_c^{+.7} \\
 \hat{\delta V}_c^{.-.7} \\
 \hat{C}_{IP} \\
 \hat{C}_{IO}
 \end{bmatrix}
 =
 \begin{bmatrix}
 -.058 & 0 & .517 & 0 & .459 & 0 & 0 & 0 & .082 & 0 \\
 -.140 & 0 & -.459 & 0 & .401 & 0 & 0 & 0 & .197 & 0 \\
 -.779 & 0 & .435 & 0 & .656 & 0 & 0 & 0 & -.313 & 0 \\
 0 & 1 & 0 & 0 & 0 & 0 & 0 & 0 & 0 & 0 \\
 0 & 0 & 0 & 1 & 0 & 0 & 0 & 0 & 0 & 0 \\
 1.101 & 0 & -.615 & 0 & -.928 & 1 & -.5 & 1 & .442 & -.5 \\
 0 & 0 & 0 & 0 & 0 & 0 & .5 & 0 & 0 & .5 \\
 -.197 & 0 & -.649 & 0 & .568 & 0 & -1 & 0 & .279 & 1 \\
 -1.101 & 0 & .615 & 0 & .928 & 0 & 1 & -2 & -.442 & 1
 \end{bmatrix}
 \begin{bmatrix}
 \dot{M}^4 \\
 \dot{M}^5 \\
 \dot{M}^6 \\
 \dot{M}^1 \\
 \dot{M}^2 \\
 \dot{M}^7 \\
 \dot{M}^9 \\
 \dot{M}^{10} \\
 \dot{M}^{11} \\
 \dot{M}^{12}
 \end{bmatrix}$$

$j=3$
 $j=3$
 $j=3$

•The \dot{M}_j^m terms are computed as indicated in Tables B-2, B-3 and B-4.
 •Not shown are compensations for rotary axis tilt error (from vertical).

TABLE C-4 ACCELEROMETER SCALE FACTOR ERROR ESTIMATION

EQUATIONS

The following calculations are performed for each accelerometer(j)

$$\left. \begin{aligned} \hat{A}_b &= (F_4 Z_0 - F_2 Z_2) / (KF_4 - F_2^2) \\ \hat{D}_1 &= (F_6 Z_1 - F_4 Z_3) / (F_2 F_6 - F_4^2) \\ \hat{D}_2 &= (KZ_2 - F_2 Z_0) / (KF_4 - F_2^2) \\ \hat{D}_3 &= (F_2 Z_3 - F_4 Z_1) / (F_2 F_6 - F_4^2) \end{aligned} \right\} \text{General form-for } \pm \text{ pairs of inputs}$$

where

$$\begin{aligned} Z_0 &\equiv \sum_1^K (\delta \dot{V}_c)_k & F_2 &\equiv \sum_1^K (a_{i_k})^2 \\ Z_1 &\equiv \sum_1^K (a_{i_k}) (\delta \dot{V}_c)_k & F_4 &\equiv \sum_1^K (a_{i_k})^4 \\ Z_2 &\equiv \sum_1^K (a_{i_k})^2 (\delta \dot{V}_c)_k & F_6 &\equiv \sum_1^K (a_{i_k})^6 \\ Z_3 &\equiv \sum_1^K (a_{i_k})^3 (\delta \dot{V}_c)_k & K &= \text{number of data samples} \end{aligned}$$

and

$$\begin{aligned} (\delta \dot{V}_c)_1 &\equiv \delta \dot{V}_c^{-1}, & (a_{i_1})_1 &= -g \\ (\delta \dot{V}_c)_2 &\equiv \delta \dot{V}_c^{-.7}, & (a_{i_2})_2 &= -g/\sqrt{2} \\ (\delta \dot{V}_c)_3 &\equiv \hat{A}'_b, & (a_{i_3})_3 &= 0 \\ (\delta \dot{V}_c)_4 &\equiv \delta \dot{V}_c^{+.7}, & (a_{i_4})_4 &= +g/\sqrt{2} \\ (\delta \dot{V}_c)_5 &\equiv \delta \dot{V}_c^{+1}, & (a_{i_5})_5 &= +g \end{aligned}$$

For the inputs shown, the above general estimation equations may be simplified, to yield:

$$\left. \begin{aligned} \hat{A}_b &= (2.5 Z_0 - 3Z_2/g^2) / 3.5 \\ \hat{D}_1 &= (2.25 Z_1 - 2.5Z_3/g^2) / .5g^2 \\ \hat{D}_2 &= (-3 Z_0 + 5 Z_2/g) / 3.5 g^2 \\ \hat{D}_3 &= (-2.5 Z_1 + 3 Z_3/g^2) / .5g^2 \end{aligned} \right\} \text{For the data obtained in Tables C-2 and C-3}$$

in which only the Z terms need to be computed.

TABLE C-5 GYRO NONORTHOGONALITY AND RATE ERROR
ESTIMATION EQUATIONS

Define $c^{m-} \equiv \pi(w^{T+} - w^{T-})^m / 360$

$$\begin{array}{c} \text{Gyro \#1} \\ \left[\begin{array}{c} \hat{\text{NOA}} \\ \hat{\text{NSA}} \\ \hat{\delta\dot{\psi}}_c^+ \\ \hat{\delta\dot{\psi}}_c^- \end{array} \right]_{j=1} = \left[\begin{array}{cccc} 0 & 0 & 0 & 1/c^{61-} \\ 0 & 0 & 1/c^{51-} & 0 \\ 1 & 0 & 0 & 0 \\ 0 & 1 & 0 & 0 \end{array} \right]_{j=1} \left[\begin{array}{c} \dot{M}^{c_1^+} \\ \dot{M}^{c_1^-} \\ \dot{M}^{51} \\ \dot{M}^{61} \end{array} \right]_{j=1} \end{array}$$

where $c_1 \equiv$ a function of table rate (w^T) used = 71, 72, 73,

$$\begin{array}{c} \text{Gyro \#2} \\ \left[\begin{array}{c} \hat{\text{NOA}} \\ \hat{\text{NSA}} \\ \hat{\delta\dot{\psi}}_c^+ \\ \hat{\delta\dot{\psi}}_c^- \end{array} \right]_{j=2} = \left[\begin{array}{cccc} 0 & 0 & 0 & -1/c^{51-} \\ 0 & 0 & -1/c^{41-} & 0 \\ 1 & 0 & 0 & 0 \\ 0 & 1 & 0 & 0 \end{array} \right]_{j=2} \left[\begin{array}{c} \dot{M}^{c_2^+} \\ \dot{M}^{c_2^-} \\ \dot{M}^{41} \\ \dot{M}^{51} \end{array} \right]_{j=2} \end{array}$$

where $c_2 \equiv$ a function of table rate (w^T) used = 91, 92, 93,

$$\begin{array}{c} \text{Gyro \#3} \\ \left[\begin{array}{c} \hat{\text{NOA}} \\ \hat{\text{NSA}} \\ \hat{\delta\dot{\psi}}_c^+ \\ \hat{\delta\dot{\psi}}_c^- \end{array} \right]_{j=3} = \left[\begin{array}{cccc} 0 & 0 & 0 & 1/c^{61-} \\ 0 & 0 & -1/c^{41-} & 0 \\ 1 & 0 & 0 & 0 \\ 0 & 1 & 0 & 0 \end{array} \right]_{j=3} \left[\begin{array}{c} \dot{M}^{c_3^+} \\ \dot{M}^{c_3^-} \\ \dot{M}^{41} \\ \dot{M}^{61} \end{array} \right]_{j=3} \end{array}$$

where $c_3 \equiv$ a function of table rate (w^T) used = 81, 82, 83,

The units of $\hat{\delta\dot{\psi}}_c$ and \dot{M} are deg/hr., $\hat{\text{NOA}}$ and $\hat{\text{NSA}}$ are in $\widehat{\text{sec}}$, and w^T in deg/sec. The \dot{M}_j^m terms are computed as indicated in Tables B-5, B-6, and B-7.

TABLE C-6 GYRO MINIMUM CALIBRATION ESTIMATION EQUATIONS

Gyro #1

$$\begin{bmatrix} \hat{R}_b^i \\ \hat{gB}_I^A \\ \hat{gB}_S^A \\ \hat{gB}_O^A \end{bmatrix}_{j=1} = \begin{bmatrix} 0 & .25 & .25 & .25 & .25 \\ 1 & -.25 & -.25 & -.25 & -.25 \\ 0 & 0 & -.5 & 0 & .5 \\ 0 & .5 & 0 & -.5 & 0 \end{bmatrix}_{j=1} \begin{bmatrix} \dot{M}^4 - g^2 C_{II} \\ \dot{M}^{50} \\ \dot{M}^{60} - g^2 C_{SS} \\ \dot{M}^1 \\ \dot{M}^2 - g^2 C_{SS} \end{bmatrix}_{j=1}$$

Gyro #2

$$\begin{bmatrix} \hat{R}_b^i \\ \hat{gB}_I^A \\ \hat{gB}_S^A \\ \hat{gB}_O^A \end{bmatrix}_{j=2} = \begin{bmatrix} .25 & .25 & 0 & .25 & .25 \\ -.25 & -.25 & 1 & -.25 & -.25 \\ 0 & .5 & 0 & -.5 & 0 \\ -.5 & 0 & 0 & 0 & .5 \end{bmatrix}_{j=2} \begin{bmatrix} \dot{M}^{40} \\ \dot{M}^{50} - g^2 C_{SS} \\ \dot{M}^6 - g^2 C_{II} \\ \dot{M}^1 - g^2 C_{SS} \\ \dot{M}^3 \end{bmatrix}_{j=2}$$

Gyro #3

$$\begin{bmatrix} \hat{R}_b^i \\ \hat{gB}_I^A \\ \hat{gB}_S^A \\ \hat{gB}_O^A \end{bmatrix}_{j=3} = \begin{bmatrix} .25 & 0 & .25 & .25 & .25 \\ -.25 & 1 & -.25 & -.25 & -.25 \\ 0 & 0 & -.5 & .5 & 0 \\ -.5 & 0 & 0 & 0 & .5 \end{bmatrix}_{j=3} \begin{bmatrix} \dot{M}^{40} \\ \dot{M}^5 - g^2 C_{II} \\ \dot{M}^{60} - g^2 C_{SS} \\ \dot{M}^2 - g^2 C_{SS} \\ \dot{M}^3 \end{bmatrix}_{j=3}$$

- The \dot{M}_j^m terms are computed as indicated in Tables B-5, B-6 and B-7.
- Not shown are compensations for earth rate coupling through NOA and NSA.

TABLE C-7 GYRO PARTIAL CALIBRATION ESTIMATION EQUATIONS

Gyro #1

$$\begin{bmatrix} R_b^A \\ gB_I^A \\ gB_S^A \\ gB_O^A \\ g^2 C_{II}^A \\ g^2 C_{SS}^A \end{bmatrix}_{j=1} = \begin{bmatrix} -.014 & .497 & -.015 & .500 & .003 & .004 & .024 \\ .268 & .474 & -.150 & -.081 & .026 & -.786 & .249 \\ .118 & .021 & -.379 & -.004 & .479 & -.034 & -.201 \\ -.020 & .496 & -.021 & -.500 & .004 & .006 & .034 \\ .551 & -1 & -.036 & -.413 & .006 & .839 & .060 \\ -.069 & -.512 & .429 & -.498 & .512 & .020 & .118 \end{bmatrix} \begin{bmatrix} \dot{M}^4 \\ \dot{M}^{50} \\ \dot{M}^{60} \\ \dot{M}^1 \\ \dot{M}^2 \\ \dot{M}^{7+.5g^2C_{IO}} \\ \dot{M}^{8+.5g^2C_{IS}} \end{bmatrix}_{j=1}$$

Gyro #2

$$\begin{bmatrix} R_b^A \\ gB_I^A \\ gB_S^A \\ gB_O^A \\ g^2 C_{II}^A \\ g^2 C_{SS}^A \end{bmatrix}_{j=2} = \begin{bmatrix} .414 & .003 & -.083 & -.015 & .515 & .142 & .024 \\ -.150 & -.081 & .268 & .474 & .026 & .249 & -.786 \\ .021 & .499 & .020 & -.496 & -.004 & -.034 & -.006 \\ -.379 & -.004 & .118 & .021 & .479 & -.201 & -.034 \\ -.465 & .085 & .620 & -.494 & -.506 & -.058 & .819 \\ -.429 & .498 & .069 & .512 & -.512 & -.118 & -.020 \end{bmatrix}_{j=2} \begin{bmatrix} \dot{M}^{40} \\ \dot{M}^{50} \\ \dot{M}^6 \\ \dot{M}^1 \\ \dot{M}^3 \\ \dot{M}^{8+.5g^2C_{IO}} \\ \dot{M}^{9-.5g^2C_{IS}} \end{bmatrix}_{j=2}$$

Gyro #3

$$\begin{bmatrix} R_b^A \\ gB_I^A \\ gB_S^A \\ gB_O^A \\ g^2 C_{II}^A \\ g^2 C_{SS}^A \end{bmatrix}_{j=3} = \begin{bmatrix} .515 & -.083 & .003 & -.015 & .414 & .142 & .024 \\ .026 & .268 & -.081 & .474 & -.150 & .249 & -.786 \\ .004 & -.020 & -.499 & .496 & -.021 & .034 & .006 \\ -.479 & -.118 & .004 & -.021 & .379 & .201 & .034 \\ -.506 & .620 & .085 & -.494 & -.465 & -.058 & .819 \\ -.512 & .069 & .498 & .512 & -.429 & -.118 & -.020 \end{bmatrix}_{j=3} \begin{bmatrix} \dot{M}^{40} \\ \dot{M}^5 \\ \dot{M}^{60} \\ \dot{M}^2 \\ \dot{M}^3 \\ \dot{M}^{7-.5g^2C_{IO}} \\ \dot{M}^{9+.5g^2C_{IS}} \end{bmatrix}_{j=3}$$

Notes: (1) The \dot{M}_j^m terms are computed as indicated in Tables B-5, B-6 and B-7.

(2) Not shown are compensations for earth rate coupling through NOA and NSA.

TABLE C-8 GYRO FULL CALIBRATION ESTIMATION EQUATIONS

Gyro #1

$$\begin{bmatrix} R_b^A \\ g_{B_I}^A \\ g_{B_S}^A \\ g_{B_O}^A \\ g_{C_{II}}^{2A} \\ g_{C_{SS}}^{2A} \\ g_{C_{IS}}^{2A} \\ g_{C_{IO}}^{2A} \\ g_{C_{OS}}^{2A} \end{bmatrix} = \begin{bmatrix} -.025 & .498 & -.011 & .498 & -.011 & .004 & .022 & .004 & .022 & 0 \\ .217 & .193 & -.084 & .193 & -.084 & -.385 & .168 & -.385 & .168 & 0 \\ 0 & 0 & -.5 & 0 & .5 & 0 & 0 & 0 & 0 & 0 \\ 0 & .5 & 0 & -.5 & 0 & 0 & 0 & 0 & 0 & 0 \\ .460 & -.716 & -.054 & -.716 & -.054 & .433 & .107 & .433 & .107 & 0 \\ -.123 & -.509 & .448 & -.509 & .448 & .018 & .105 & .018 & .105 & 0 \\ 0 & 0 & .707 & 0 & -.707 & 0 & -1 & 0 & 1 & 0 \\ 0 & .707 & 0 & -.707 & 0 & -1 & 0 & 1 & 0 & 0 \\ .174 & .220 & -1.133 & -1.194 & .281 & -.255 & -.148 & -.255 & -.148 & 1 \end{bmatrix} \begin{bmatrix} \dot{M}^4 \\ \dot{M}^5 \\ \dot{M}^6 \\ \dot{M}^1 \\ \dot{M}^2 \\ \dot{M}^7 \\ \dot{M}^8 \\ \dot{M}^{10} \\ \dot{M}^{11} \\ \dot{M}^{12} \end{bmatrix}$$

$j=1$ $j=1$ $j=1$

Gyro #2

$$\begin{bmatrix} R_b^A \\ g_{B_I}^A \\ g_{B_S}^A \\ g_{B_O}^A \\ g_{C_{II}}^{2A} \\ g_{C_{SS}}^{2A} \\ g_{C_{IS}}^{2A} \\ g_{C_{IO}}^{2A} \\ g_{C_{OS}}^{2A} \end{bmatrix} = \begin{bmatrix} .336 & -.006 & -.138 & .037 & .466 & .168 & -.304 & 0 & .071 & -.030 & .097 \\ .325 & -.054 & .199 & .315 & -.388 & .062 & -.261 & 0 & -.504 & -.261 & .566 \\ -.093 & .474 & .083 & -.348 & .050 & .043 & -.126 & 0 & .101 & -.126 & -.058 \\ -.379 & .021 & -.001 & -.122 & .479 & -.100 & .101 & 0 & -.101 & .101 & .001 \\ -.827 & .085 & .547 & -.493 & -.217 & .045 & .409 & 0 & .431 & .409 & -.387 \\ -.300 & .525 & .079 & .356 & -.501 & -.198 & .119 & 0 & -.142 & .119 & -.056 \\ .460 & -.076 & .281 & .446 & -.548 & .088 & .630 & 0 & -.713 & -1.370 & .801 \\ .364 & -.059 & .004 & .346 & -.646 & -.717 & -.287 & 0 & .286 & -.287 & .997 \\ .028 & -.128 & -.315 & .749 & 1.036 & -.065 & .379 & -2 & -.287 & .379 & .223 \end{bmatrix} \begin{bmatrix} \dot{M}^{40} \\ \dot{M}^{50} \\ \dot{M}^6 \\ \dot{M}^1 \\ \dot{M}^3 \\ \dot{M}^8 \\ \dot{M}^9 \\ \dot{M}^{10} \\ \dot{M}^{11} \\ \dot{M}^{12} \\ \dot{M}^{13} \end{bmatrix}$$

$j=2$ $j=2$ $j=2$

TABLE C-8 GYRO FULL CALIBRATION ESTIMATION EQUATIONS

(cont.)

Gyro #3													
\hat{R}_b^A		.504	-.073	.048	.004	.372	.124	-.051	.124	.031	-.051	-.031	\dot{M}^{40}
\hat{g}_I^B		-.001	.441	.189	.206	.048	-.046	-.395	-.046	-.012	-.395	.012	\dot{M}^5
\hat{g}_S^B		-.124	-.026	-.358	.376	.080	.044	-.018	.044	.188	-.018	-.188	\dot{M}^{60}
\hat{g}_O^B		-.371	-.087	-.074	.129	.239	.132	-.055	.132	-.144	-.055	.144	\dot{M}^2
\hat{g}_{II}^{2A}	=	-.498	.546	-.181	-.205	-.570	.068	.386	.068	.017	.386	-.017	\dot{M}^3
\hat{g}_{SS}^{2A}		-.505	.103	.433	.495	-.319	-.176	.073	-.176	-.044	.073	.044	\dot{M}^7
\hat{g}_{IS}^{2A}		-.175	-.036	-.506	.532	.113	.062	-1.026	.062	.265	.974	-.265	\dot{M}^9
\hat{g}_{IO}^{2A}		.002	-.624	-.268	-.291	-.068	1.066	.559	-.934	.016	.559	-.016	\dot{M}^{10}
\hat{g}_{OS}^{2A}		.502	-.043	.528	.502	.425	.073	-.030	.073	-.982	-.030	-1.018	\dot{M}^{11}
													\dot{M}^{12}
													\dot{M}^{13}

Notes: (1) The M_j^m terms are computed as indicated in Tables B-5, B-6 & B-7

(2) Not shown are compensations for earth rate coupling through NOA and NSA.

TABLE C-9 GYRO SCALE FACTOR ERROR ESTIMATION EQUATIONS

$$\left. \begin{aligned} \hat{R}_b &= (Z_0 - F_2 Z_2) / (KF_4 - F_2^2) \\ \hat{Q}_1 &= Z_1 / F_2 \\ \hat{Q}_2 &= KZ_2 / (KF_4 - F_2^2) \end{aligned} \right\} \text{general form - for } \pm \text{ pairs} \\ \text{of inputs.}$$

where

$$\begin{aligned} Z_0 &\equiv \sum_1^K (\delta \dot{\psi}_c)_k \\ Z_1 &\equiv \sum_1^K (W^T)_k z_k \\ Z_2 &\equiv \sum_1^K (W^T)_k^2 z_k \end{aligned} \quad \begin{aligned} F_2 &\equiv \sum_1^K (W^T)_k^2 \\ F_4 &\equiv \sum_1^K (W^T)_k^4 \end{aligned}$$

k = number of data samples

$$Z_3 \equiv \sum_1^K (W^T)_k^3 z_k \quad z_k \equiv (\delta \dot{\psi}_c)_k - Z_0/k$$

and $z = \hat{R}_b'$ for $W^T = 0$ is included. The $(\delta \dot{\psi}_c^+, \delta \dot{\psi}_c^-)$ pairs for various W^T are obtained from Table C-5.

If a third order coefficient (Q_3) is to be estimated, the F_6 terms in Eqs. (9-7) and (9-9) must be retained, where

$$F_6^G \equiv \sum_1^K (W^T)_k^6$$

APPENDIX D

EFFECT OF ENVIRONMENTAL ERROR SOURCES

The environmental error sources are as specified in Figs. 10-1 and 10-2 of Section 10.3. In the case of $\Delta\phi_n$, the angular motion of the test stand base, the effect is to cause cross coupling of (1) earth rate components to the IA's of the gyros and (2) components of specific force due to gravity to the IA's of the accelerometers. Components of the rate of change of $\Delta\phi_n$ (i. e., $\dot{\Delta\phi}_n$) in the direction of the gyro IAs are sensed directly as erroneous rate errors. In the case of a_v , the linear vibration of the test stand, the effect is significant only at the input to the accelerometers.

This appendix presents the transfer functions and resulting effects associated with the above error sources. The equations are presented in this appendix and plots are provided in Appendices E and F. The analyses used in the UNIVAC report (Ref. 4) are utilized, and in several instances apparent inconsistencies were noted.* Some of these were resolved; others are more involved and require more detailed analyses beyond the scope of this study.

D.1 EFFECT ON ACCELEROMETERS

The component of $\delta\dot{M}$ due to the $\Delta\phi_n$ and a_v environmental error sources are given in the time domain as follows:

*These are identified wherever they occur.

$$(\ddot{e}_n^A)^m = (\dot{e}_n^A)^m = \frac{1}{\Delta t^m} \int_0^{\Delta t} [(\dot{e}_{\Delta\phi_n}^A)^m + (a_v)^m] dt \quad (D-1)$$

where

$$(\dot{e}_{\Delta\phi_n}^A)^m = \begin{cases} g(\Delta\phi_n) & \text{for IA level} & (D-2) \\ g(\Delta\phi_n)/\sqrt{2} & \text{for IA at } 45^\circ \text{ to level} & (D-3) \\ 0 & \text{for IA vertical} & (D-4) \end{cases}$$

Since $\Delta\phi_n$ and a_v are given in terms of power spectral densities (PSDs), the autocorrelation function and Fourier Transform of Eq. (D-1) is computed. This was done in Appendix A of Ref. 4 and the results are summarized as follows:

Accelerometer IA vertical

$$\sigma^2(\ddot{e}_n^A) = \left(\frac{1}{\Delta t^m}\right)^2 \left[\int_0^\infty \frac{2(1 - \Delta t^m \cos 2\pi f)}{(\Delta t^m 2\pi f)^2} \{ \text{PSD}(a_v) \} df \right] \quad (D-5)$$

Accelerometer IA at 45° to level

$$\sigma^2(\ddot{e}_n^A) = \left(\frac{1}{\Delta t^m}\right)^2 \left[\int_0^\infty \frac{2(1 - \Delta t^m \cos 2\pi f)}{(\Delta t^m 2\pi f)^2} \left\{ \text{PSD}(a_v) + \frac{g^2}{2} \text{PSD}(\Delta\phi_n) \right\} df \right] \quad (D-6)$$

Accelerometer IA level

$$\sigma^2(\ddot{e}_n^A) = \left(\frac{1}{\Delta t^m}\right)^2 \left[\int_0^\infty \frac{2(1 - \Delta t^m \cos 2\pi f)}{(\Delta t^m 2\pi f)^2} \left\{ \text{PSD}(a_v) + g^2 \text{PSD}(\Delta\phi_n) \right\} df \right] \quad (D-7)$$

where the PSDs are given in Figs. 10-2 and 10-1 and approximated as shown in Tables 10-2 and 10-1, for the case when the bubble levels are not used.

These equations have been solved (in Appendix A of Ref. 4) and the equations that relate the PSD's to $\sigma^2(\dot{e}_n^A)$ are repeated here as follows:

$$\left. \begin{array}{l} \sigma^2(\dot{e}_n^A) \text{ due to} \\ \text{PSD}(a_v) \end{array} \right\} = \frac{1.1 \times 10^{-15}}{\Delta t} + \frac{1.92 \times 10^{-8}}{(\Delta t)^2} \quad (\text{D-8})$$

$$\left. \begin{array}{l} \sigma^2(\dot{e}_n^A) \text{ due to} \\ g^2 \text{ PSD}(\Delta\phi_n) \end{array} \right\} = 9.4 \times 10^{-9} - 2.3 \times 10^{-14} \Delta t + \frac{6.7 \times 10^{-15}}{(\Delta t)^2} \quad (\text{D-9})$$

$$\left. \begin{array}{l} \sigma^2(\dot{e}_n^A) \text{ due to} \\ \frac{g^2}{2} \text{ PSD}(\Delta\phi_n) \end{array} \right\} = 4.7 \times 10^{-9} - 1.15 \times 10^{-14} \Delta t + \frac{3.35 \times 10^{-15}}{(\Delta t)^2} \quad (\text{D-10})$$

where $\sigma^2(\dot{e}_n^A)$ has units of g^2 and t is the run time in minutes. The effect a_v is shown plotted in Fig. E-6 of Appendix E (as reproduced from Table 1-1 of Ref. 8, Fig. 2-3 of Ref. A, and Eq. (D-8), which is derived in Appendix A of Ref. 4).^{*} It will be assumed that the curve from Ref. 8 is the correct one since the others are based on it and are inconsistent with each other. Even if Fig. 2-3 of Ref. 4 were the correct curve, the effect on the measurement errors would be small (see Table E-2).

Without bubble level compensation, the effect of $\Delta\phi_n$ as given by Eqs. (D-9) and (D-10) is to cause excessively large errors (viz., 97 and 68 μg for IA horizontal and at 45°, respectively). However, when bubble levels are used, as is the case considered in the error analysis, the terms in Eqs. (D-9) and (D-10) are reduced considerably. Upon applying the

^{*}The curve from Ref. 8 is assumed correct, particularly since the two from Ref. A are apparently inconsistent.

two bubble level models discussed in Section 10.3, the resulting average accelerometer output errors are as shown in Fig. E-5 of Appendix E.

D.2 EFFECT ON GYROS

The component of $\delta \dot{M}$ due to random gyro drift (\dot{e}_{nr}^G) and the $\Delta\phi_n$ and $\Delta\dot{\phi}_n$ environmental error sources are given in the time domain as follows:

$$\tau_{\dot{e}_n^G} = (\dot{e}_n^G)^m = \frac{1}{\Delta t^m} \int_0^{\Delta t^m} [\dot{e}_{nr}^G + (\dot{e}_{\Delta\phi_n}^G)^m + (\dot{e}_{\Delta\dot{\phi}_n}^G)^m] dt \quad (D-11)$$

where

$$\dot{e}_{nr}^G = \text{gyro internal noise (in terms of rate)} \quad (D-12)$$

$$\dot{e}_{\Delta\phi_n}^G = \begin{cases} (w_e \cos L) \Delta\phi_n & \text{for IA vertical} \\ (w_e \sin L) \Delta\phi_n & \text{for IA horizontal} \end{cases} \quad (D-13)$$

$$\dot{e}_{\Delta\dot{\phi}_n}^G = \begin{cases} 0 & \text{for IA vertical} \\ \Delta\dot{\phi}_n & \text{for IA horizontal} \end{cases} \quad (D-14)$$

Since \dot{e}_{nr}^G and $\Delta\dot{\phi}_n$ are given in terms of power spectral densities (PSDs), the autocorrelation function and Fourier Transform for Eq. (D-11) is computed. This was done in Appendix A of Ref. 4 and the results are summarized as follows:

Gyro IA vertical

$$\sigma^2 (\dot{e}_n^G)^m = \left(\frac{1}{\Delta t^m} \right)^2 \left[\int_0^\infty \frac{2(1 - \Delta t^m \cos 2\pi f)}{(\Delta t^m 2\pi f)^2} \{ \text{PSD}(\dot{e}_{nr}^G) + (w_e \cos L)^2 \text{PSD}(\Delta\phi_n) \} df \right] \quad (D-16)$$

Gyro IA Horizontal

$$\sigma^2(\dot{e}_n^G)^m = \left(\frac{1}{\Delta t^m}\right)^2 \left[\int_0^{\infty} \frac{2(1 - \Delta t^m \cos 2\pi f)}{(\Delta t^m 2\pi f)^2} \{ \text{PSD}(\dot{e}_{nr}^G) + (w_e \sin L)^2 \text{PSD}(\Delta \phi_n) + \text{PSD}(\Delta \dot{\phi}_n) \} df \right] \quad (D-17)$$

where

$$\text{PSD}(\dot{e}_{nr}^G) \equiv \text{PSD of } \dot{e}_{nr}^G$$

$$\text{PSD}(\Delta \phi_n) \equiv \text{PSD of angular motion of test stand base, about level axes}$$

$$\text{PSD}(\Delta \dot{\phi}_n) \equiv \text{PSD of angular vibration of test stand, about level axes}$$

$$= (2\pi f)^2 \text{PSD}(\Delta \phi_n)$$

where the PSDs are given in Tables 4-6 and Fig. 10-1. The standard deviation of Eq. (D-17) is plotted in Fig. F-8 of Appendix F. Each of the terms in Eqs. (D-16) and (D-17) have been solved separately (in Appendix A of Ref 4) and the equations that relate the PSD's to $\sigma^2(\dot{e}_n^G)$ are repeated here as follows:

$$\left. \begin{array}{l} \sigma^2(\dot{e}_n^G) \text{ due to} \\ \text{PSD}(\dot{e}_{nr}^G) \end{array} \right\} = 1.7 \times 10^{-7} + \frac{2.6 \times 10^{-7}}{\Delta t} + \frac{5.5 \times 10^{-9}}{(\Delta t)^2} \quad (D-18)$$

$$\left. \begin{array}{l} \sigma^2(\dot{e}_n^G) \text{ due to} \\ \left(\frac{15}{\sqrt{2}}\right)^2 \text{PSD}(\Delta \phi_n) \end{array} \right\} = 1.8 \times 10^{-7} - 2.4 \times 10^{-12} \Delta t - \frac{8.5 \times 10^{-12}}{(\Delta t)^2} \quad (D-19)$$

$$\left. \begin{array}{l} \sigma^2(\dot{\epsilon}_n^G) \text{ due to} \\ \text{PSD } (\Delta\dot{\phi}_n) \end{array} \right\} = \frac{4.35 \times 10^{-2}}{\Delta t} + \frac{2.11 \times 10^{-1}}{(\Delta t)^2} \quad (\text{D-20})$$

where the variances have units of (deg/hr.)² and Δt is in minutes.

Fig. 2-1 of Ref. 4 is a plot of Eqs. (D-18) and (D-19) and indicates $\sigma(\dot{\epsilon}_n^G)$ is equal to 1.4 mdh for $\Delta t > 2.5$ min. Although this is inconsistent with the above equations, it is used in the error analysis (see Table F-2) since the equations in Ref. 4 appear to be inconsistent dimensionally and it is more likely that the final results (in the form of curves) are correct.

Fig. 2-1 of Ref. 4 also contains a plot of Eq(D-20)*, which is reproduced in Fig. F-8 of Appendix F. Again the equation and curve are inconsistent and the curve is chosen as being correct. Results using the equations indicate very large calibration errors which appear to be unrealistic. The results using the curve are one of the largest error sources, as shown in Table F-2, and so further analyses are recommended to verify results. Fig. F-8 also shows the effect when the gyro IA is at 45° to the vertical.

The effect on $\sigma^2(\dot{\epsilon}_n^G)$ in Eq. (D-19) due to using bubble levels, which changes PSD $(\Delta\dot{\phi}_n)$, is not significant since the effect was small in the first place.

* Although Fig. 2-1 of Ref. 4 includes Eqs. (D-18) and (D-19), the pre-dominant term is that in Eq. (D-20).

APPENDIX E

ACCELEROMETER ERROR EQUATIONS

The form of the propagation of the accelerometer error sources into the accelerometer output errors ($\delta\dot{M}$) are shown in Table E-1 for accelerometer #1 ($j = 1$). Each component of $\delta\dot{M}$ is identified by a dash number following the letter "A" and is related to the potentially significant error sources of Table 10-3 as shown in Tables E-1 and E-2. The sensitivities of the error propagations are indicated by the matrix elements in Table E-1. This information is used, in conjunction with numerical values for the error sources as listed in Table 10-3, to determine the components of $\delta\dot{M}$ for each group of accelerometer orientations (m) and run times (Δt). Those calculations are shown in Table E-2, along with the statistical combination* of the $\delta\dot{M}$ components to yield estimates of the expected errors in \dot{M} (viz., $\delta\dot{M}$) for each test condition (m). The total sum-squared error for each test condition (m) is designated e_{ss}^m . Although the error propagation equations of Table E-1 are only for accelerometer #1, the errors can be grouped according to ISU orientation and run time (Δt) and then extended to the other two accelerometers in accordance with like conditions. The results are summarized in Table E-2. Not included in the Table are pre-calibration alignment errors, which will be considered separately as discussed in Section 10.2 and 10.3.

*The errors are assumed to be statistically independent and therefore are combined on a sum-squared basis.

Table E-1 Propagation of Accelerometer #1 Error Sources *

$\delta \dot{M}^4$	$g/2$	$g/2$	$-g^2$	g^2	-	-	$g/\Delta t$	$1/\Delta t$	-	$f(\Delta t) -$ see Fig. E-6	1	$(MIA)^2$ $(\underline{B} \cdot \underline{L})^2$ $C_{IO}(MIA)$ $C_{IP}(MIA)$ $C_{IP}(\underline{O}^A \cdot \underline{B})$ $C_{IO}(\underline{P} \cdot \underline{B})$ $\delta(\Delta t)$ q^A $\Delta\phi_n$ a_v δg^{**}	Accelerometer Error Source No. (A-1) (A-2) (A-3) (A-4) (A-5) (A-6) (A-7) (A-8) (A-9) (A-10) (A-11)	
$\delta \dot{M}^5$	-	-	$-g^2$	-	-	-	-	-	$f(\Delta t, \phi's)$ see Fig. E-5	-	$(MIA)^2$			(A-1)
$\delta \dot{M}^6$	-	-	-	-	-	-	-	-	-	-	$(\underline{B} \cdot \underline{L})^2$			(A-2)
$\delta \dot{M}^1$	-	-	g^2	-	-	-	-	-	-	-	$C_{IO}(MIA)$			(A-3)
$\delta \dot{M}^2$	-	-	-	-	-	-	-	-	-	-	$C_{IP}(MIA)$			(A-4)
$\delta \dot{M}^3$	$g/2$	$g/2$	$-g^2$	g^2	-	-	$g/\Delta t$	-	-	-	$C_{IP}(\underline{O}^A \cdot \underline{B})$			(A-5)
$\delta \dot{M}^7$	-	-	-	$g^2/\sqrt{2}$	$g^2/\sqrt{2}$	-	$g/\sqrt{2}\Delta t$	-	$f(\Delta t, \phi's)$ see Fig. E-5	-1	$C_{IO}(\underline{P} \cdot \underline{B})$			(A-6)
$\delta \dot{M}^8$	-	-	$g^2/\sqrt{2}$	$-g^2/\sqrt{2}$	-	$g^2/\sqrt{2}$	$g/\sqrt{2}\Delta t$	-	-	$-1/\sqrt{2}$	$\delta(\Delta t)$			(A-7)
$\delta \dot{M}^9$	-	-	$-g^2/\sqrt{2}$	$g^2/\sqrt{2}$	-	-	-	-	-	$+1/\sqrt{2}$	q^A			(A-8)
$\delta \dot{M}^{10}$	-	-	-	$-g^2/\sqrt{2}$	-	-	$g/\sqrt{2}\Delta t$	-	-	$-1/\sqrt{2}$	$\Delta\phi_n$			(A-9)
$\delta \dot{M}^{11}$	-	-	$-g^2/\sqrt{2}$	-	-	$g^2/\sqrt{2}$	$g/\sqrt{2}\Delta t$	-	-	$+1/\sqrt{2}$	a_v			(A-10)
$\delta \dot{M}^{12}$	-	-	$-g^2/\sqrt{2}$	$g^2/\sqrt{2}$	-	-	-	-	-	-	δg^{**}			(A-11)
$\delta \dot{M}^{13}$	-	-	$-g^2/\sqrt{2}$	-	-	$g^2/\sqrt{2}$	$g/\sqrt{2}\Delta t$	-	-	$-1/\sqrt{2}$				

* Pre-calibration alignment errors not included
 ** This error source causes correlations in $\delta \dot{M}^m$

Table E-2 Calculation of Accelerometer Error Covariance Matrix Elements (1)

Error Source 1				Error Source 2				Sensitivity (4)		Error Component		
No.	Symb.	Value	Units	No.	Symb.	Value	Units	Value	Units	Value	Units	No.
11	(MIA) ²	(5/3) ²	min ²					$\frac{10^6}{2(60 \cdot 57.3)^2}$	$\frac{\mu g}{\text{min}^2}$.12	μg	A-1
14	(E·L) ²	(10.4/3) ²	min ²					"	"	.51	"	A-2
11	(MIA)	5/3	min	16	C _{IO}	10	$\frac{\mu g}{g^2}$	$\frac{1^{(2)}}{(60 \cdot 57.3)}$	$\frac{g^2}{\text{min}}$.005	"	A-3
11	(MIA)	5/3	min	15	C _{IP}	"	"	"	"	"	"	A-4
12	(Q ^A ·E)	10/3	min	15	C _{IP}	"	"	$\frac{\sqrt{2}}{(60 \cdot 57.3)}$	"	.014	"	A-5
13	(P·E)	10/3	min	16	C _{IO}	"	"	"	"	"	"	A-6

Δt = 5 min				Δt = 10 min			
OA and PA not at 45° to Vertical				OA and/or PA at 45°			
IA Vert.	IA Horiz.	IA Vert.	Horiz	IA 45°	IA Horiz		
.1		.1					
.5		.5					
negl.	negl.	negl.	negl.	negl.	negl.		
"		"		"	"		
				"			

17	δ(Δt)	100	μsec					f(Δt, M)- See Fig. E-3	-	-	-	A-7
18	q ^A	.0025/√6	fps					$\frac{1}{(32.2 \cdot 60)\Delta t}$	$\frac{\mu g}{\text{fps}}$	-	-	A-8
21	Δφ _n	see Fig. 10-1	-					f(Δt, φ's) see Fig. E-5	-	-	-	A-9
22	a _v	see Fig. 10-2	-					f(Δt) see Fig. E-6	-	-	-	A-10
3	δg	3	μg					Errors Correlated	-	see Sect. 10.4.2	-	A-11

.33	-	.17	-	.10	-
.11	.11	.05	.05	.05	.05
-	6.2	-	5.0	5.0/√2	5.0
~.1	~.1	.04	.04	.04	.04
-	-	-	-	-	-

- Notes: (1) Pre-calibration alignment errors are not included.
 (2) This is the sensitivity to g². The g²/√2 sensitivity is not shown since it is negligible.
 (3) Δt is in minutes.
 (4) Error sensitivity plots of Error Components A-1 through A-10 are contained in Figs. E-1 through E-6.

e _{ss} ^m (μg) ²	.39	38.44	.29	25.00	12.63	25.00
δM (μg)	.63	6.2	.54	5.00	3.56	5.00
m for j=1	4	5, 6	3	1, 2	7, 8, 10 11, 13	9, 12
m for j=2	6	4, 5	2	1, 3	8, 9, 11 12, 13	7, 10
m for j=3	5	4, 6	1	2, 3	7, 9, 10, 12	8, 11 13

Plots of the effect on $\delta \dot{M}$ of each potentially significant error source are shown in Figures E-1 thru E-6. These sensitivity curves are useful in providing a "balanced design" such that trade-offs can be performed to ease equipment requirements whenever possible, without compromising calibration precision unnecessarily. Figure E-1 graphically shows the estimation precision goals stated in Table 4-3 and provides a basis for determining acceptable levels of the various error sources. However, to use the curves effectively, the propagation of the $\delta \dot{M}^m$ errors into errors in the estimates of the calibration terms must be considered. This sensitivity is given by the calibration estimation equations themselves (Equations C-1 thru C-3), in which the weighting factors are generally less than unity and in some cases will attenuate the errors by more than a factor of 10.

The curves in Figure E-6, as reproduced from Refs. 4 and 8, show inconsistencies. The plot of Equation (D-8) is most likely incorrect since the equations in Ref. 4 are dimensionally inconsistent and are numerically inconsistent with Figure 2-3 of the same report (Ref. 4). Figure 2-3 probably reflects the final result with less chance for typographical errors, etc. The difference between Figure 2-3 of Ref. 4 and Table 1-1 of Ref. 8 is not important since the error source is not major (see Table E-2). Since Figure 2-3 of Ref. 4 was based on data from Ref. 8, the curve from Ref. 8 is assumed to be the correct one.

The curves presented in Figure E-5 are based on the use of bubble levels and reflect the difference between two models for PSD ($\Delta \phi_n$) that were considered (see Sections 10.2, 10.3 and D.1). Since this is the critical error source, it is recommended that further analyses in this area be conducted, as discussed in Section 10.3.

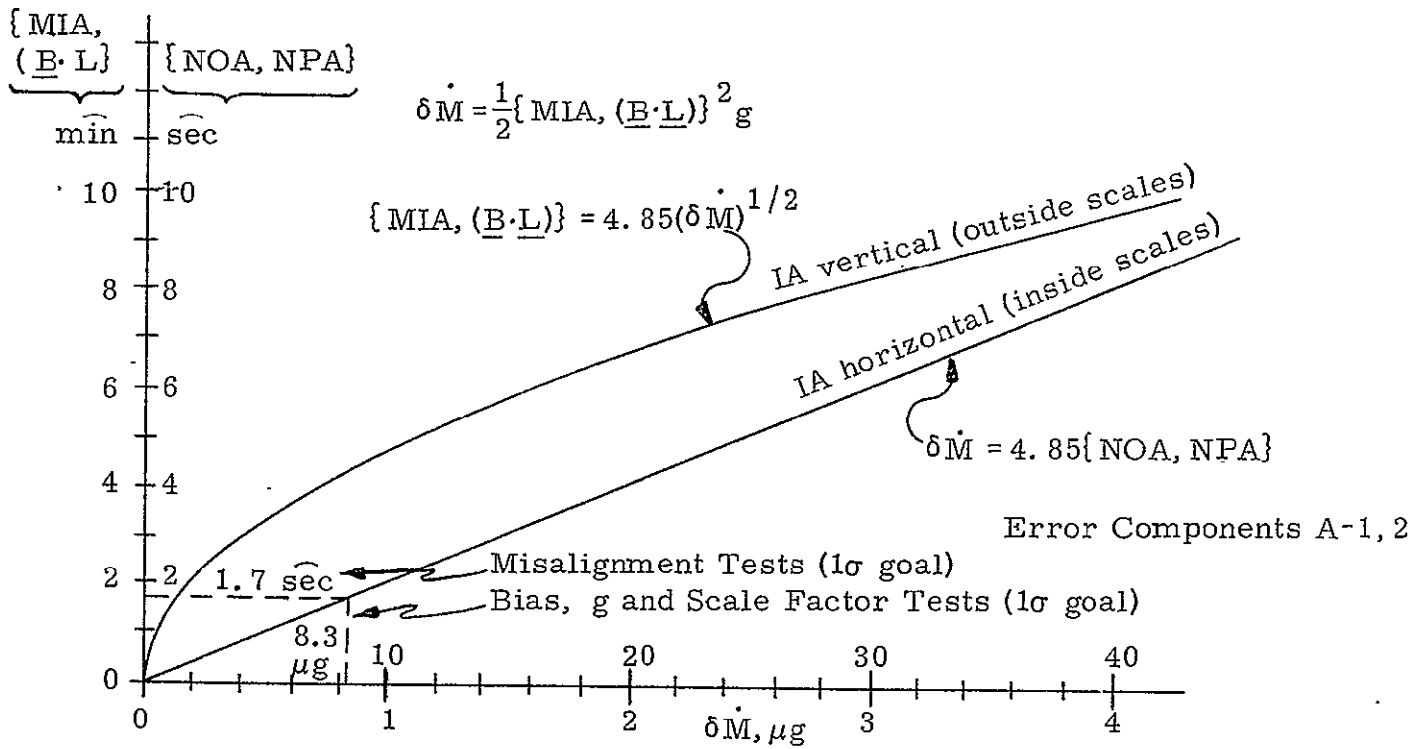


Figure E-1 Sensitivity of $\delta \dot{M}$ to Misalignment Between Accelerometer IA and Gravity Vector

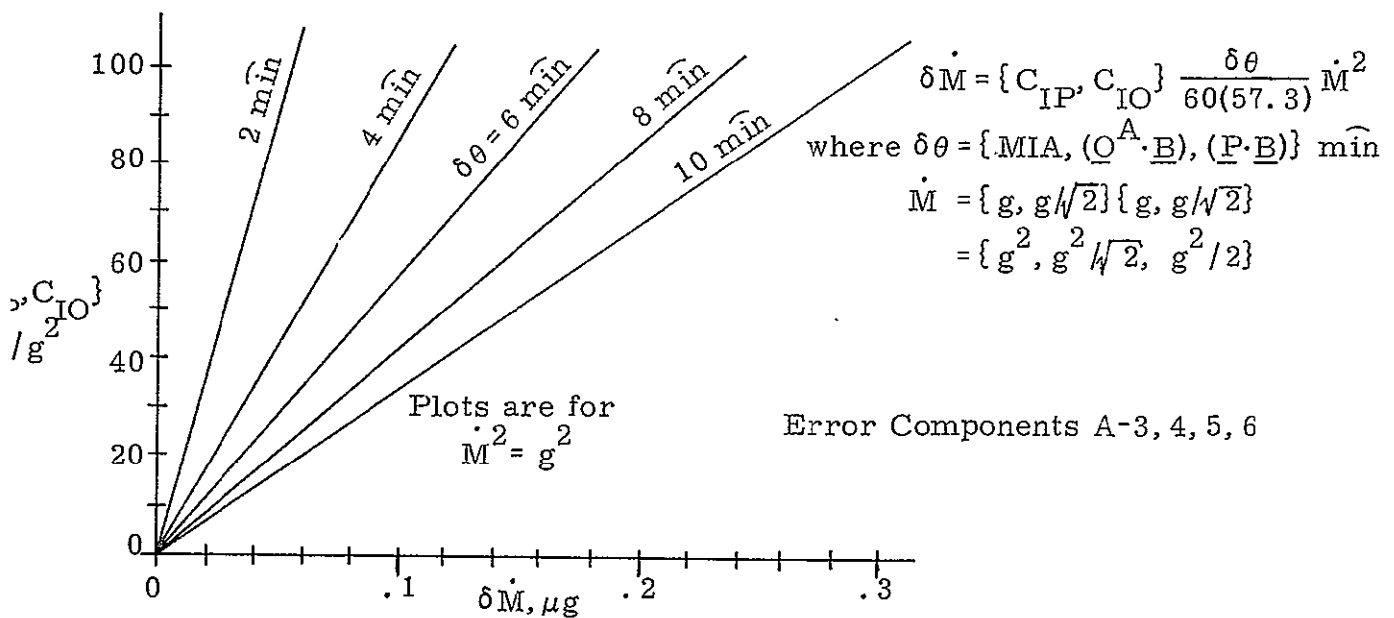


Figure E-2 Sensitivity of $\delta \dot{M}$ to Compliance Cross Coupling

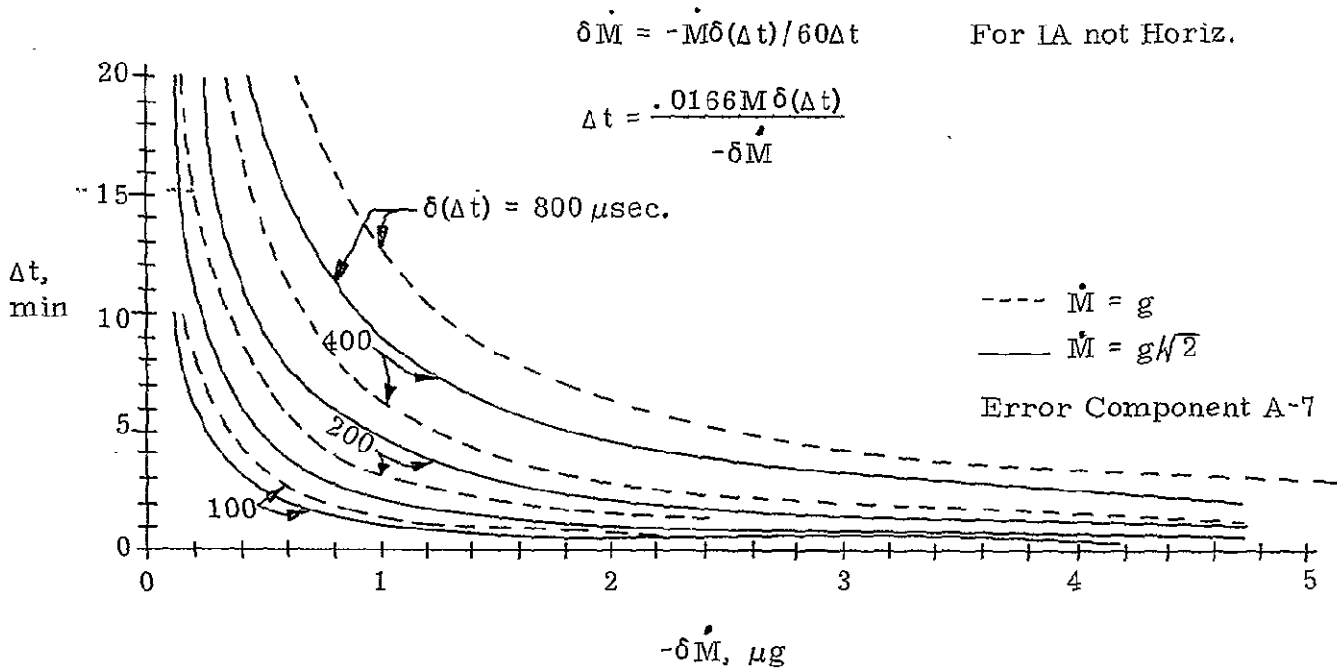


Figure E-3 Sensitivity of $\delta \dot{M}$ to Sampling Time Error ($\delta(\Delta t)$)

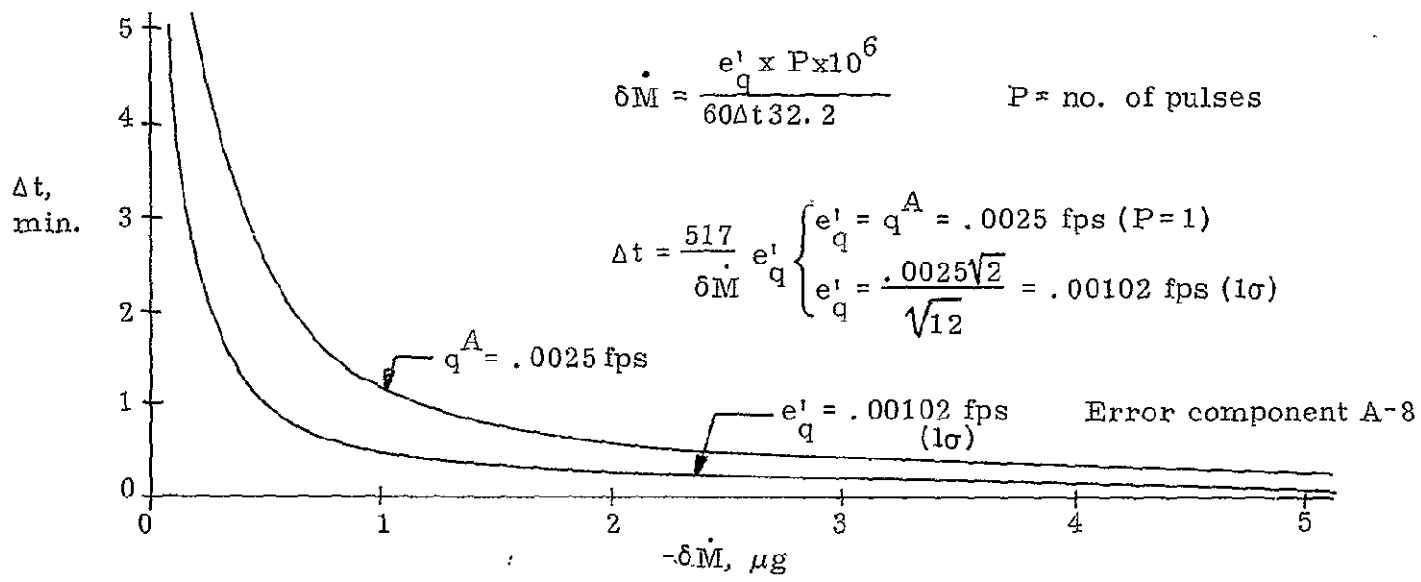


Figure E-4 Sensitivity of $\delta \dot{M}$ to Quantization of Accelerometer Output (e'_q)

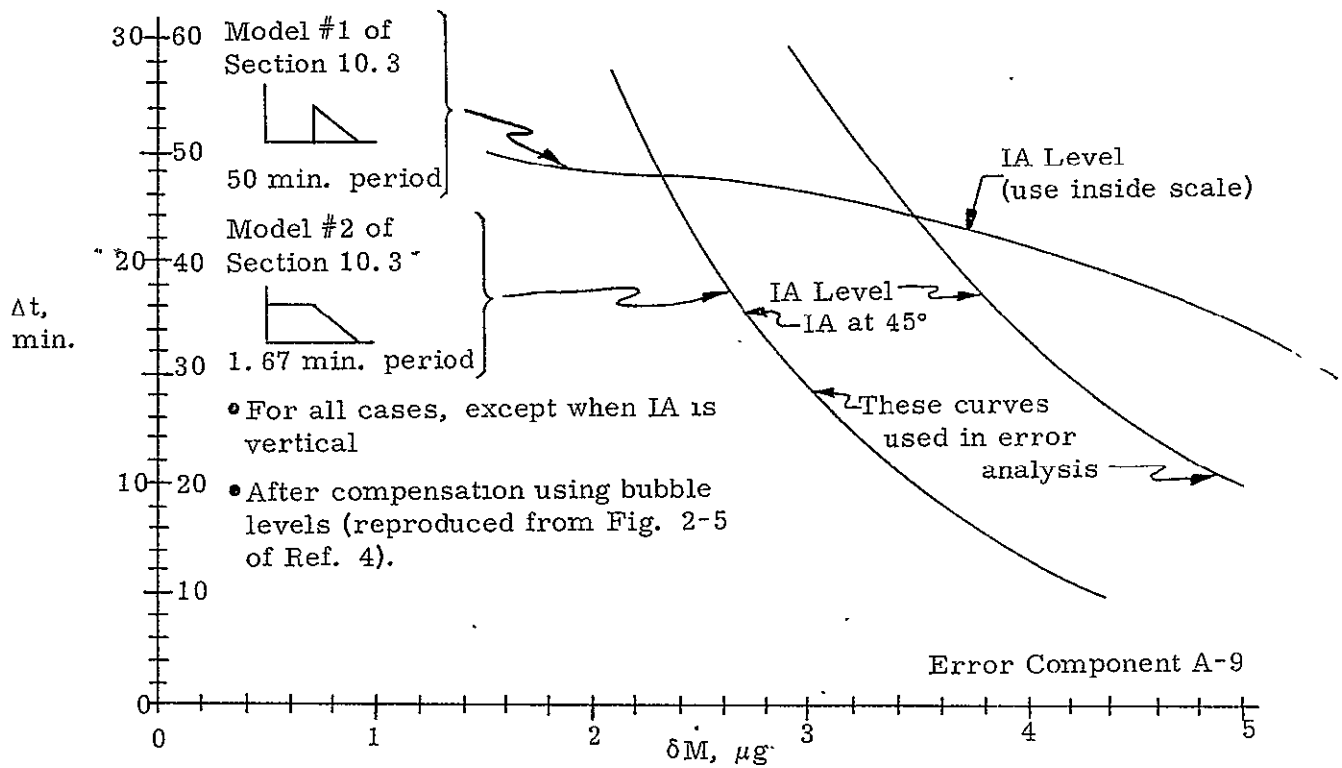


Figure E-5 Sensitivity of δM to Angular Base Motion ($\Delta\phi_n$) of Test Stand

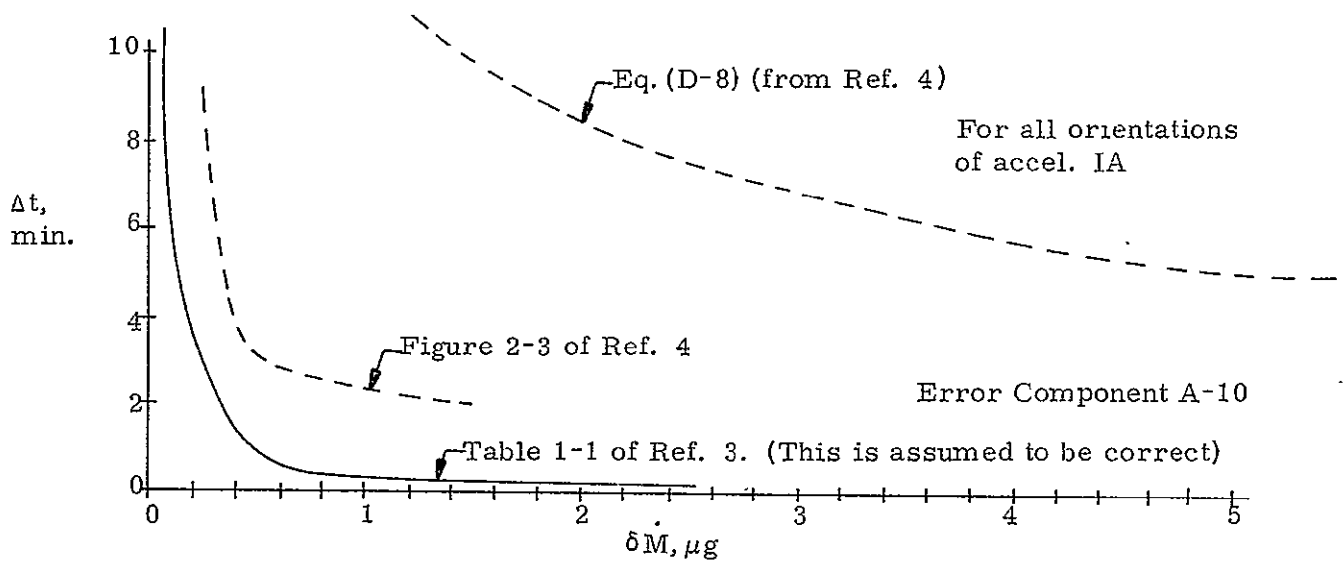


Figure E-6 Sensitivity of δM to Linear Vibration (a_v)

APPENDIX F

GYRO ERROR EQUATIONS

The form of the propagation of the gyro error sources into the gyro output errors ($\delta\dot{M}$) are shown in Table F-1 for gyro #1 ($j = 1$). Each component of $\delta\dot{M}$ is identified by a dash number following the letter "G" and is related to the potentially significant error sources of Table 10-5 as shown in Tables F-1 and F-2. The sensitivities of the error propagations are indicated by the matrix elements in Table F-1. This information is used, in conjunction with numerical values for the error sources as listed in Table 10-5, to determine the components of $\delta\dot{M}$ for each group of gyro orientations (m), run times (Δt) and table rates (W^T). Those calculations are shown in Table F-2, along with the statistical combination* of the $\delta\dot{M}$ components to yield estimates of the expected errors in \dot{M} (viz., $\delta\dot{M}$) for each test condition (m). The total sum-squared error for each test condition (m) is designated e_{SS}^m . Although the error propagation equations of Table F-1 are only for Gyro #1, the errors can be grouped according to ISU orientation, run time (Δt) and table rate (W^T) and then extended to the other two gyros in accordance with like conditions. The results are summarized in Table F-2. The effect of pre-calibration alignment errors is expected to have little effect on the e_{SS}^m in Table F-2. They are important, however, in the estimation precision of \hat{T}^{BG} , which is discussed in Section 10.5.2.

Plots of the effect on \dot{M} of each potentially significant error source are shown in Figs. F-1 thru F-8. These sensitivity curves are useful in

*The errors are assumed to be statistically independent and therefore are combined on a sum-squared basis.

Table F-1 Propagation of Gyro #1 Error Sources

δM^{42+}	w_N	-	-	w_N	-	-	-	R	r	$w^T/2$	$w^T/2$	-	$(w^T)^2$	-	w_N	w_N	$w^T/\Delta t$	$1/\Delta t$	-	-	$1/\Delta t$	$f(\Delta t)$ -sec Eq. D-18	f_2 -sec Eq. D-19	-	$f(\Delta t)$ -sec Fig. F-8	δQ_c	G-1	
δM^{52+}	w_V	-	-	-	-	g	R	g	g	-	-	$(w^T)^2$	$(w^T)^2$	w_N	-	-	negl.	$1/\Delta t$	$1/\Delta t$	$1/\Delta t$	$1/\Delta t$	f_3	f_3	$f(\Delta t)$	$\delta(G^L)$	G-2		
δM^{02+}	w_V	-	-	-	-	g	g	-	-	-	-	$(w^T)^2$	-	w_N	-	-	-	$1/\Delta t$	$1/\Delta t$	$1/\Delta t$	$1/\Delta t$	f_3	f_3	$f(\Delta t)$	(L^N)	G-3		
δM^{51}	-	-	-	-	-	0	0	0	0	-	-	negl.	negl.	1/2 Diff	-	-	-	1/2 Diff	1/2 Diff	1/2 Diff	$\delta \epsilon_E$	G-4						
δM^{01}	-	-	-	-	-	0	0	-	-	-	-	negl.	-	1/2 Diff	-	-	-	1/2 Diff	1/2 Diff	1/2 Diff	$\delta \epsilon_N$	G-5						
δM^{72}	0	w_N	-	0	-	-	-	0	0	$w^T/2$	$w^T/2$	-	$(w^T)^2$	-	w_N	w_N	$w^T/\Delta t$	$1/\Delta t$	-	-	Diff	Diff	Diff	-	$B_1(MUA)$	G-6		
δM^{14}	w_V	w_N	-	w_N	-	-	-	g	g	-	-	-	-	-	-	-	negl.	-	-	-	$1/\Delta t$	f_2	-	-	$B_1(B^L)$	G-7		
δM^{50}	w_V	-	-	-	-	g	g	g	g	-	-	$(w^T)^2$	$(w^T)^2$	1/2 Sum	-	-	-	negl.	1/2 Sum	1/2 Sum	1/2 Sum	1/2 Sum	1/2 Sum	1/2 Sum	$B_S(\Sigma^G, E)$	G-8		
δM^{60}	-	-	-	-	-	-	-	-	-	-	-	$(w^T)^2$	-	1/2 Sum	-	-	-	negl.	1/2 Sum	1/2 Sum	1/2 Sum	1/2 Sum	1/2 Sum	1/2 Sum	$B_S(B^L)$	G-9		
δM^{11}	w_N	-	-	w_N	-	-	-	R	R	-	-	-	-	-	-	-	negl.	-	-	-	$1/\Delta t$	f_3	$f(\Delta t)$	$f(\Delta t)$	$(MUA)^2$	G-10		
δM^{22}	w_N	-	-	w_N	-	-	-	R	R	-	-	-	-	-	-	-	negl.	-	-	-	$1/\Delta t$	f_3	$f(\Delta t)$	$f(\Delta t)$	$(B^L)^2$	G-11		
δM^{72}	$-w_V$	w_N	-	w_N	-	-	-	g	g	-	-	-	-	-	-	-	-	-	-	-	-	f_3	$f(\Delta t)$	$f(\Delta t)$	MB_1	G-12		
δM^{77}	f_1	f_1	-	f_1	-	$g/\sqrt{2}$	$g/\sqrt{2}$	g	g	-	-	-	-	-	-	-	-	-	-	-	-	f_2	-	-	MB_S	G-13		
δM^{88}	$w_V/\sqrt{2}$	$w_V/\sqrt{2}$	$w_N/\sqrt{2}$	$-w_N/\sqrt{2}$	$-w_V/\sqrt{2}$	$g/\sqrt{2}$	$g/\sqrt{2}$	$g/\sqrt{2}$	$g/\sqrt{2}$	$g/\sqrt{2}$	$g/\sqrt{2}$	$g/\sqrt{2}$	$g/\sqrt{2}$	f_4	$f(\Delta t)/\sqrt{2}$	NUWT	G-14											
δM^{99}	-	w_V	w_N	-	$-w_V$	r	R	$g/\sqrt{2}$	$g/\sqrt{2}$	$g/\sqrt{2}$	$g/\sqrt{2}$	$g/\sqrt{2}$	f_3	$f(\Delta t)$	$f(\Delta t)$	NUWT(B^L)	G-15											
δM^{10}	f_1	f_1	-	f_1	-	$g/\sqrt{2}$	$g/\sqrt{2}$	g	g	-	-	-	-	-	-	-	-	-	-	-	-	f_3	$f(\Delta t)$	$f(\Delta t)$	NUWT(MUA)	G-16		
δM^{11}	$w_V/\sqrt{2}$	$w_V/\sqrt{2}$	$w_N/\sqrt{2}$	$-w_N/\sqrt{2}$	$-w_V/\sqrt{2}$	$g/\sqrt{2}$	$g/\sqrt{2}$	$g/\sqrt{2}$	$g/\sqrt{2}$	$g/\sqrt{2}$	$g/\sqrt{2}$	$g/\sqrt{2}$	$g/\sqrt{2}$	f_3	$f(\Delta t)/\sqrt{2}$	$\delta(\Delta t)$	G-17											
δM^{12}	-	w_V	w_N	-	$-w_V$	R	R	$g/\sqrt{2}$	$g/\sqrt{2}$	$g/\sqrt{2}$	$g/\sqrt{2}$	$g/\sqrt{2}$	$g/\sqrt{2}$	$g/\sqrt{2}$	$g/\sqrt{2}$	f_3	$f(\Delta t)$	$\delta(\Delta \epsilon_2)$	G-18									
δM^{13}	$-w_V/\sqrt{2}$	$w_V/\sqrt{2}$	$w_N/\sqrt{2}$	$w_N/\sqrt{2}$	$-w_V/\sqrt{2}$	$g/\sqrt{2}$	$g/\sqrt{2}$	$g/\sqrt{2}$	$g/\sqrt{2}$	$g/\sqrt{2}$	$g/\sqrt{2}$	$g/\sqrt{2}$	$g/\sqrt{2}$	f_3	$f(\Delta t)/\sqrt{2}$	$\delta(\Delta \epsilon_2)(B^L)$	G-19											
$j=1$																										$\delta(\Delta \epsilon_2)(MUA)$	G-20	

Definitions of Functions

- $w_N = w_c \cos L$
- $w_V = w_c \sin L$
- $f_1 = w_c (f \cos L, \sin L) / \sqrt{2}$
- $f_2 = w_N f(\Delta t)$
- $f_3 = w_V f(\Delta t)$
- $f_4 = w_c (f \cos L, \sin L) f(\Delta t) / \sqrt{2}$

Notes

- (1) Not all $f(\Delta t)$ and $f(\cos L, \sin L)$ are necessarily the same
- (2) "Diff" refers to difference of errors, computed as shown in Table B-5
- (3) "Sum" refers to sum of errors, computed as shown in Table B-5
- (4) Pre-calibration alignment errors in δM^{11} and δM^{12} are not included

Gyro Error Source No.

δQ_c	G-1
$\delta(G^L)$	G-2
(L^N)	G-3
$\delta \epsilon_E$	G-4
$\delta \epsilon_N$	G-5
$B_1(MUA)$	G-6
$B_1(B^L)$	G-7
$B_S(\Sigma^G, E)$	G-8
$B_S(B^L)$	G-9
$(MUA)^2$	G-10
$(B^L)^2$	G-11
MB_1	G-12
MB_S	G-13
NUWT	G-14
NUWT(B^L)	G-15
NUWT(MUA)	G-16
$\delta(\Delta t)$	G-17
$\delta(\Delta \epsilon_2)$	G-18
$\delta(\Delta \epsilon_2)(B^L)$	G-19
$\delta(\Delta \epsilon_2)(MUA)$	G-20
ϵ^G	G-21
ϵ^{nr}	G-22
$\Delta \epsilon_n$	G-23
$\Delta \epsilon_n$	G-24

Table F-2 Calculation of Gyro Error Covariance Matrix Elements

Error Source 1				Error Source 2				Sensitivity ⁽⁴⁾		Error Component		Δt = 6 minutes		Δt = 10 minutes		Δt = 5		Δt = 6		Δt = 10 minutes			
No.	Symb.	Value	Units	No.	Symb.	Value	Units	Value ⁽³⁾	Units	Value	Units	No.	Units	w ^T = 2°/sec				OA and/or SA at 45°					
												w ^T = 2°/sec				OA and SA not at 45° to Vertical (w ^T = 0)				OA and/or SA at 45°			
												IA Vert.	IA Horiz.	IA Vert.	IA Horiz.	IA Vert.	IA Horiz.	IA Vert.	IA Horiz.	IA 45°	IA Horiz.		
12	δQ _c	200/3	ppm					15(.707) ⁽¹⁾	°/hr	.71	mdh	G-1		-	-	.71	.71	.71	-	.5	-		
6	δ(G·L)	<.5/3	min					"	"	.52	"	G-2		.5	-	.5	-	.5	.5	.35	.5		
13	(L·N)	20	sec					"	"	1.03	"	G-3		-	-	1.03	-	-	.73	1.03			
19	δφ _E	.2	min					"	"	.62	"	G-4		-	-	.62	.62	-	.44	-			
21	δφ _N	.2	"					"	"	"	"	G-5		-	-	.62	-	-	.14	.62			
17	B _I	1.5	°/hr g	14	MLA	5/3	min	60(57.3)	rad min	.67	mdh g	G-6		-	-	.67	-	.67	.17	.67			
17	B _I	"	"	16	(B·L)	10.4/3	"	"	"	1.38	"	G-7		-	-	1.38	-	1.38	.97	1.38			
18	B _S	"	"	15	(S·B)	10/3	"	"	"	1.33	"	G-8		-	-	1.33	1.33	1.33	1.33	.94	.94		
18	B _S	"	"	16	(B·L)	10.4/3	"	"	"	1.38	"	G-9		-	-	1.38	1.38	1.38	1.38	.97	.97		
Sub Total of w ^T & Time Independent										(δM) ² (mdh) ²				.25	-	1.81	8.36	4.81	6.28	4.28	5.87		
Sub Total of w ^T Dependent										(δM) ² (mdh) ²				.5	-	2.19	2.89	2.19	2.51	2.07	2.42		
14	(MLA) ²	(5/3) ²	min ²					w ^T 2(57.3) ²	°/hr min ²	1.67	mdh	G-10		1.67	-	-	-	-	-	-	-		
16	(B·L) ²	(10.4/3) ²	"					"	"	7.24	"	G-11		7.24	-	-	-	-	-	-	-		
22	m	10	in	17	B _I	1.5	°/hr g	(w ^T) ² 12(57.3) ² 32	deg g hr in	.04	"	G-12		-	.04	-	-	-	negl.	-	-		
22	m	"	"	18	B _S	"	"	"	"	"	"	G-13		.04	-	-	-	-	negl.	-	-		
Sub Total of w ^T Dependent										(δM) ² (mdh) ²				55.21	negl.	-	-	-	negl.	-	-		
Sub Total of w ^T Dependent										(δM) ² (mdh) ²				7.43	negl.	-	-	-	negl.	-	-		
Sub Total of w ^T Dependent										(δM) ² (mdh) ²				m for j=1	72	51, 61	3	1, 2	4	50, 60	7, 8, 10, 11, 13	9, 12	
Sub Total of w ^T Dependent										(δM) ² (mdh) ²				m for j=2	92	41, 51	2	1, 3	6	40, 50	8, 9, 11, 12, 13	7, 10	
Sub Total of w ^T Dependent										(δM) ² (mdh) ²				m for j=3	82	41, 61	1	2, 3	5	40, 60	7, 9, 10, 12	8, 11, 13	

Notes: (1) Latitude sensitive terms are evaluated at L=45°.
 (2) Pre-calibration alignment errors are not included in δM¹¹, δM⁵¹ or δM⁶¹.
 (3) Δt is in minutes and w^T in deg/sec.
 (4) Error sensitivity plots of Error Components G-1 through G-24 (except G-14, 15, 16, 19 & 20) are contained in Figs F-2 through F-8.

Continued on next page

Table F-2 Calculation of Gyro Error Covariance Matrix Elements

Error Source 1				Error Source 2				Sensitivity ⁽⁴⁾		Error Component			Δt = 6 minutes w ^T = 2 °/sec		Δt = 10 minutes OA and SA at 45° to Vertical (w ^T = 0)		Δt=5		Δt=6		Δt = 10 minutes OA and/or SA at 45°			
No.	Symb.	Value	Units	No.	Symb.	Value	Units	Value ⁽³⁾	Units	Value	Units	No.	IA Vert.	IA Horiz.	IA Vert.	IA Horiz.	IA Vert.	IA Horiz.	IA Vert.	IA Horiz.	IA 45°	IA Horiz.		
20	NUWT	3.05 ⁽¹⁾	$\frac{\text{sec}}{\text{rev}}$	-	-	-	-	$\frac{w^T}{360}$	$\frac{\text{°/hr}}{\text{sec}}$	17.0	mdh rev	G-14	-	$\frac{17.0}{\sqrt{2}\sqrt{2}}$	-	-	-	-	$\frac{17.0}{\sqrt{2}\sqrt{2}}$	-	-	-	-	
20	NUWT	"	"	16	(B.L)	10.4/3	min	$\frac{w^T \times 10^{-6}}{1.237}$	$\frac{\text{°/hr}}{\text{sec min}}$	<.005	"	G-15	negl.	-	-	-	-	-	-	-	-	-	-	
20	NUWT	"	"	14	MIA	5/3	"	"	"	<.003	"	G-16	negl.	-	-	-	-	-	-	-	-	-	-	
23	δ(Δt)	100	μsec	-	-	-	-	$60(10)^{-3} \frac{w^T}{\Delta t}$	$\frac{\text{mdh}}{\mu\text{sec}}$	2.0	mdh	G-17	2.0	-	-	-	-	-	-	-	-	-	-	
Sub Total of w ^T & Time Dependent												$(\delta M)^2$	(mdh) ²	4.00	72.25	-	-	-	-	72.3	-	-	-	-
Sub Total of w ^T & Time Dependent												δM	mdh	2.0	8.50	-	-	-	-	8.50	-	-	-	-
24	δ(Δφ ₂)	6	sec	-	-	-	-	$\frac{10^3}{60\Delta t}$	$\frac{\text{mdh}}{\text{sec}}$	16.7	mdh x min	G-18	16.7	-	-	-	-	-	-	-	-	-	-	
24	δ(Δφ ₂)	"	"	16	(B.L)	10.4/3	min	$\frac{10^3/\Delta t}{3600(57.3)}$	$\frac{\text{mdh}}{\text{sec min}}$.05	mdh	G-19	-	negl.	-	-	-	-	negl.	-	-	-	-	
24	δ(Δφ ₂)	"	"	14	MIA	5/3	"	"	"	.03	"	G-20	-	negl.	-	-	-	-	negl.	-	-	-	-	
25	q _G	see Note 5	sec	-	-	-	-	$\frac{\sqrt{2}/\sqrt{2}}{60 \Delta t}$	$\frac{\text{°/hr}}{\text{sec}}$	$\frac{5.74}{\Delta t}$	mdh x min	G-21	.96/2	.96/√2	.57	.57	1.15	.96/√2	.57	.57	-	-	-	
26	ε _{nr}	see Table 4-6	-	-	-	-	-	see Eq. (D-18)	-	-	-	G-22	-	-	-	-	-	-	-	-	-	-	-	
28	Δφ _n	see Fig. 10-1	-	-	-	-	-	see Eq. (D-19)	-	-	-	G-23	1.4√2	1.4/√2	1.4	1.4	1.4	1.4/√2	1.4	1.4	1.4	1.4	1.4	
29	Δφ _n	see Eq. (D-17)	-	-	-	-	-	see Fig. F-8	-	-	-	G-24	-	10/√2	-	12.0	-	10/√2	12/√2	12	12	12	12	
Sub Total of Time Dependent												$(\delta M)^2$	(mdh) ²	284.59	51.71	2.28	146.28	3.28	51.71	74.71	146.28	-	-	
Sub Total of Time Dependent												δM	(mdh)	16.87	7.19	1.51	12.09	1.81	7.19	8.64	12.09	-	-	
Sum Squared Error												e _{ss} ^m	(mdh) ²	344.05	123.96	7.09	154.64	8.09	130.29	78.99	162.15	-	-	
Sum Squared Error												δM	(mdh)	18.55	11.13	2.66	12.44	2.84	11.41	8.89	12.34	-	-	
Sum Squared Error												m for j=1		72	51, 61	3	1, 2	4	50, 60	7, 8, 10, 11, 13	9, 12	-	-	
Sum Squared Error												m for j=2		92	41, 51	2	1, 3	6	40, 50	8, 9, 11, 12, 13	7, 10	-	-	
Sum Squared Error												m for j=3		82	41, 61	1	2, 3	5	40, 60	7, 9, 10, 12	8, 11, 13	-	-	

- Notes: (1) Latitude sensitive terms are evaluated at L=45°.
 (2) Pre-calibration alignment errors are not included in δM⁴¹, δM⁵¹ or δM⁶¹.
 (3) Δt is in minutes and w^T in deg/sec.
 (4) Error sensitivity plots of Error Components G-1 through G-24 (except G-14, 15, 16, 19 & 20) are contained in Figs. F-2 through F-8.
 (5) q_G = .844 sec for |w| < 30°/sec and 1.688 sec for 30 < |w| < 60°/sec.
 (6) The value 1.4 was chosen conservatively between two inconsistent values, as discussed in Appendix D.

providing a "balanced design" such that trade-offs can be performed to ease equipment requirements whenever possible, without compromising calibration precision unnecessarily. Figs. F-1 thru F-3 graphically show the estimation precision goals stated in Table 4-5 and provides a basis for determining acceptable levels of the various error sources. However, to use the curves effectively, the propagation of the $\delta \dot{M}^m$ errors into errors in the estimates of the calibration terms must be considered. This sensitivity is given by the calibration estimation equations themselves (Eqs. C-5 thru C-8), in which the weighting factors are generally less than unity and in some cases will attenuate the errors by more than a factor of 10.

The "IA Horiz. " curve in Fig. F-8 was reproduced from Fig. 2-1 of Ref. 4. Although Eq. (D-20) is inconsistent with this curve, the curve is assumed correct, as explained in Appendix D-2. Because the angular rate vibration ($\Delta \dot{\phi}_n$) is one of the largest error sources, as shown in Table F-2, further analyses are recommended.

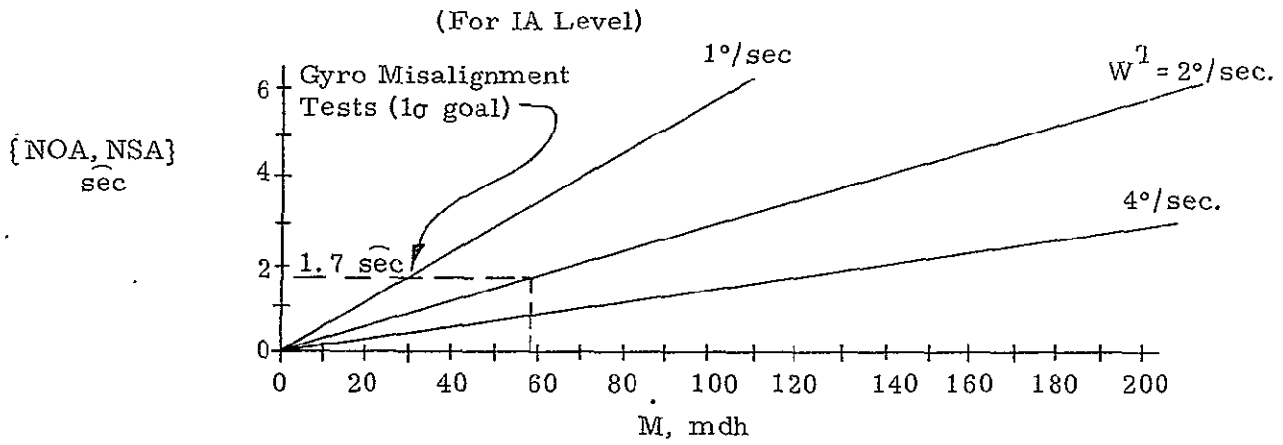


Figure F-1 Sensitivity of \dot{M} to Gyro IA Nonorthogonality with Rotary Axis

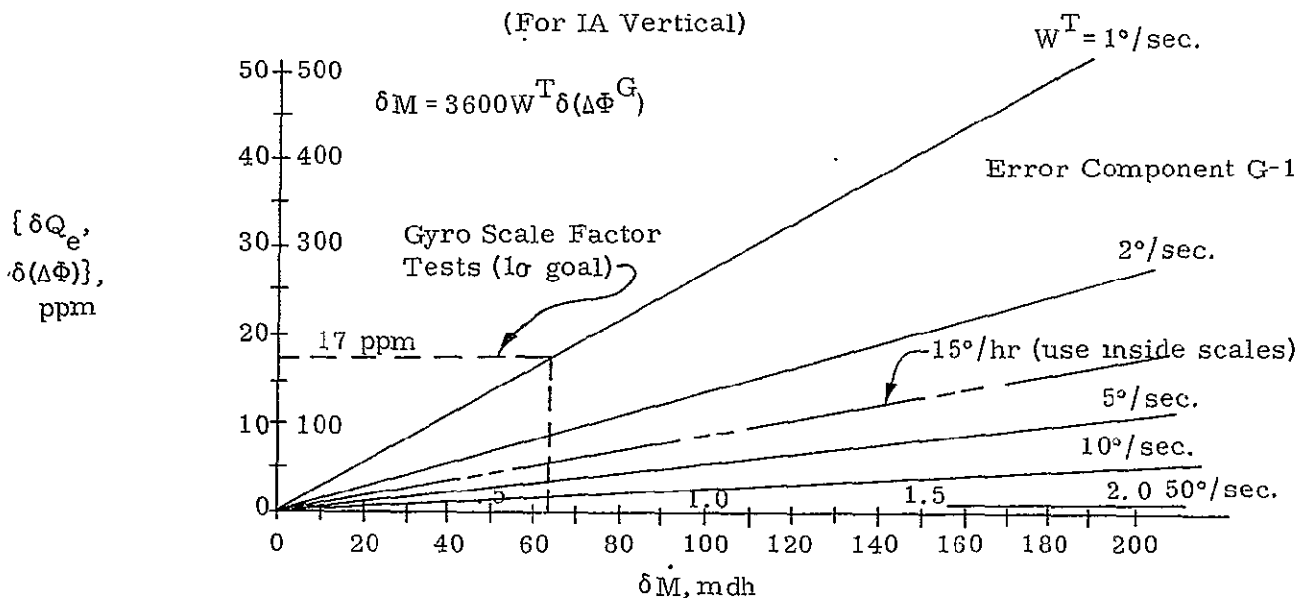


Figure F-2 Sensitivity of $\delta\dot{M}$ to Gyro Scale Factor Error

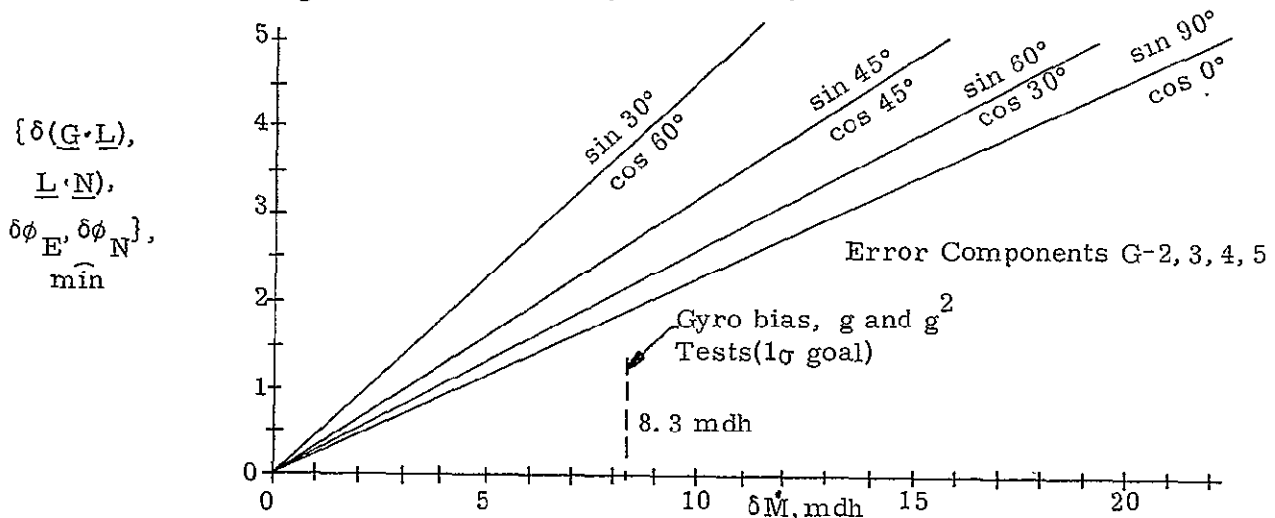


Figure F-3 Sensitivity of $\delta\dot{M}$ to Earth Rate Cross Coupling

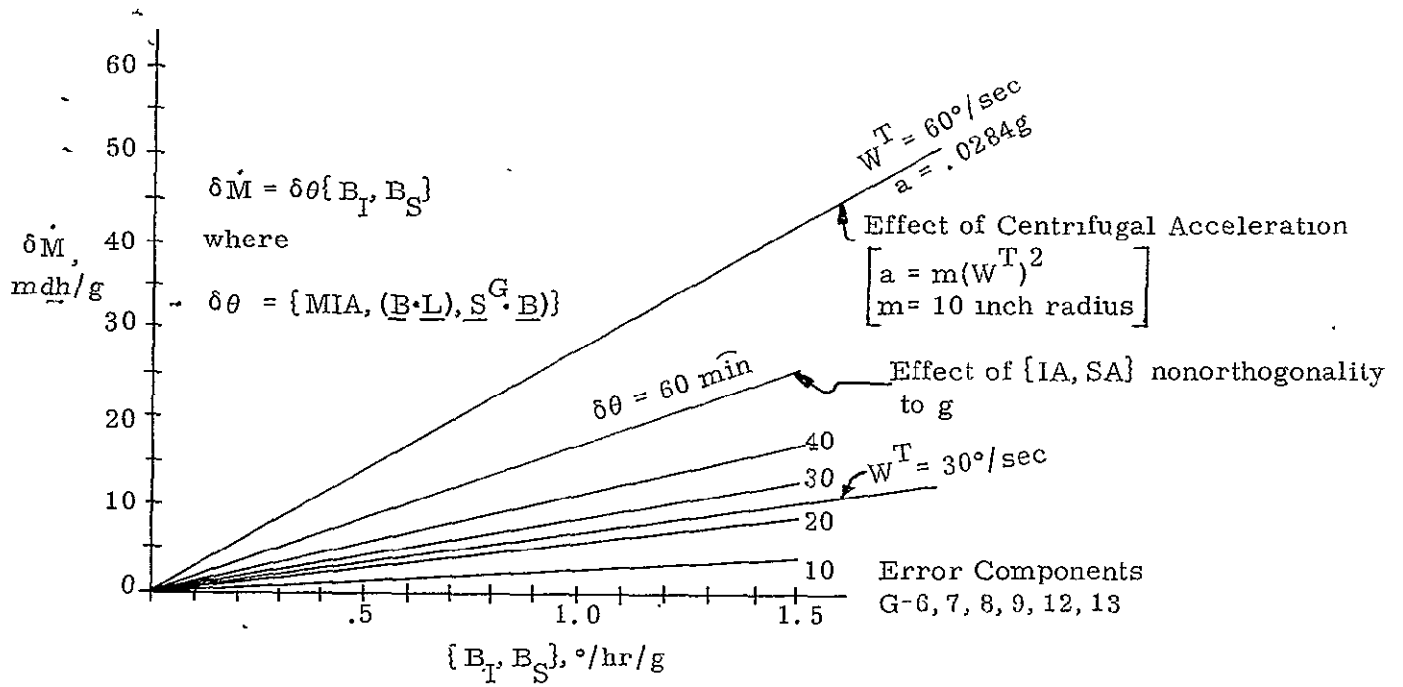


Figure F-4 Sensitivity of δM to Centrifugal Acceleration and Misalignments of IA and SA

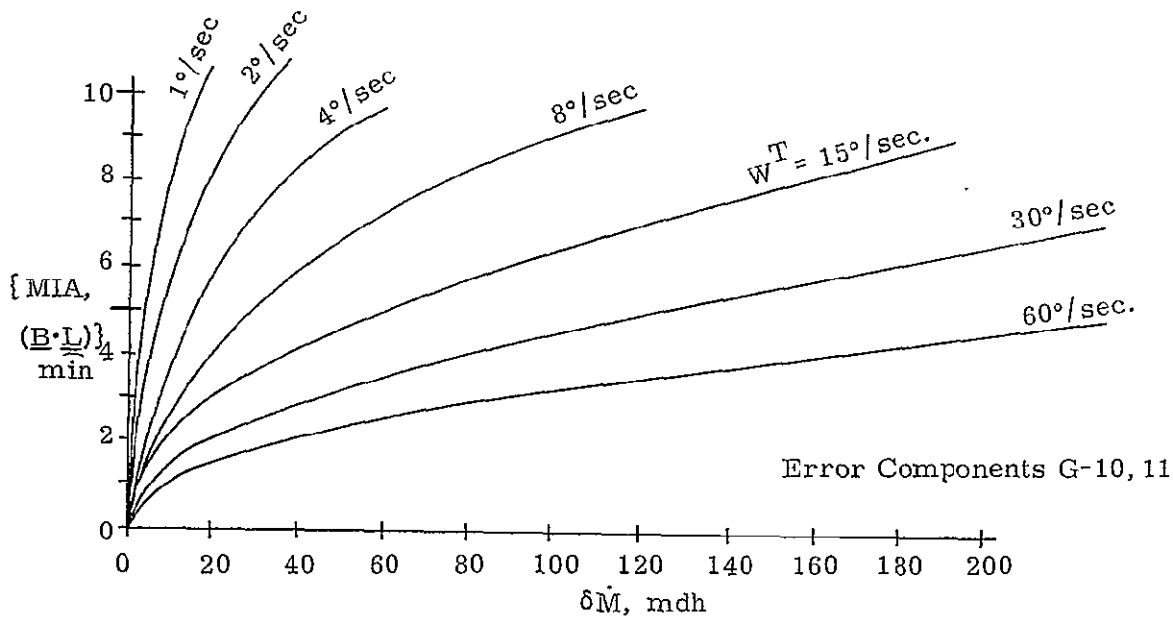


Figure F-5 Sensitivity of δM to Misalignment Between Gyro IA and Rotary Axis

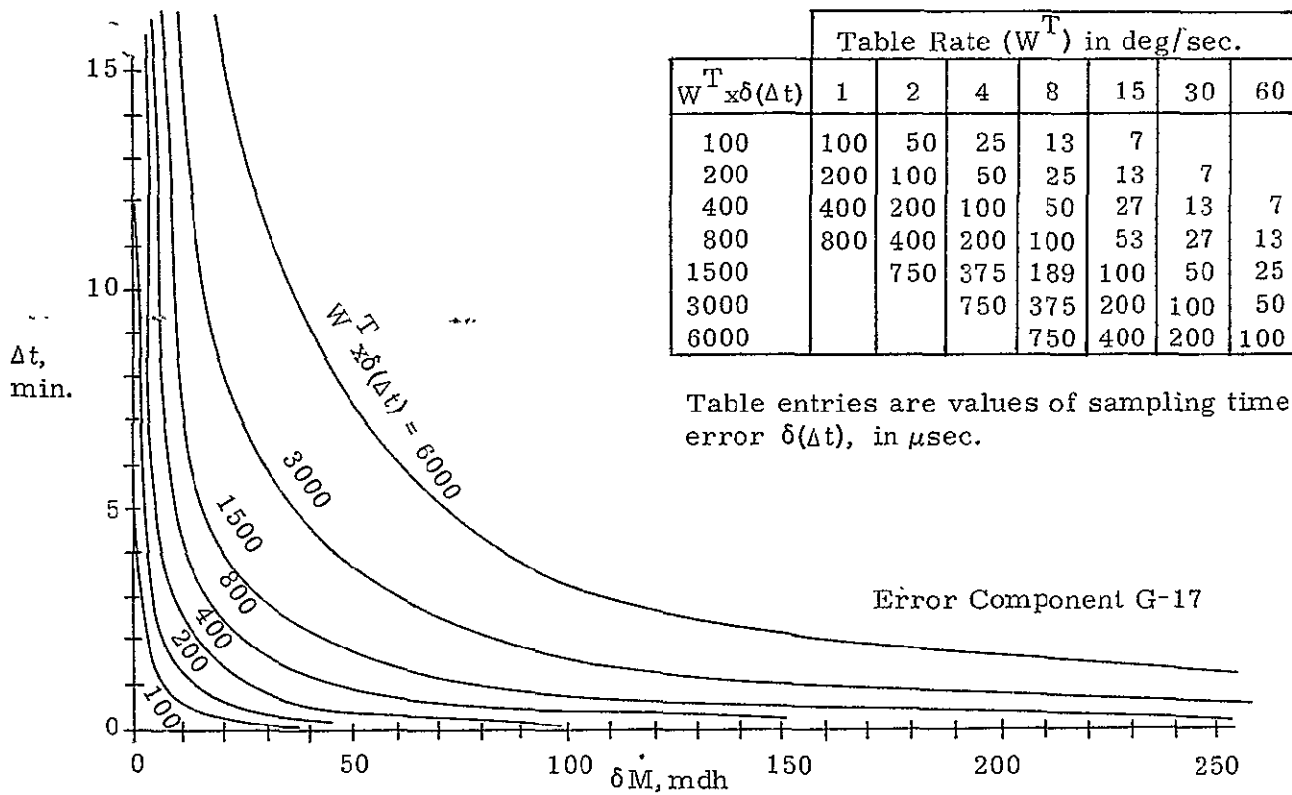


Figure F-6 Sensitivity of $\delta \dot{M}$ to Sampling Time Error

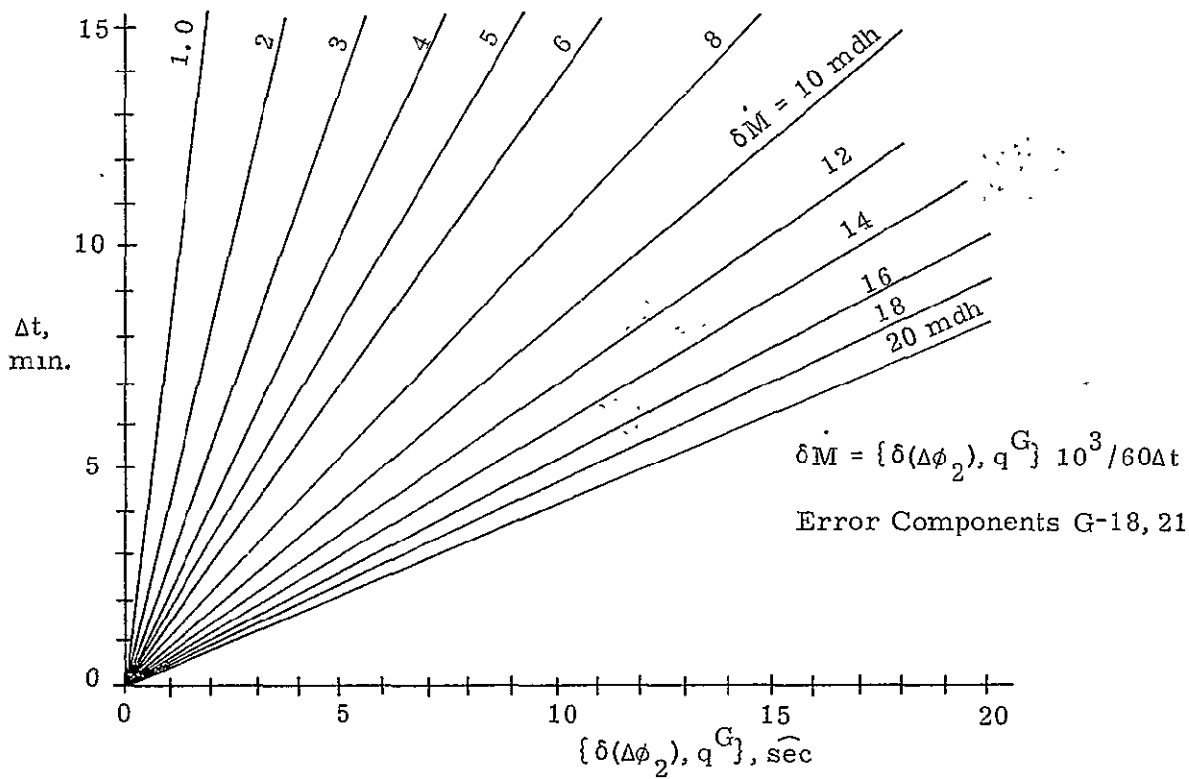


Figure F-7 Sensitivity of $\delta \dot{M}$ to Quantization of Test Table and Gyro Outputs
F-8

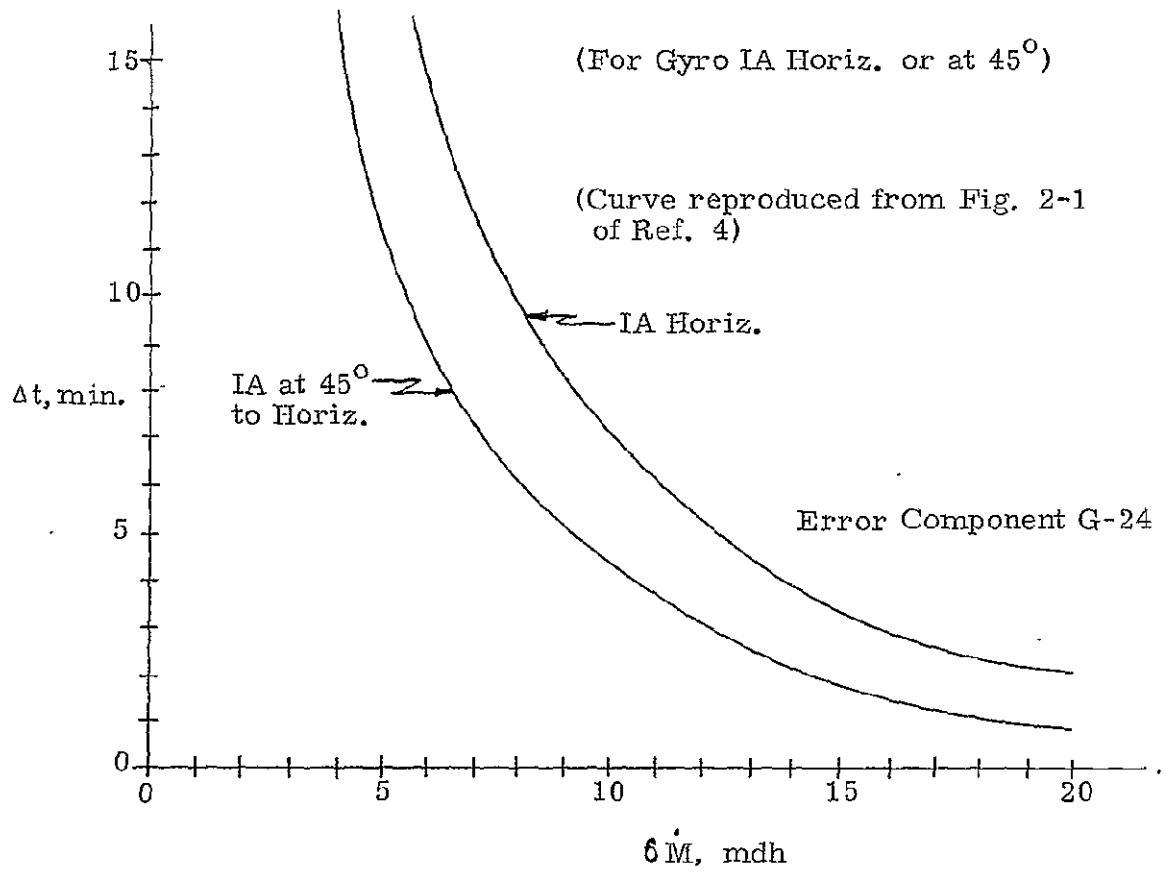


Figure F-8 Sensitivity of $\delta \dot{M}$ to Angular Rate Vibration ($\Delta \dot{\phi}_n$) of Test Stand

APPENDIX G

GLOSSARY

FORMATION OF SYMBOLS

- Wherever possible symbols will be used which suggest the name of the parameter involved.
- Lower case subscripts are used to modify prime symbols and to index over several items of the same kind.
- The lowercase script m is used to index over different test conditions.
- Uppercase superscripts will be used to indicate coordinate frames. For example, T is used to identify a transformation matrix and lettered superscripts such as ML in T^{ML} identify the particular transformation, as being in this case from the L frame to the M frame.
- Matrices will be denoted by capital letters.
- An underline will identify a vector.
- Unit vectors are used to identify lines in space such as instrument axes and the axes of all frames of reference.
- The component of any vector along any axis is indicated by a dot product of that vector with the unit vector along the axis of interest.
- A triple line symbol (\equiv) will be used for definitions.
- A superior "-" denotes an average of the quantity, but is omitted when the meaning is clear.
- A superior $\hat{\cdot}$ " " denotes an estimate of a vector or scalar.
- A superior "dot" denotes scalar differentiation.

- The abbreviation "exp" is used to indicate an exponent (e. g. , $A \text{ exp } B = A^B$), but only when necessary to avoid ambiguity.
- The Greek sigma (Σ) will be used for summations. Where the limits of summation are clear from the context, they will not be indicated with the symbol.
- The Greek Δ is generally used to indicate a change.
- The Greek δ is always used to indicate an error.
- $S\phi$ and $C\phi$ are sometimes used to identify the sine and cosine of the angle ϕ .
- Misalignments expressed in the form $\underline{M}_{ab} \cdot \underline{L}_c$ are interpreted as the misalignment of \underline{M}_a about \underline{L}_b with respect to \underline{L}_c , measured about the positive \underline{L}_b axis in accordance with the right-hand rule.

LIST OF PRIME SYMBOLS

<u>Old Symbol</u>	<u>Symbol</u>	<u>Definition</u>
	a	acceleration or specific force, defined as sum of applied acceleration and gravitational attraction.
a^e [3]	a_v	acceleration due to vibration of test stand base
	\underline{A}	unit vector representing accelerometer input axis
Redefined [3]	$\underline{A}_1, \underline{A}_3, \underline{A}_2$	unit vectors representing the accelerometer system coordinates as defined by the accelerometer IAs.
D_o [3]	A_b, A_b'	accelerometer bias, prime refers to quantity modeled in calibration equation
	$a_i, a_o,$ a_s, a_p	accelerations along IA, OA, SA and PA of gyros and accelerometers, as applicable
	B_I, B_S, B_O	gyro mass unbalance coefficients due to acceleration along IA, SA and OA, respectively. $B_I = -MUSA$ and $B_S = -MUIA$
	$\underline{B}_1, \underline{B}_2, \underline{B}_3$	unit vectors representing the ISU body axes, as defined by the ISU optical cube faces corresponding to the nominal directions of the gyro IAs (assumed to be orthogonal)
	$\underline{B}_i \cdot \underline{A}_j$	elements of T^{BA}
	$\underline{B}_c \cdot \underline{G}_j$	elements of T^{BG}

<u>Old Symbol</u>	<u>Symbol</u>	<u>Definition</u>
	BL	Bubble Level
	c	gyro damping coefficient; constant (defined where used); abbreviation for cosine
	C_k, C_T, C_M	count of pulses in rebalance loop
	C_{II}, C_{SS}	major compliance coefficients of gyro
	C_{IS}, C_{IO}, C_{OS}	cross compliance coefficients of gyro
	C_{IP}, C_{IO}	cross compliance coefficients of accelerometer (C_{IP} is the vibro- pendulous coefficient and C_{IO} is the compliance of the pendulous axis).
	D	gyro damping coefficient (= $-C/Hr$); down
	D_b	accelerometer dynamic bias
	D_1, D_2, D_3	accelerometer scale factor error coefficients
	e	error
	e^A, e^G	errors in accelerometer and gyro outputs, as defined in Eqs. (7-2) and (7-10)
$\Delta n, n_A, n_G$ [3]	e_n^A, e_n^G	error in accelerometer and gyro outputs due to noise
	\dot{e}^A, \dot{e}^G	average rate of change of e^A and e^G over time Δt
	e_{ss}^m	sum squared error in δM^m , due to all independent error sources, for test condition m
	E	East

<u>Old Symbol</u>	<u>Symbol</u>	<u>Definition</u>
	$E[]$	expected value of quantity in brackets
	\underline{E}	unit vector in East direction
	$\underline{E}_1 \underline{E}_2 \underline{E}_3$	unit vectors representing the Earth's coordinate system (\underline{E}_1 is up, \underline{E}_2 is East and \underline{E}_3 is North)
	f	frequency (H_z)
	f()	function of quantity in parenthesis; numerical subscripts refer to functions defined where used
Redefined [3]	f_1, f_2, f_3	functions of inputs to inertial sensors used in scale factor error estimation equations
	F_2, F_4, F_6	
	$\underline{F}_1 \underline{F}_2 \underline{F}_3$	unit vectors representing SATS frame of coordinates of base
	g	magnitude of specific force due to gravitational attraction
	\underline{g}	the vector directed up that presents the specific force due to gravitational attraction. Corresponding to popular convention, this is referred to as the "gravity vector"
	\underline{G}	unit vector representing gyro input axis
	$\underline{G}_1 \underline{G}_2 \underline{G}_3$	unit vectors representing the gyro system coordinates, as defined by the gyro IAs
	H	angular momentum of gyro

<u>Old Symbol</u>	<u>Symbol</u>	<u>Definition</u>
	\underline{H}	row vector of coefficients that relates \underline{Y} to M
	I	gyro moments of inertia (I_{II} , I_{SS} , I_{OO})
	$\underline{I}_1, \underline{I}_2, \underline{I}_3$	unit vectors representing the TAF inner gimbal coordinate system
	IA	Input Axis
	ISU	Inertial Sensing Unit
	j	$\sqrt{-1}$
	J	moment of inertia ratio ($= I_{OO}/H_r$)
Redefined [3]	K	constant (defined where used); total number of samples used in estimating scale factor error coefficients
	l	radius arm of proof mass in accelerometer
	L	latitude
	$\underline{L}_1, \underline{L}_2, \underline{L}_3$	unit vectors representing the Bubble Level coordinate system which is nominally defined by the TAF inner gimbal coordinate system
	m	moment arm of gyro from test table axis; mass
	mdh	millidegrees per hour ($= \text{deg/hr} \times 10^{+3}$)
Redefined [3]	$\underline{M}_1, \underline{M}_2, \underline{M}_3$	unit vectors representing the ISU mirror (optical cube) coordinate system (assumed to be orthogonal)
Redefined [3]	M^A, M^G	adjusted measurements of accelerometer and gyro outputs
	$\underline{M}_c \cdot \underline{L}_l$	elements of T^{ML}

<u>Old Symbol</u>	<u>Symbol</u>	<u>Definition</u>
	$M\tilde{O}\tilde{3}'$	misalignment between O' and O coordinate frames, about \underline{O}_3' , representing the nonorthogonality between the TAF inner and outer gimbal axes
	$MR3'$	misalignment between R' and R coordinate frames, about \underline{R}_3' , representing the nonorthogonality between the rotary and outer gimbal axes
	MUIA, MUSA	Mass unbalance along IA and SA of gyro (MUIA = $-B_S$ and MUSA = $-B_I$)
	MOA, MPA, MSA	misalignments of IA about OA, SA and PA, relative to ISU optical cube
	MIA	misalignment of IA ($=\sqrt{MOA^2 + MSA^2}$ or $=\sqrt{MOA^2 + MPA^2}$)
	NOA, NPA, NSA	nonorthogonalities of IA about OA, PA and SA, relative to earth coordinates for the accelerometers and relative to the test table axis for the gyro
Partially redefined [3]	N	number of data sampling periods of inertial instrument output that are made available to the computer; North
	\underline{N}	unit vector in the direction of true North
	NUWT	nonuniform test table rate
	$\underline{O}^A, \underline{O}^G$	unit vectors representing accelerometer and gyro output axes
	$\underline{O}_1 \underline{O}_2 \underline{O}_3$	unit vectors representing the TAF outer gimbal coordinate system. The primed coordinate frame is defined in Section 5.
	OA	Output Axis

<u>Old Symbol</u>	<u>Symbol</u>	<u>Definition</u>
	\underline{P}	unit vector representing accelerometer pendulous axis
P [3]	PSD()	power spectral density, as a function of f, of the quantity in parenthesis
	P^A	pulse count out of accelerometer, over time $\Delta t (= \sum^N C_k^A)$
	P^G	pulse count out of gyro over time $\Delta t (= \sum^N C_k^G)$
	P^Φ	pulse count out of test table, over time Δt
	$P^{\Delta t}$	pulse count out of time reference
	PA	Pendulous Axis of accelerometer
E_q [3]	q^A, q^G	quantization in accelerometer and gyro outputs to computer
	Q_{IS}	anisoinertia coefficient relating $w_i w_s$ to gyro output rate error $(= (I_{SS} - I_{II}) / H_r)$
	Q_{IP}	anisoinertia coefficient relating $w_i w_p$ to accelerometer output acceleration error
α_1, α_2 [1] } Q_{II} [3] }	Q_1, Q_2	gyro scale factor error coefficients
	R_b, R'_b	gyro bias rate error, prime refers to quantity modeled in calibration equation
	$\underline{R}_1 \underline{R}_2 \underline{R}_3$	unit vectors representing rotary axis coordinate frame that rotates with test table. The primed coordinate frame is defined in Section 5.
	$\underline{R}'_1 \underline{R}'_2 \underline{R}'_3$	
	s	abbreviation sine

<u>Old Symbol</u>	<u>Symbol</u>	<u>Definition</u>
	S	South
	\underline{S}	unit vector representing autocollimator line of sight
	S^G	unit vector representing gyro spin axis
	S^ϕ	scale factor of test table ϕ_2 angle output pulses
	$S^{\Delta t}$	scale factor of time reference
	SA	Spin Axis of gyro
	SATS	Single-Axis Test Stand
	SE()	Standard error of quantity in parenthesis
	t_o, t_N	times at beginning and end of calibration run, over which N sensor readouts are provided to the computer —
	T	torque; transformation matrix relating one coordinate system to another
Q^A [3]	T^{BA}	transformation matrix for coordinatizing vector components in the A coordinate frame (accelerometer IAs) to vector components in the B frame (body axes)
Q^G [3]	T^{BG}	transformation matrix for coordinatizing vector components in the G coordinate frame (gyro IAs) to vector components in the B frame (body axes)
	T^{ML}	transformation matrix indicating the misalignment of the ISU cube (mirror) coordinate system relative to the Bubble Level coordinate system.

<u>Old Symbol</u>	<u>Symbol</u>	<u>Definition</u>
	$\underline{T}_1 \underline{T}_2 \underline{T}_3$	unit vectors representing test table coordinate frame
	TAF	Two-Axis Fixture
	\underline{U}	unit vector in the up direction
	U	Up
	V	velocity
	\dot{V}_c	computer determined acceleration input to accelerometer
ω	w	angular velocity
[3]		
ω^E	w_e	earth rate
[3]	w_i, w_o, w_s	rates with respect to inertial space about IA, OA and SA, respectively
ω^T	w^T	angular rate of test table
[3]	W	West
	y	elements of vector \underline{Y}
	$\underline{Y}^A, \underline{Y}^G$	vector of accelerometer and gyro calibration terms to be estimated
Redefined	z_k, z_o thru	functions of outputs of inertial sensors, used in scale factor error estimation equations
[3]	z_3	
	δ	error in quantity following symbol
	Δ	change in quantity following symbol

<u>Old Symbol</u>	<u>Symbol</u>	<u>Definition</u>
D_1 [3]	$\Delta\Phi^A$	accelerometer scale factor in velocity units
	$\Delta\Phi^G$	gyro scale factor in angle units
$\Delta\theta$ [3]	$\Delta\phi_n$	change in ϕ angles (specifically ϕ_N and ϕ_E) due to motion of test stand base
ω^e [3]	$\dot{\Delta\phi}_n$	angular rate of test stand base ($=\sqrt{\dot{\phi}_N^2 + \dot{\phi}_E^2}$)
	Δt	time over which measurement M is obtained ($= t_N - t_o$)
$\left[\int_{t_o}^{t_N} a_i dt \right]_{ind}$ [1]	ΔV_c	computer determined change in accelerometer input velocity, using accelerometer output pulse count and scale factor ($=\Delta\Phi^A P^A$)
$(\theta_i)_{ind}$ [1]	$\Delta\psi_c$	computer determined change in gyro input angle, using gyro output pulse count and scale factor ($=\Delta\Phi^G P^G$)
	θ_o	gyro gimbal-to-case angular misalignment about OA
	$\phi_1, \phi_2,$ ϕ_3, ϕ_4	angles of Single-Axis Test Table and Two-Axis Fixture that define orientation of ISU (ϕ_1 is about trunnion axis, ϕ_2 about rotary axis, ϕ_3 about outer gimbal axis and ϕ_4 about inner gimbal axis)
	$\dot{\psi}_c$	computer determined rate input to gyro
	$\sigma()$	standard deviation of quantity in parenthesis
	$\sigma^2()$	variance of quantity in parenthesis

<u>Old Symbol</u>	<u>Symbol</u>	<u>Definition</u>
$\Sigma \gamma, \Sigma \delta$ [3]	N ΣC_k	summation of pulses out of inertial sensor
	τ	data sampling period at input to computer
	ω	angular frequency (rad/sec)

List of Subscripts

a	accelerometer
b	bias
c	computer; index associated with ISU optical cube
e	earth; index used to identify error sources
E	East
g	gyro
i	input axis;
j	inertial sensor designator
k	index associated with inertial sensor pulse rebalance loops; index associated with data used to estimate scale factor errors
l	index associated with bubble level axes
M	time - modulation rebalance loop
n	noise; nominal value

<u>Symbol</u>	<u>Definition</u>
N	North; reference to number of inertial sensor data samplings made available to computer
o	output axis; initial value (as used in t_0)
p	pendulous axis
q	quantization
r	random; record; gyro rotor
reb	rebalance
s	spin axis
T	ternary rebalance loop
u	uncertainty
v	vibration
V	vertical
z	value resulting from zeroing process

List of Superscripts

A	accelerometer; coordinate frame defined by accelerometer IAs
B	body coordinate frame
E	earth coordinate frame
F	SATS frame of coordinates relative to tilt of rotary axis about North
G	gyro; coordinate frame defined by gyro IAs
I	TAF inner gimbal coordinate frame
L	Bubble Level coordinate frame

<u>Symbol</u>	<u>Definition</u>
m	index associated with test conditions for each calibration run
M	mirror coordinate frame defined by ISU optical cube
O	TAF outer gimbal coordinate frame
R	rotary axis coordinate frame that rotates with test table coordinate
S	coordinate frame of autocollimator(s)
T	test table; transpose of matrix or vector; test table coordinate frame (of base) relative to tilt about East
Φ	reference to test table rotary angle output
+	plus input rate into gyro
-	minus input rate into gyro
+1	+1 g input acceleration into accelerometer
-1	-1 g input acceleration into accelerometer
+ .7	+ .707 g input acceleration into accelerometer
- .7	- .707 g input acceleration into accelerometer